PHILOSOPHICAL TRANSACTIONS OF THE ROYAL SOCIETY A MATHEMATICAL, PHYSICAL & ENGINEERING SCIENCES

# Propagation of Elastic Wave Motion from an Impulsive Source along a Fluid/Solid Interface. I. Experimental Pressure Response. II. Theoretical Pressure Response. III. The Pseudo-Rayleigh Wave

W. L. Roever, T. F. Vining and E. Strick

*Phil. Trans. R. Soc. Lond. A* 1959 **251**, 455-523
doi: 10.1098/rsta.1959.0009

# PROPAGATION OF ELASTIC WAVE MOTION FROM AN IMPULSIVE SOURCE ALONG A FLUID/SOLID INTERFACE†

## I. EXPERIMENTAL PRESSURE RESPONSE

By W. L. ROEVER and T. F. VINING

## II. THEORETICAL PRESSURE RESPONSE

By E. STRICK

## III. THE PSEUDO-RAYLEIGH WAVE

By E. STRICK

(*Communicated by Sir Edward Bullard, F.R.S.—Received* 11 *August* 1958)

Parts I and II of this report compare the experimentally observed pressure response for the impulse-excited fluid/solid interface problem with that derived from a corresponding theoretical investigation. In the experiment a pressure wave is generated in the system by a spark and detected with a small barium titanate probe. The output of the probe is displayed on an oscilloscope and photographed. Two cases are investigated: one where the transverse wave velocity is lower than the longitudinal wave velocity of the fluid and the other where the transverse wave velocity is higher. Both of these observed responses are shown to agree even as to details of wave-form, with exact computations made for a delta-excited line source. This comparison is justified by making an approximate calculation for the decaying point source and showing that at these distances it does not differ appreciably from the delta-excited line source.

In the case of low transverse wave velocity one finds, besides critically refracted *P*, direct, and reflected waves, a Stoneley type of interface wave. Although the emphasis in recent years has been towards minimizing the importance of Stoneley waves, the evidence here is that a Stoneley wave can be the largest contributor to a response curve.

In the case of high transverse wave velocity the critically refracted *P* wave is smaller, and the Stoneley wave, though it tends to maintain a rather constant amplitude, becomes compressed in time and arrives very soon after the reflexion. Between the critically refracted *P* wave and the direct arrivals one finds both experimentally and theoretically a pressure build-up preceding the arrival time that might be expected for a critically refracted transverse wave.

In part III this pressure build-up is investigated and found to consist of the superposition of three arrivals. The most prominent of these is a pseudo-Rayleigh wave. The others are the critically refracted transverse wave and the build-up to the later arriving Stoneley wave. Detailed investigation of the pseudo-Rayleigh wave shows it to have the velocity of a true Rayleigh wave which is independent of the existence of the fluid. Furthermore, it has the same retrograde particle motion as the true Rayleigh wave. However, it is radiating into the fluid as it progresses and therefore has many of the properties of a critically refracted arrival when measurements are made in the fluid. Mathematically it differs from the true Rayleigh wave in that its origin is not from a pole on the real axis of the plane of the variable of integration, but rather from a pole which lies on a lower Riemann sheet in the complex plane. In the high transverse wave velocity case this pole is not too far removed from the real axis and the imaginary part of the pole location might be interpreted as a decay factor. The real part, however, yields only approximately the velocity of the pseudo-Rayleigh

† Publication No. 173, Shell Development Company, Exploration and Production Research Division, Houston, Texas.

Vol. 251. A. 1000. (Price £1. 3*s*. 6*d*.) 57 [Published 15 September 1959

wave, for the actual velocity as pointed out above is precisely that of the true Rayleigh wave velocity. The migration of this complex pole explains why such a pseudo-Rayleigh wave was not observed in parts I and II in the low transverse velocity case.

The problem under discussion is intimately related to the classic work of Horace Lamb *On the propagation of tremors over the surface of an elastic solid*. One need make only a minor re-interpretation of the source function in order to compare directly the wave-forms (excluding of course the Stoneley wave contribution).

Finally, a method is suggested for obtaining the solid rigidity of bottom sediments in water-covered areas from *in situ* measurements of the pseudo-Rayleigh wave and/or Stoneley wave velocities and arrival times.

CONTENTS†



# I. EXPERIMENTAL PRESSURE RESPONSE

By W. L. ROEVER and T. F. VINING

## 1. Introduction

The purpose of this investigation is to obtain complete solutions to a problem in elastic wave propagation both experimentally and theoretically with emphasis on experimentally duplicating as nearly as possible the parameters and conditions assumed in the theory. It is

† The system of numbering the sections is based on (*a*) the correspondence between part I and part II and (*b*) the dependence of part III on part II.

believed that such a dual attack may lead to a better understanding of the solution and give an idea of the relative merits of the two methods in obtaining solutions to more complicated problems. This type of comparison between model seismology and theoretical seismology has been made before for the 'Lamb problem' by Kaufman & Roever (1951), Northwood & Anderson (1953), and most recently by Tatel (1954), who has shown good wave-form agreement between theory and experiment.

We have chosen for this investigation the somewhat more complicated problem of propagation in the vicinity of a fluid/solid interface. The theory for plane waves reflected from such an interface goes back to Knott (1899), but since true plane waves are difficult to approximate in the laboratory this theory has not been experimentally verified. Weinstein (1952) has performed experiments on an aluminium/water interface using a harmonic beam; he finds a discrepancy between his results and the theory which may result from the finite width of beam used.

Arons & Yennie (1950) have made field observations of the wave-form of spherical pulses reflected from the sea bottom for various geometries. These wave-forms are compared with the wave-form predicted from the theory for reflexion of a plane pulse from a fluid/fluid interface. The predicted phase shift on reflexion results in a change in shape of the reflected pulse which is in good agreement with that observed.

Von Schmidt (1938) investigated, by the schlieren visual technique, the wave-fronts generated by a spark which arrived before the reflected wave. In his paper one finds a beautiful demonstration of the existence of the critically refracted† wave-fronts which had been utilized for many years in the interpretation of earthquake and seismic prospecting data.

Very recently, O'Brien (1955), in a seismic model study somewhat similar to ours, has investigated the dependence on distance of the peak amplitude of critically refracted waves. He varied the distance both along and normal to water/wax, water/concrete, and oil/sodium chloride interfaces and showed that the theoretical expression derived for the amplitude in the neighbourhood of the wave-front also appears to give good agreement when applied to the amplitude maximum.

Although certain discrete arrivals such as the critically refracted and reflected wave-fronts have been studied in recent years, the complete wave-form has not been investigated. The Stoneley interface wave, although it has been studied theoretically, has not, to our knowledge, been demonstrated experimentally. It is our goal in this paper to obtain complete pressure-response curves both experimentally and theoretically in order to indicate the relative importance of the various arrivals.

## 2. Statement of the problem; technique of solution

We consider here the problem of the pressure wave generated by an impulse-excited point source in a large, three-dimensional fluid medium in contact with a similarly large solid medium. The particular objective of these studies will be to observe accurately the effect of

† We shall use critically refracted wave to refer to the arrival corresponding to the minimum time path which has variously been called the 'head wave' (Von Schmidt, 1938; O'Brien 1955) and conical wave (Cagniard 1939). We shall designate the critically refracted longitudinal wave as $P_{cr}$ and the critically refracted transverse wave as $S_{cr}$ from the terms 'primary' and 'secondary' used in earthquake seismology.




PHILOSOPHICAL TRANSACTIONS OF THE ROYAL SOCIETY A MATHEMATICAL, PHYSICAL & ENGINEERING SCIENCES

the presence of solids of various elastic constants on the pressure wave-form observed at a point in the fluid. By a large medium we mean one with linear dimensions sufficiently great that reflexions from the outer boundaries will reach the detector after all events associated with the interface have been recorded. To generate a suitable pressure pulse we use a spark because this enables us to release a relatively large amount of energy from a small source. Otherwise the technique is very similar to that used in many of the earlier model experiments mentioned previously.

## 3. Apparatus (experimental)

A capacitor discharging across the spark gap under the water creates a pressure pulse and, at the same time, by inductive coupling, triggers the horizontal sweep of a Tektronix-type 511-AD oscilloscope. A pressure-sensitive, barium titanate probe measures the resulting pressure which, after suitable amplification, is presented to the vertical amplifier of the oscilloscope. The detector and pre-amplifier can be manually replaced by a time mark generator as the need arises (see figure 1).

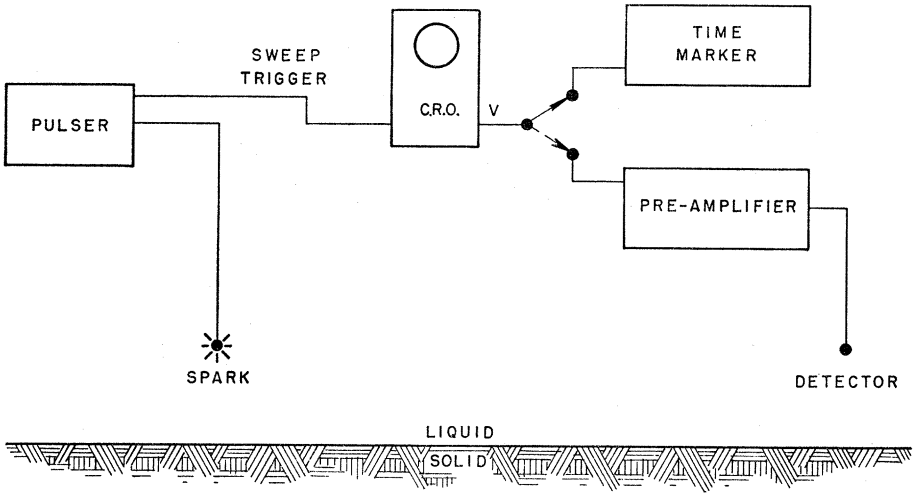


Figure 1. Block diagram of equipment.

### (a) *Nature of the source*

The power source for the spark consists simply of an 800 V supply which charges a 1 $\mu$F capacitor through a 10 k$\Omega$ resistor. A type OA 5 thyratron is used to discharge the capacitor across the spark gap (see figure 2*a*). A peak discharge current of the order of 800 A flows across the gap when the thyratron is triggered.

The spark gap is made by squeezing a $\frac{1}{8}$ in. o.d., thick-walled copper tube onto a 0·035 in. diameter copper wire having extruded nylon insulation. In this manner, the outside diameter of the tip is reduced to $\frac{1}{16}$ in. and the nylon insulation is reduced to about 0·001 in. The gap, which becomes eroded after 50 to 100 firings, can be rejuvenated by filing a small amount of metal off the tip. Observations of the current flowing in the spark circuit as a function of time indicate that most of the energy is dissipated in the first 2 $\mu$s. Figure 2*b* shows the pressure response as a function of time as observed in a large tank of water (to which sodium chloride has been added to increase the conductivity) at a distance of 10 cm from the spark. From figure 2*b* one observes that the pressure pulse can be approximated by an instantaneous rise in pressure, followed by an exponential decay to $1/e$ of the peak value in

about 5 $\mu$s. The amplitude of the frequency spectrum of such a pulse is given by $\frac{1}{2}\pi\sqrt{(\alpha^2+\omega^2)}$, where $\alpha$ is the decay constant which in this case is $1/5\times10^{-6}=2\times10^5$/s. Thus the frequency where the amplitude is down to one-half its low-frequency value is given by

$$\omega=\sqrt{3}\alpha=2\sqrt{3}\times10^5\,\text{rad/s}\quad\text{or}\quad 2\sqrt{3}/2\pi\times10^5\sim55\,\text{kc/s},$$

which corresponds to a wavelength in the water of 2·7 cm. Since the diameter of the source is about 3 mm, the source and also the detector to be described will appear to be good point sources and point detectors when placed in a practical fluid such as water. The spark creates an oscillating bubble, the first oscillation having a period of about 600 $\mu$s, so that the complication of multiple arrivals can be avoided by making sure that all interesting events occur well within that time.

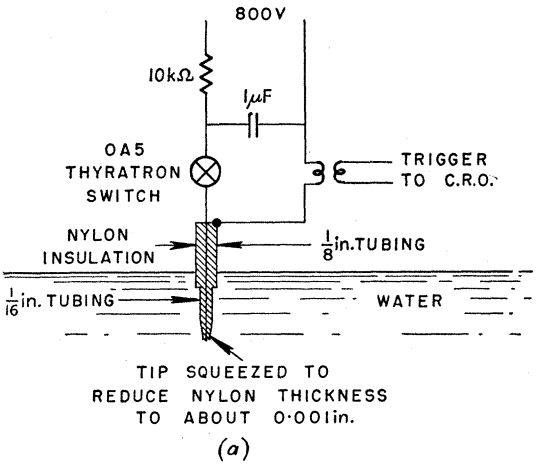


FIGURE 2*a*. Diagram of spark source.

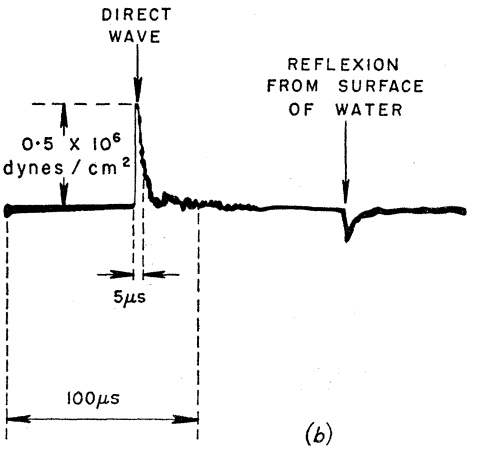


FIGURE 2*b*. Pressure pulse observed at 10 cm.

### (*b*) *Nature of the detector*

The pressure probe consists of a $\frac{1}{8}$ in. by $\frac{1}{8}$ in. barium titanate cylinder mounted on the end of a 4 in. long piece of $\frac{1}{16}$ in. hypodermic needle tubing which is in turn mounted on the end of an 18 in. piece of $\frac{1}{8}$ in. tubing. An insulated wire drawn through the hole in the tubing provides the electrical contact to the inner surface of the sensitive element. The aim in this construction is to minimize the effect of the probe on the pressure field and also to minimize acoustic energy travelling along the support. A very similar construction is described by Heuter & Bolt (1955) in more detail. By the reciprocity technique of calibration, it has been established that the probe has a response of $-130\pm4$ db with respect to 1 V dyn$^{-1}$cm$^{-2}$ within the range of 5 to 100 kc/s, with some response well above 100 kc/s.

### (*c*) *Nature of the fluid and solid media*

The fluid for our experiments is ordinary tap water having a compressional velocity of about 1500 m/s. The exact value depends upon the temperature, the air content, and the type and concentration of salt. In order to obtain a value accurate to within 10 m/s, we make the velocity measurement on the same fluid used in the experiment. This is accomplished by making a time-distance profile in the fluid with the solid sufficiently far removed. Since the plot of arrival time against source-detector distance must be a straight line with

the reciprocal of the slope yielding the desired velocity of compressional wave propagation in the fluid, the velocity is obtained by carrying out a straight-line least-squares fit with readings taken in, say, 1 cm intervals. Such an analysis shows that twenty to thirty such readings will yield the desired accuracy in velocity measurement. One consequence of this straight-line least-squares fit is that the resulting straight line does not necessarily go through zero when the centre-to-centre source-detector distance is taken to be zero. This non-zero intercept of the time axis is applied as a zero-time correction to the time axis of the interface response curves. The numerical values and probable errors for the fluid velocity and zero-time correction are included below in the data for the solid media because, as we have already stated, the fluid velocity does vary from one experiment to another.

The choice of solid is dependent upon whether or not its rotational velocity $b$ is greater or less than the fluid velocity $c$, for only when $b$ is greater than $c$ will one observe $S_{cr}$ (i.e. a critically refracted wave-front which has apparently travelled along the solid with the transverse velocity of the solid) in addition to $P_{cr}$. It would, therefore, be desirable to have a solid medium for which this refracted transverse wave is present, and one for which it is not. After some consideration, the following selections for the solid media were made:

Case 1, $b < c$. The solid is a very high viscosity pitch with the trade designation Kopper's 85 °C ring and ball softening point pitch.

Case 2, $b > c$. The solid is plaster of paris with additives (trade designation, Halliburton's Cal-Seal type LT 60) mixed three parts powder to one part water by weight.

TABLE 1. PHYSICAL CONSTANTS MEASURED FOR CASES 1 AND 2

| | case 1 | case 2 |
|---|---|---|
| specific gravity | 1·27 | 1·89 |
| longitudinal wave velocity, $a$ (m/s) | 2463 | 3192 |
| transverse wave velocity, $b$ (m/s) | 1003 | 1814 |
| attenuation of longitudinal waves at 500 kc/s (approximate) (db/cm) | 1 | 0·6 |
| attenuation of transverse waves at 25 kc/s (approximate) (db/cm) | 0·6 | 0·2 |
| fluid compressional wave velocity, $c$ (m/s) | $1496 \pm 5$ | $1484 \pm 6$ |
| zero-time correction ($\mu$s) | $-0{\cdot}7 \pm 0{\cdot}1$ | $-1{\cdot}2 \pm 0{\cdot}2$ |

Although at low frequencies pitch behaves as a viscous fluid it can be seen from table 1 that at the frequencies involved in these experiments it behaves as an elastic solid and has, in fact, properties quite similar to those of Lucite. The value of attenuation as measured for the pitch is of the same order of magnitude as that for the plaster of paris, and indicates that losses should not be too serious at distances of the order of 10 cm.

The characteristic velocities $a$ and $b$ of cases 1 and 2 were measured by pulse techniques which are independent of the method diagrammed in figure 1, although the physical principle involved is similar. Cylindrical rods of an appropriate length, say about 10 cm, and of 2 to 3 cm diameter were cored from the solid block on which the propagation study had been made. The compressional velocity is determined by measuring the time for a longitudinal pulse to travel between a barium titanate transducer used to generate the wave at one end of the cylinder and a similar transducer used to detect the wave at the other end.

The transverse wave velocity is measured in a similar arrangement where a torsional wave

instead of a longitudinal wave is transmitted along the cylinder. The transducers used to generate this torsional wave are made by arranging eight polarized, circular sectors of barium titanate to approximate a circumferentially polarized disk. When voltage is applied between the faces of the disk there is a rotation of one face relative to the other. This twisting motion is used to generate a torsional wave in the sample and, since these are reciprocal transducers, another disk of the same type is used to detect the torsional wave. A construction similar to this has been discussed by Kennel (1955). The velocities measured by this method are reproducible to within 2 to 3 %.

Attenuation is measured by plotting the logarithm of the amplitude of the received pulse against sample length for a number of different length samples. The slope of the straight line averaging the resulting points is taken as the attenuation. Although this is not a very accurate method because the coupling varies from one sample to another, it is sufficient for determining the relative desirability of various solid materials. The frequency at which the attenuation is measured is estimated from the period of the first cycle of the observed pulse.

## 4. Pressure response determination

Referring to the experimental arrangement of figure 1, and the co-ordinate designations as shown in figure 3, we must select the source-detector distance $r$, source-interface distance $H$, and detector-interface distance $H-z$ in such as manner that the experimental and

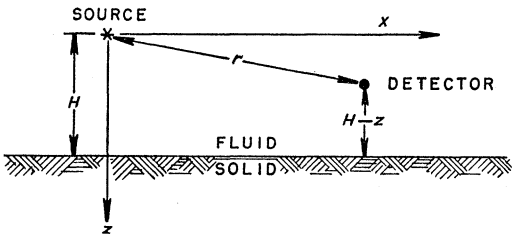


Figure 3. Co-ordinate designations.

theoretical investigations of this and the following part will describe similar uations. Since we should like to be able to attach characteristic wave-forms to those parts of the pressure response curve which follow the corresponding arriving wave-fronts, it apparent that we must select a source-detector distance which is sufficiently great that the arriving fronts are well separated in time. On the other hand, the attenuation measurements on rods of the solid media as listed in §3 are of the order of magnitude of $\frac{1}{2}$ db/cm and probably increase with frequency. This means that we cannot use too large a source-detector distance if we desire to keep losses and the consequent high-frequency attenuation from severely limiting our correlation of theory with experiment. Since the source-detector combination has a pass band from 5 to 100 kc/s and the materials used have velocities ranging from 900 to 4000 m/s, we are able to observe wavelengths in the range of 80 to 0·9 cm. Choosing the source-detector spacing ($x$) as 10 cm makes $x$ fall in the cross-over range where

$$10\lambda > x > 0{\cdot}1\lambda.$$

This cross-over region is of great interest because the most widely used theoretical techniques, i.e. the asymptotic and normal mode methods, are not accurate within this region. At 10 cm, the attenuation in plaster of paris and pitch will not be too severe, and the

initial requirement, i.e. that $x$ be sufficiently large that the events of physical interest be well separated in time, will be shown to be satisfied both by this experiment and by the theoretical analysis to follow.

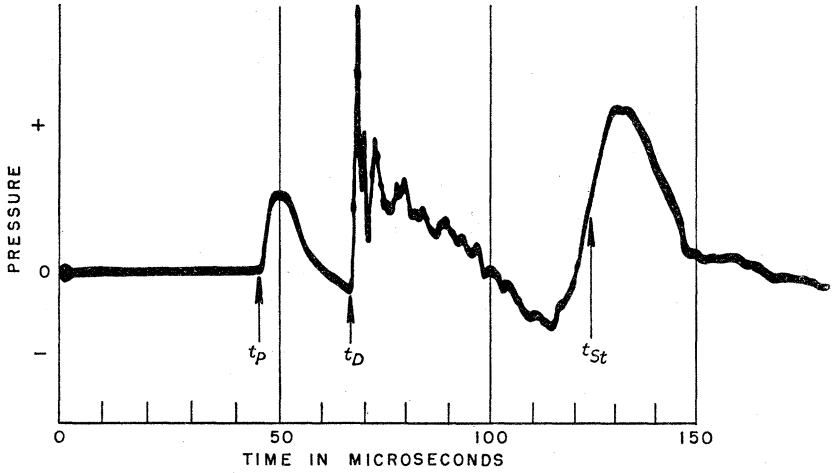


FIGURE 4. Pressure response due to water/pitch interface, $b < c$.

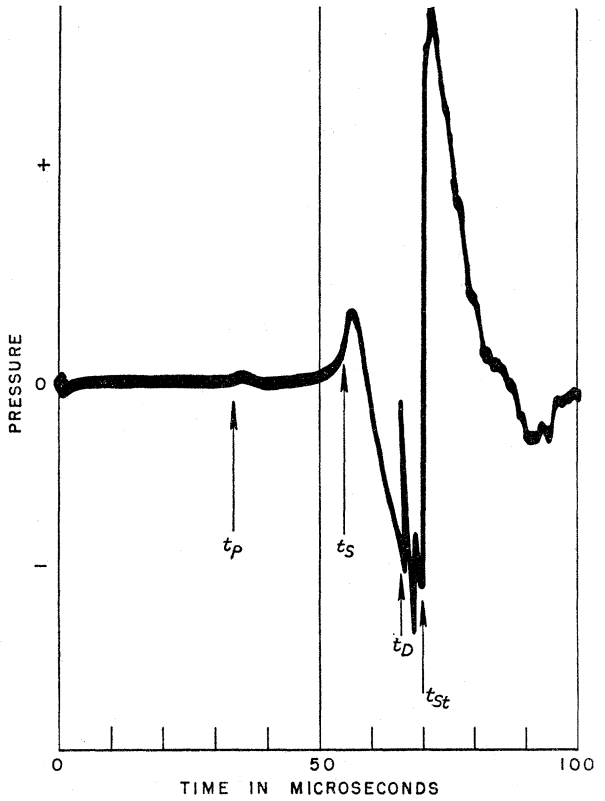


FIGURE 5. Pressure response for a spark source near a plaster of paris interface, $b > c$.

The limitations on the choice of source-interface distance $H$ and detector-interface distance $H-z$ are not as severe. Preliminary experiments indicated that the amplitude of interface waves decreased rapidly as either the source or detector or both were removed from the interface. At a distance of about 0·5 cm from the interface for both source and detector, the

amplitude of the interface wave was such that all parts of the wave-form could be observed with a single attenuation setting.

With the source and detector located at the distances stated above, the pressure response curves of figures 4 and 5 have been obtained. Figure 4 was made with pitch as the solid medium and figure 5 with plaster of paris. Shown below each curve is a time scale which has been zero-corrected in accordance with the discussion in §3.

These response curves are reproduced in figures 8 and 9 of the theoretical treatment in part II, where one notes that a close wave-form correlation exists between the experimental and theoretical solutions of the problem. In the following § (5), figures 4 and 5 of this paper will be interpreted in the light of the existing wave-front arrival time technique that has become rather standardized in recent years, and in part II, a complete wave-form analysis will be shown to answer many of the questions that cannot be treated in the arrival time analysis.

## 5. Discussion of results

### (a) *Wave-form interpretation*

In accordance with a previous statement, the interpretation of the wave-forms of figures 4 and 5 will be limited here to a discussion of the arrival times of the various wave-fronts and the surface waves. Since the water velocity is determined to $\pm 10$ m/s and the source-detector distance is measured to $\pm 1$ mm, the computed arrival time $t_D$ for the direct wave-front is immediately located to approximately $\pm 1$ $\mu$s on the response curves. The direct wave is, in both cases, a distinct arrival at the computed time characterized by high frequency and some oscillation which probably represents resonances in the detector system above 100 kc/s. The reflected wave cannot be recognized as a separate arrival in this geometry since for the 10 cm spacing and 1500 m/s velocity in the water, the time difference between the direct and reflected arrivals is only of the order of $\frac{1}{8}$ $\mu$s, which is less than the resolution of our apparatus. Since the pressure wave suffers a phase reversal upon reflexion, the net effect is to reduce the amplitude observed in the direct wave region.

The first arrival, $t_P$, on both response curves can be identified as a critically refracted wave-front from the well-known minimum travel-time formula

$$t_P = \frac{x}{a} + \frac{2H-z}{c}\sqrt{\left\{1-\left(\frac{c}{a}\right)^2\right\}}.$$

These critically refracted rays apparently travel from the source to the interface with the fluid velocity $c$ and at the critical angle $\theta = \sin^{-1}(c/a)$ for total reflexion and then along the interface, with the compressional velocity of the solid, generating a front in the fluid at the same angle of total reflexion. Application of the above minimum travel-time formula to the plaster of paris and pitch data of cases (1) and (2) in §3 yields $t_P = 35{\cdot}71$ $\mu$s for plaster of paris and $t_P = 46{\cdot}5$ $\mu$s for pitch, these values being within 1 $\mu$s of the observed arrival times of the responses in figures 4 and 5. The velocity of this arrival was determined by the usual time-distance plot for comparison with the velocity obtained from a small sample.

It is also well known that if the rotational velocity $b$, as well as the compressional velocity $a$, of the solid is greater than the fluid velocity $c$, then a second minimum time arrival can exist travelling along the solid part of the interface with the rotational velocity instead of the compressional velocity of the solid. The same minimum travel-time formula holds, except




PHILOSOPHICAL TRANSACTIONS OF THE ROYAL SOCIETY A MATHEMATICAL, PHYSICAL & ENGINEERING SCIENCES

that $a$ is replaced by $b$. Since the data of case (2) for plaster of paris are consistent with $b > c$, they can be applied to the modified travel-time formula and yield an arrival time for the front of the so-called critically refracted transverse wave of 58·3 $\mu$s. This arrival time is designated as $t_S$ on figure 5 and falls just ahead of the peak of large positive pressure response occurring before the direct wave-front arrival. The identification of this peak pressure response with that of the $S_{cr}$ wave raises a question concerning the nature of the pressure build-up occurring just before this arrival, which in a sense seems to anticipate this minimum time arrival. This and experiments on other materials, where the arrival falls still farther ahead of the peak, indicate that there is no visible 'break' on the curve that can be associated with the $S_{cr}$ wave. Therefore, in general, true shear velocities cannot be obtained from the usual time-distance plot, although in all cases examined the velocity of the pressure maximum was a good approximation to $b$.

The extremely large pressure variation which occurs after the arrival of the direct wave-front has the general appearance of a boundary wave. If we identify this part of the response as a Stoneley interface wave and insert the velocity data for plaster of paris into the Stoneley wave equation (Stoneley 1924) we arrive at a velocity of 1345 m/s for the Stoneley wave, which for an interface distance of 10 cm yields an arrival time of 74·3 $\mu$s. This is very close to the observed arrival time of a point of zero pressure amplitude in figure 5.

TABLE 2. CHARACTERISTIC VELOCITIES IN METRES/SECOND

| | rod data (§3) | profile data | average data |
|---|---|---|---|
| *case* 1 | | | |
| $b < c$ (pitch) compressional velocity $a$ | 2463 | 2470 | 2467 |
| $V_{St}$ | — | 824 | — |
| rotational velocity, $b$ | 1003 | 1008† | 1006 |
| fluid velocity, $c$ | — | 1496 | 1496 |
| *case* 2 | | | |
| $b > c$ (plaster of paris) compressional velocity, $a$ | 3192 | 3370 | 3281 |
| $V_{St}$ | — | 1365 | — |
| rotational velocity, $b$ | 1814 | 1889† | 1852 |
| fluid velocity, $c$ | — | 1484 | 1484 |

† Computed from the Stoneley wave equation using measured value of $V_{St}$.

When $c > b$, as in the pitch of case 1, the minimum travel-time formula for the $S_{cr}$ wave becomes complex and such a wave-front does not exist. However, we can make use of the measured characteristic velocities for pitch as listed in §3 and of the Stoneley wave equation to arrive at a Stoneley wave velocity of 818 m/s and a corresponding travel time of 122·2 $\mu$s for the arrival time of the zero-pressure amplitude of the Stoneley wave. This is within about 2 $\mu$s of the zero as observed on the response for pitch in figure 4. Therefore, in order to obtain a value for the rotational velocity from the profile data which can be compared with the rod data listed in §3, we can resort to the profile for the velocity $V_{St}$ of the point of symmetry of the Stoneley wave and, making use of the compressional velocities from such profile data and the previously mentioned Stoneley wave equation, we can determine the rotational velocity of the solid. Profile data obtained in this way are listed in table 2, together with the average of these values which will be used in computation of the results of the theoretical analysis of part II.

Extensive charts of the solutions of the Stoneley wave equation, which enable one to determine quickly one of the parameters, $a$, $b$, $c$, $V_{St}$, or $\rho^f/\rho^s$ when all others are known, have been prepared in this laboratory for a wide range of values of the parameters and have been published elsewhere (Strick & Ginzbarg 1956).

### 6. Conclusions

Measurements of the pressure-time history resulting from a transient point source in the vicinity of a fluid/solid interface show the arrival of a Stoneley interface wave in addition to the arrivals anticipated from simple ray path theory. This to our knowledge is the first experiment to confirm the existence of the Stoneley wave.

The measured response curves indicate that, although there is no 'sharp break' associated with the arrival of the critically refracted transverse wave, the pressure maximum occurring near this time travels with approximately the transverse wave velocity.

The velocities of the Stoneley wave (where it can be identified), the direct wave, and the critically refracted longitudinal wave may be substituted into the Stoneley wave equation to obtain a supplementary check on the transverse wave velocity. This procedure can be used regardless of whether the transverse wave velocity is greater than or less than the fluid velocity and in fact, in the latter case, is the only method of obtaining a value of transverse wave velocity from profile data.

## II. THEORETICAL PRESSURE RESPONSE

By E. STRICK

### 1. Introduction

As in the preceding, experimental part, the main purpose of this investigation is to obtain accurate pressure response curves from an impulsive point source in the vicinity of the fluid/solid interface of homogeneous isotropic elastic media. Although the procedure for obtaining the exact response to a non-periodic point source exciting a solid/solid interface was given by Cagniard (1939) as early as 1939, the complexity of his solution has up to the present time limited the applications of his method to simpler boundary-value problems such as the source located on the free boundary of a semi-infinite elastic solid. In this paper we shall call this latter problem the Lamb problem, since it was first discussed with a rather complete mathematical development by Horace Lamb (1904). Lamb considered both line and point sources on the surface having an impulse excitation. Although his results were qualitatively very good, his method was very intricate. Recently Pekeris (1955*a*) gave a solution in closed form to this Lamb problem for the case of a point pressure source with a Heaviside step excitation in the vertical stress. The Lamb problem becomes somewhat more involved if the location of the source is modified to be within the semi-infinite solid. Using the mathematically simpler line rather than point source, Nakano (1925) and Lapwood (1949) have given qualitative asymptotic solutions of this problem. Garvin (1956) and Gilbert (1956) have obtained the exact closed form solution for the same problem utilizing

the method of Cagniard, whereas Takeuchi & Kobayashi (1955) have obtained exactly the same result by means of the Fourier integral. For a point source, numerically incomplete solutions have since been given by Pinney (1954) and Pekeris (1955*b*).

## 2. Statement of the problem; technique of solution

The procedure for constructing integrals of the solutions of elastic wave boundary-value problems is closely related to the technique originally developed by Sommerfeld (1949) for solving problems of radio wave propagation. An integral representation for a periodic source alone having the form of a Fourier integral is first established and the integrand is then interpreted as a periodic elementary plane or cylindrical wave of complex propagation constant. With boundaries present, other convergent Fourier integrals are similarly constructed to account for the wave amplitudes in the various media due to the reflexion and refraction of these periodic inhomogeneous plane waves at the boundaries. A sufficient number of amplitude coefficients are introduced into these integrands to allow the boundary conditions to be satisfied. If the wave equations are also satisfied and the integrals are convergent, then the uniqueness theorem is employed to prove that this is the desired solution. In order to obtain a non-periodic from this periodic solution one can invoke the unit function integral operator (Muskat 1933; Lapwood 1949) to determine the response to a Heaviside step excitation of the source, or one can introduce the Laplace transform variable $s$ by $s = \pm i\omega$ and utilize this powerful tool as Cagniard does to avoid the double integration as required in the former method. The details of Cagniard's procedure are rigorously and elaborately discussed in his book (Cagniard 1939). Dix (1954) has recently summarized the method of Cagniard and remarks that the method appears to be particularly attractive in that it permits one to formulate an elastic wave-boundary value problem in the case of non-periodic source excitations that is free of the *a priori* assumption that steady-state solutions exist. As Dix further points out, Cagniard shows that these periodic solutions form a class from which solutions of pulse problems can be synthesized. However, even though one can in this manner formulate the problems without reference to the existence of the periodic waves, in this paper we shall adhere to the procedure of first establishing the integral for the periodic solution that satisfies both wave and boundary equations and then obtain the non-periodic solution from it. That is, by considering the coefficient of $e^{\pm i\omega t}$ with $\omega$ replaced by $\pm is$ to be the $s$-multiplied (McLachlan 1953) Laplace transform of the response to a step function excited source we can immediately go over into the Cagniard formalism. In this way we can facilitate comparison of the integral with those already established in the literature.

The desired solution of the problem of the response to a step function point source exciting a fluid/solid interface would be to evaluate Cagniard's integrals in the limit as the rotational velocity of the elastic medium in which the point source is located is made to vanish. However, the resulting evaluation would still be quite involved, and in order to simplify calculations as well as to obtain information on the effect that the geometry of the source has upon the resulting wave-form a slightly different approach was indicated. It was decided to carry out the Cagniard calculation first for the case of a delta-function-excited line source, for in this case, as in all problems involving line sources with plane parallel boundaries, the

solution can be expressed in a closed algebraic form, i.e. not requiring further integration. Then a similar calculation will be made using instead a source that closely approximates at large distances to a delta-function-excited point source, but still has the form of the previous line source representation. In this way it can be shown that at large distances the geometric difference of the two sources will not appreciably affect the wave-form of the pressure response. The close agreement of these calculations with the experimental response curves of part I will further strengthen this conclusion. As a result, it was not considered necessary to carry out the tedious Cagniard problem for the exact exponentially decaying point source.

Because our problem is in some respects almost a special case of the solid/solid interface problem treated by Cagniard, many of his arguments for solving the problem on a rigorous basis are also valid here. For this reason, our early mathematical development will be rather brief. Since the essential difference is in the nature of the source, special emphasis will be placed on its mathematical representation.

## 3. Apparatus; theoretical

### (a) *Nature of the source*

(i) *The line source*

Consider a cylindrical pressure source of radius $r_0$ immersed in an infinite fluid of velocity $c$. For a step-function excitation of the source the radially symmetric pressure response is shown in appendix 1 to have the form†

$$p_0^f(r,t;\text{step}) = \frac{P_0}{2\pi i}\int_\Omega \frac{d\omega}{\omega}\frac{H_0^{(2)}(\omega r/c)}{H_0^{(2)}(\omega r_0/c)}e^{i\omega t}. \tag{3·1}$$

Considering $(1/2\pi i)\int_\Omega (d\omega/\omega)$ as a unit function operator (Lapwood 1949) it is apparent that the periodic response to a line source is correctly given by

$$p_0^f(r,t;\,e^{i\omega t}) = P_0 \lim_{r_0\to 0}\frac{H_0^{(2)}(\omega r/c)}{H_0^{(2)}(\omega r_0/c)}e^{i\omega t} \to \tfrac{1}{2}\pi i P_0 \lim_{r_0\to 0}\frac{H_0^{(2)}(\omega r/c)}{\ln(\omega r_0/c)}e^{i\omega t}. \tag{3·2}$$

The zero-frequency singularity in (3·1) is avoided by the path of the contour $\Omega$. If the upper limit of the angular frequency $\omega$ contained in the source is such that $\omega \ll \lim_{r_0\to 0} c/r_0$, the logarithm term has the form of a slowly varying large negative number whose magnitude can be absorbed into the constant $P_0$, and we have for the simple line source

$$p_0^f(r,t;\,e^{i\omega t}) = -\tfrac{1}{2}\pi i P_0 H_0^{(2)}(\omega r/c)e^{i\omega t}. \tag{3·3}$$

In his text, Sommerfeld (1949) shows that our reduced form (3·3) of the line source does indeed represent physically an outgoing cylindrical wave at large radial distances. If we make use of the Sommerfeld representation for the Hankel function as given by

$$H_0^{(2)}\left(\frac{\omega r}{c}\right) = \frac{1}{\pi}\int_{a-i\infty}^{b+i\infty}\exp\{-i(\omega r/c)\cos w\}\,dw, \quad \text{with} \quad \begin{cases} -\pi < a < 0, \\ 0 < b < \pi, \end{cases} \tag{3·4}$$

† In this paper we have adopted the convention that the symbol which follows the semicolon in the functional parenthesis of the response variable shall describe the source excitation for which that particular response is being determined.

then upon applying the above unit function operator it is easy to show (Lapwood 1949) by elementary integration that the response to the step function excited simple line source is

$$p_0^f(r,t;\ \text{step}) = P_0 \operatorname{arc\,cosh}(ct/r)\,\mathbf{H}\{t-(r/c)\}, \tag{3·5}$$

where $\mathbf{H}(t-r/c)$ is the step function which is zero for $t<r/c$ and unity for $t>r/c$. By time differentiation we obtain the response to a delta-function excitation of the simple line source

$$p_0^f(r,t;\ \text{delta}) = \frac{c}{r}P_0\frac{\mathbf{H}\{t-(r/c)\}}{\sqrt{\{(ct/r)^2-1\}}}. \tag{3·6}$$

Now, our choice of harmonic line-source representation, as given by inserting (3·4) with $a=-\frac{1}{2}\pi$, $b=+\frac{1}{2}\pi$ into (3·3), yields

$$p_0^f(r,t;\ \mathrm{e}^{\mathrm{i}\omega t}) = \frac{1}{2\mathrm{i}}\int_{-\frac{1}{2}\pi-\mathrm{i}\infty}^{\frac{1}{2}\pi+\mathrm{i}\infty}\exp\{-\mathrm{i}(\omega r/c)\cos w\}\,\mathrm{d}w\,\mathrm{e}^{\mathrm{i}\omega t}, \tag{3·7}$$

which is not suitable as a basis for constructing integrals for the potentials which can satisfy boundary conditions on plane boundaries. A procedure which has been successfully carried

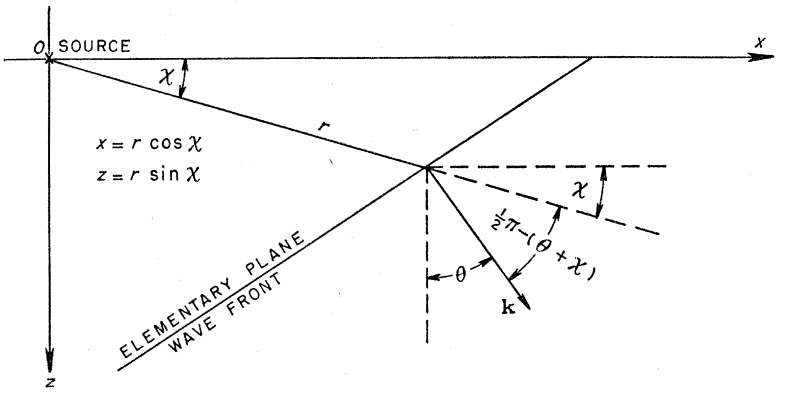


FIGURE 6. Propagation of an elementary plane wave-front in rectangular co-ordinates with $z$ axis positive downwards.

out by Lamb (1904) and Lapwood (1949) is to introduce the new integration variable [say $q=(\omega/c)\sin w$] and express the exponent in rectangular co-ordinates. An equivalent, but better physical approach is to follow to some extent the procedure of Sommerfeld (1949) in deriving the desired expression by considering the line source response to be due to the superposition in the polar co-ordinates $(r,\chi)$ of figure 6, of plane waves of propagation constant $k=\omega/c$ travelling at an angle $\theta$ with respect to the $z$ axis. The $z$ axis taken to be positive downwards is taken as the reference direction, because later in the development a plane boundary will be placed at $z=H$, and it is customary in plane wave-propagation problems to define angles of incidence with respect to the normal to the boundary. Then at the point $D$ in the fluid we have the elementary plane wave

$$p_0^f=\rho^f\omega^2\phi_0^f=P_0\exp\{-\mathrm{i}[(\omega r/c)\cos(\tfrac{1}{2}\pi-\theta-\chi)-\omega t]\}=P_0\exp\{-\mathrm{i}[(\omega r/c)\sin(\chi+\theta)-\omega t]\}, \tag{3·8}$$

which is a periodic solution to

$$\nabla^2\phi_0^f=\ddot{\phi}_0^f/c^2 \tag{3·9}$$

and corresponds to outgoing plane waves as in figure 6.

If we form the integral superposition of plane waves of this type over a range of angles of incidence $\theta$ (the use of the word incidence here will become clear when we apply this source integral to the boundary value problem of §4) as follows

$$p_0^f(r,\chi;\,e^{i\omega t}) = \frac{P_0}{2i}\int_a^b \exp\{-i(\omega/c)\,r\sin(\chi+\theta)\}\,d\theta\,e^{i\omega t}, \quad \text{where} \quad \begin{cases} -\pi < a < 0 \\ 0 < b < \pi \end{cases} \tag{3·10}$$

and permit $\theta$ to enter the complex plane, and if we also make the transformation of variable to $w = \frac{1}{2}\pi - \theta - \chi$, we arrive at a Sommerfeld type integral. Expanding the exponent $r\sin(\chi+\theta)$ and identifying as in figure 6

$$x = r\cos\chi, \quad z = r\sin\chi \tag{3·11}$$

we obtain (since the $z$ axis is positive downwards, the range $0 \leqslant \chi \leqslant \pi$ corresponds to the bottom half of figure 6 and therefore increasing $\chi$ corresponds to a clockwise rotation about the orgin of figure 6):

$$p_0^f(x,z;\,e^{i\omega t}) = \frac{P_0}{2i}\int_{-\frac{1}{2}\pi-i\infty}^{\frac{1}{2}\pi+i\infty} \exp\{-i(\omega/c)\,(z\cos\theta + x\sin\theta)\}\,d\theta\,e^{i\omega t}. \tag{3·12}$$

Although we shall confine our calculations in this paper to $0 \leqslant z \leqslant H$, i.e. to positive $z$, it is desirable that we indicate how (3·12) need be interpreted should we decide to extend our calculations to negative $z$. By definition our pressure source must be invariant to $z \to -z$. Since our line source consists of plane waves travelling away from the origin, we must simultaneously require that $\theta \to \pi - \theta$. Thus, $z\cos\theta$ and therefore $p_0^f$ is invariant to $z \to -z$. With this convention we find that the vertical component of displacement changes sign on $z \to -z$ as it should.

The form (3·12) of the integral contains the desired separation of variables in rectangular co-ordinates that will permit us to satisfy the boundary conditions at $z = H$ for all $x$. Since this is equivalent to matching the propagation constant in the $x$ direction along the interface, an algebraically simpler procedure obtained by introducing the new variable of integration $q$ by

$$q = (1/c)\sin\theta \tag{3·13}$$

is indicated. Then (3·12) becomes

$$p_0^f(x,z;\,e^{i\omega t}) = \frac{P_0}{2i}\int_{-\infty}^{+\infty} \frac{\exp\{-i\omega(qx+\Gamma z)\}}{\Gamma}\,dq\,e^{i\omega t}, \tag{3·14}$$

where

$$\Gamma = \frac{1}{c}\cos\theta = \sqrt{\left(\frac{1}{c^2} - q^2\right)}. \tag{3·15a}$$

We have implicitly assumed here that our radical (3·15$a$) has a phase zero for $|q| > 1/c$. The radical $\sqrt{\{(1/c^2) - q^2\}}$ is subject to the convergence condition

$$\mathscr{I}\sqrt{\{(1/c^2) - q^2\}} \gtreqless 0 \quad \text{for} \quad \omega \gtreqless 0. \tag{3·15b}$$

Under the transformation (3·13) the saddle points at $\theta = \pm\frac{1}{2}\pi - \chi$ are replaced by branch points at $q = \pm 1/c$. For convergence the contour passes below the branch point at $q = -1/c$ and above that at $q = +1/c$. Note that (3·14) has the desired exponential form of the Fourier integral. As was previously indicated, the transform of the response to a step function excitation of the line source is obtained from (3·14) by introducing $s = i\omega$ into the coefficient

of $e^{i\omega t}$ and then distorting the contour 90° to follow the imaginary axis. We then obtain for $s$ positive real:

$$\bar{p}_0^f(x, z; \text{step}) = \frac{P_0}{2i}\int_{-i\infty}^{+i\infty} \frac{\exp\{-s(qx+\Gamma z)\}}{\Gamma}\, dq, \tag{3·16}$$

where we now require, instead of (3·15$b$), that

$$\mathscr{R}\,\Gamma \geqslant 0.$$

In order to avoid confusion due to the fact that we are going to treat simultaneously the response to both line and point sources, and because it is customary in seismic wave-propagation problems to consider the positive $z$ direction as pointing downward into the earth, we consider the choice of co-ordinate systems for the two sources in some detail. In the line source construction which has the form given by equation (3·3), we imagine an expanding physically significant cylindrical wave of radius $r$ whose axis is normal to the plane of figure 6 and in particular to the downward $z$ direction, that is, the axis of this source lies along the $y$ axis of figure 6. In equation (3·14) we obtained an integral representation of this radially symmetric line source which could be interpreted as a superposition of non-physical (i.e. elementary) plane waves travelling along the horizontal $x$ axis and having for $q > 1/c$ an exponential decay along the $z$ axis.

(ii) *The point source*

In a discussion of the response from a harmonic point source the radially symmetric and physically significant point source function in three dimensions is decomposed into an integral sum of non-physical cylindrical waves of radius $\rho$ travelling in the horizontal $\rho$ direction and again having an exponential decay in the $z$ direction. Note that the axis of these cylindrical waves is taken to be along the $z$ axis and is therefore perpendicular to the axis of the previously discussed two-dimensional cylindrical wave from the line source. Owing to the angular symmetry of these elementary cylindrical waves, it has been shown by Sommerfeld that the integral decomposition for the point source can be expressed in the form

$$p_0^f(\rho, z; e^{i\omega t}) = \frac{P_0 \exp\{-i\omega[(R/c)-t]\}}{R} = P_0\int_0^\infty \frac{J_0(\lambda\rho)\exp[-\sqrt{\{\lambda^2-(\omega/c)^2\}}\,|z|]}{\sqrt{\{\lambda^2-(\omega/c)^2\}}}\,\lambda\, d\lambda\, e^{i\omega t}, \tag{3·17}$$

where $\mathscr{R}\sqrt{\{\lambda^2-(\omega/c)^2\}} > 0$.

Dix (1954) has shown by direct application of the Cagniard formalism to (3·17) that the transform of (3·17) does indeed lead to the response to a step-function-excited point source in an infinite medium as given by

$$p_0^f(R; \text{step}) = \frac{P_0 \mathbf{H}(t-R/c)}{R}, \tag{3·18}$$

where

$$R^2 = \rho^2 + z^2. \tag{3·19}$$

The form (3·17), however, corresponds to standing cylindrical waves in the radial direction and for this reason is physically not desirable for use in our simple interface problem.

In order to arrive at an alternate representation we introduce the new variable of integration $q$ by

$$\lambda = -isq, \tag{3·20}$$

together with $s = i\omega$ so that

$$\bar{p}_0^f(\rho, z; \text{step}) = -sP_0 \int_0^{i(\infty/s)} \frac{I_0(sq\rho) \exp(-s\Gamma|z|)}{\Gamma} q\, dq, \tag{3·21}$$

where $$\Gamma = \sqrt{\{(1/c^2) - q^2\}}$$

as in (3·15$a$). The branch cut is taken to be $(1/c, \infty)$ with phase of $\Gamma = 0$ for $q < 1/c$.

Upon transformation to the $\Gamma$ plane we obtain the branch radical

$$q = \sqrt{\{(1/c^2) - \Gamma^2\}}, \tag{3·22}$$

and (3·21) becomes

$$\bar{p}_0^f(\rho, z; \text{step}) = +sP_0 \int_{1/c}^{\infty/s} I_0(sq\rho) \exp(-s\Gamma|z|)\, d\Gamma. \tag{3·23}$$

Using the well-known relation (Watson 1952)

$$I_0(sq\rho) = \pm (i/\pi)\, [K_0(s\rho a\, e^{\pm i\pi}) - K_0(sq\rho)], \tag{3·24}$$

we find

$$\bar{p}_0^f(\rho, z; \text{step}) = \mp \frac{isP_0}{\pi} \left[ \int_{\infty/s}^{1/c} K_0(s\rho q\, e^{\pm i\pi}) \exp(-s\Gamma|z|)\, d\Gamma + \int_{1/c}^{\infty/s} K_0(s\rho q) \exp(-s\Gamma|z|)\, d\Gamma \right]. \tag{3·25}$$

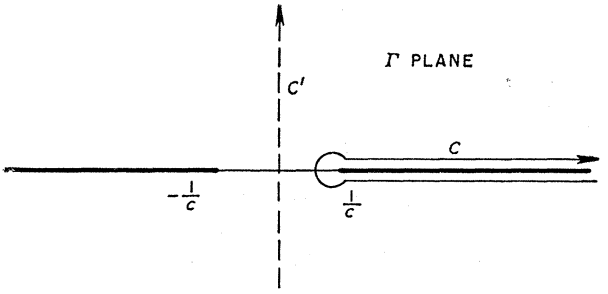


FIGURE 7. Location of the branch points and branch cut in the $\Gamma$ plane.

Just as in the $q$ plane, the radical (3·22) in the $\Gamma$ plane has phase zero to the left of the branch point at $\Gamma = 1/c$ on the real $\Gamma$ axis. The contours of both integrals in (3·25) are now taken above the branch cut from $\Gamma = 1/c$ to $\Gamma = \infty$. But since $q = \sqrt{\{(1/c^2) - \Gamma^2\}}$ has phase $-i$ above and $+i$ below the cut in the $\Gamma$ plane, it is apparent that the first integral may be set equal to one whose path is taken below the cut provided $q\, e^{i\pi}$ is replaced by $q$. We then have the single integral

$$\bar{p}_0^f(\rho, z; \text{step}) = \mp \frac{isP_0}{\pi} \int_C K_0(sq\rho)\, e^{-s\Gamma z}\, d\Gamma, \tag{3·26}$$

taken over the contour $C$ of figure 7. This contour may then be distorted into the imaginary axis $(-i\omega, 0, +i\omega)$ as is designated by $C'$ in Figure 7. Note that in accord with our established procedure, letting $s = i\omega$ and distorting the contour 90° shows (3·26) to be a Fourier integral in the $\Gamma$ plane.

Over the contour $C'$ the argument of $K_0$ is positive real. The form (3·26) for the integral representation of the step-function transform is, of course, singular for $\rho = 0$. However, this is also true of the step transform of the line source as given by (3·16).

We can now proceed to apply the method of Cagniard to show that the integral (3·26) also reduces to (3·18). This proof is given in appendix 3, where it is apparent that the major

portion of the proof consists of elementary algebraic transformation of real variables of real integrals, and it is not necessary, as in the case of the point source, to make the second transformation of variable back into the $q$ plane in order to obtain the solution (3·18) for $\rho \neq 0$. For $\rho \to 0$ it can easily be shown that the integral (3·26) converges if we do not perform the limiting process until after the integration is carried out. When (3·26) is used in boundary value problems involving layered media, the integral representations within the layered media will involve the modified Bessel function $I_0$ instead of $K_0$, which is well behaved for $\rho \to 0$. This follows since with $s = \mathrm{i}\omega$, the $K_0$ in (3·26) goes into $H_0^2$ with positive argument corresponding to only outgoing cylindrical waves from the source, whereas $I_0$ goes into $J_0$ with its corresponding standing wave interpretation.

Although we have stated that it is not necessary to make a transformation of variable back into the $q$ plane in order to reduce (3·26) to (3·18), it is desirable to work in the $q$ plane if we are to obtain a relation between the point source and line source responses. The transition to the $q$ plane is most simply carried out by applying (3·22) to (3·26) obtaining

$$\bar{p}_0^f(\rho, z; \text{step}) = \mp \frac{\mathrm{i}sP_0}{\pi} \int_{\infty,\, 1/c,\, \infty} K_0(sq\rho) \exp(-s\Gamma|z|) \frac{q}{\Gamma} \mathrm{d}q, \tag{3·27}$$

where the contour of integration which surrounds the branch cut from $q = 1/c$ to $q = \infty$ can easily be distorted to $[-\mathrm{i}(\infty/s), \mathrm{i}(\infty/s)]$. For large values of the argument, the well-known asymptotic expansion is valid,

$$K_0(sq\rho) = \mp \sqrt{\left(\frac{\pi}{2sq\rho}\right)} \mathrm{e}^{-sq\rho} \left[1 - \frac{1}{8sq\rho} + \ldots\right]. \tag{3·28}$$

Considering only the first term which is good for large $\rho$ such that

$$\rho \gg \left|\frac{1}{8sq}\right| \quad \text{or} \quad \rho \gg \left|\frac{1}{8\omega q}\right|, \tag{3·29}$$

the following approximation is obtained

$$\bar{p}_0^f(\rho, z; \text{step}) = \mp \mathrm{i}P_0 \sqrt{\left(\frac{s}{2\pi\rho}\right)} \int_{-\mathrm{i}\infty/s}^{+\mathrm{i}\infty/s} \frac{q^{\frac{1}{2}}}{\Gamma} \exp(-sq\rho - s\Gamma|z|)\, \mathrm{d}q, \tag{3·30}$$

which for $s = \mathrm{i}\omega$ becomes a Fourier integral in the $q$ plane.

Comparing (3·30) for the transform of the response to a step-excited point source with the corresponding relation (3·16) for the line source it is apparent that one can obtain (3·30) from (3·16) by merely replacing $x$ by $\rho$ and multiplying by the factor

$$-\left[\frac{2}{\pi} \frac{sq}{\rho}\right]^{\frac{1}{2}}. \tag{3·31}$$

In a comparison of point and line source responses, the existence of the factor $\rho^{-\frac{1}{2}}$ in (3·31) is to be expected. The factor $q^{\frac{1}{2}}$ is a very slowly varying quantity; for our simple interface problem where the major contributions come from $q$ essentially between $1/a$ and $3/c$, we can easily neglect it. However, retaining this term will not complicate the calculations appreciably. The expression (3·30) contains an absolute value sign on the co-ordinate $z$ which is not present in (3·16). Sommerfeld introduced this modification in order that his integral would be invariant to $z \to -z$. Sommerfeld did not, however, attempt to retain the identification of his variable of integration as an angle of incidence with respect to a later appearing

boundary and consequently did not require that $\Gamma \to -\Gamma$ as $z \to -z$. Since we are making our calculations only for positive $z$, we need not concern ourselves with any further modification due to the existence of this absolute value symbol. The remaining factor $s^{\frac{1}{2}}$ will require some discussion.

There are two ways we can deal with this factor $s^{\frac{1}{2}}$ which corresponds operationally to half-order differentiation. The first way is to make use of the product theorem for $s$-multiplied Laplace transforms to arrive at an exact interpretation of our first-order response as given by (3·30). This approach is discussed in appendix 4 and will not be used here. The second and much simpler approach is to reason along the following lines. If the factor $s^{\frac{1}{2}}$ were not present, then just as in appendix 2 the method of Cagniard would naturally lead to the response to a delta-function excitation of the source. On the other hand, if a factor $s$ instead of $s^{\frac{1}{2}}$ were present in (3·30), then in order to avoid a final time integration we would be naturally led to interpret the response as being due to a step function excitation of the source. Therefore, since $s^{\frac{1}{2}}$ lies between these two extremes, we should expect (3·30) to correspond to the response to an excitation which lies somewhere between that of a step function and a delta function. Thus the response to a point source with such an intermediate excitation should resemble the response due to a delta-function-excited line source.

In many seismological problems many investigators go to great labour to set up the response to a point source and using asymptotic methods are not able to obtain very accurate results. Since the excitation of the wave-form of an earthquake is not known, it is just as well to assume the above intermediate excitation instead of a delta or step. Then use can be made of the rigorous line-source calculations to obtain a response which at large radial distances although only an approximation in a quantitative sense shows all essential features of the response in the proper time scale. In this paper, for a comparison with experimental results for point sources, we shall make use of the approximation obtained by dropping the factor $s^{\frac{1}{2}}$, realizing at the same time that our resulting wave-form will be incorrect by an amount corresponding to a half-order time integration of the response to a delta-function-excited source. In §4 we shall see that this approximation leads to a surprisingly good agreement between the theoretical and experimental results.

### (*b*) *Nature of the detector*

For a step- or delta-function excitation of the pressure source, closed form solutions of the response (i.e. not requiring further time integration or differentiation) exist for only certain physically significant response variables. In particular, for a step-function excitation of the line source such a closed-form solution would appear for a particle acceleration detector. On the other hand, a delta-function-excitation of the same source would lead to closed-form solutions for both pressure and particle velocity detectors. Although we shall initially construct the transform of the response to a step-function excitation of the source, owing to our utilization of the $s$-multiplied Laplace transform the inversion of this transform will lead directly to closed-form expressions for pressure and particle velocity responses to a delta-function excitation of the line source. This interpretation as the response to a delta-function excitation is desirable, because after some high-frequency filtering such a response as (3·6) would roughly resemble an exponential decay or the excitation utilized in the experiment in part I.





PHILOSOPHICAL TRANSACTIONS OF THE ROYAL SOCIETY A MATHEMATICAL, PHYSICAL & ENGINEERING SCIENCES

### (*c*) *Nature of the fluid and solid media*

In our study of elastic wave propagation, both fluid and solid media are assumed to be homogeneous and isotropic. The customary equations of motion and boundary conditions are valid; that is, in two dimensions we have:

(1) For the fluid with the displacement potential $\phi^f$ defined by displacement

$$(U^f, W^f) = \operatorname{grad} \phi^f, \tag{3·32}$$

the wave equation

$$\nabla^2 \phi^f - \frac{1}{c^2} \frac{\partial^2 \phi^f}{\partial t^2} = 0, \tag{3·33}$$

where $c$ is the sound velocity of the fluid, i.e.

$$c = \sqrt{(\lambda^f / \rho^f)}. \tag{3·34}$$

The fluid pressure is obtained from the displacement potential by

$$p^f = -\sigma^f = -\rho^f (\partial^2 \phi^f / \partial t^2). \tag{3·35}$$

(2) Similarly, for the solid we have in two dimensions in terms of the displacement potentials $\phi^s$ and $\psi^s$ defined by

$$U^s = \frac{\partial \phi^s}{\partial x} + \frac{\partial \psi^s}{\partial z}, \quad W^s = \frac{\partial \phi^s}{\partial z} - \frac{\partial \psi^s}{\partial x}, \tag{3·36}$$

the wave equations

$$\nabla^2 \phi^s = \frac{1}{a^2} \frac{\partial^2 \phi^s}{\partial t^2} \quad \text{and} \quad \nabla^2 \psi^s = \frac{1}{b^2} \frac{\partial^2 \psi^s}{\partial t^2}, \tag{3·37}$$

where $a$ and $b$ are the compressional and shear (rotational) velocities, respectively, of the solid and are given by

$$a = \left[\frac{\lambda^s + 2\mu^s}{\rho^s}\right]^{\frac{1}{2}} \quad \text{and} \quad b = \left[\frac{\mu^s}{\rho^s}\right]^{\frac{1}{2}}. \tag{3·38}$$

The solid stresses are obtained from

$$\sigma^s_{zz} = \rho^s \left[\left(1 - 2\frac{b^2}{a^2}\right) \frac{\partial^2 \phi^2}{\partial t^2} + 2b^2 \left(\frac{\partial^2 \phi^s}{\partial z^2} - \frac{\partial^2 \psi^s}{\partial x \partial z}\right)\right], \tag{3·39}$$

$$\sigma^s_{xz} = \rho^s \left[\frac{\partial^2 \psi^s}{\partial t^2} + 2b^2 \left(\frac{\partial^2 \phi^s}{\partial x \partial z} - \frac{\partial^2 \psi^s}{\partial x^2}\right)\right]. \tag{3·40}$$

The expressions for the wave equations and boundary conditions for use with the point source in three dimensions can be found in Cagniard (1939). For their application to the fluid/solid interface problem we can refer to the thesis by Spencer (1956). The numerical evaluation of the exact solution of the transient excitation of the fluid/solid interface by a point source for points off the normal to the interface passing through the source would be too laborious to attempt at the present time; therefore, in accord with our approximate development in § 3 (*a*) we are going to proceed under the assumption that since the response in an infinite fluid is alike for both point and line sources the responses will remain alike (under the assumptions of § 3 (*a*)) when a solid boundary is present. Under this assumption it will not be necessary to make use of the three-dimensional equations and so the following pressure-response determination will be devoted solely to the exact two-dimensional problem.

## 4. Pressure response determination

The displacement potential due to a line source in an infinite fluid is by (3·14) and (3·35)

$$\phi_0^f(x,z;\mathrm{e}^{\mathrm{i}\omega t}) = Q_0\int_{-\infty}^{+\infty}\frac{\exp\{-\mathrm{i}\omega(\Gamma z+qx)\}}{\Gamma}\,\mathrm{d}q\,\mathrm{e}^{\mathrm{i}\omega t}, \tag{4·1}$$

where $\Gamma$ is defined by (3·15) and $$Q_0 = \frac{P_0}{2\mathrm{i}\rho^f\omega^2}. \tag{4·2}$$

When a fluid/solid interface is present at $z = H$, one has the modification of figure 6 as shown in figure 8. The additive potential $\phi_1^f$ due to a superposition of elementary plane waves reflected from the interface and solid potentials $\phi^s$, $\psi^s$ due to refraction into the solid are constructed with (4·1) as a model as follows. For $\phi_1^f$, in order to construct a source function at the image location one need simply replace $z$ in (4·1) by $2H-z$ and insert a reflexion

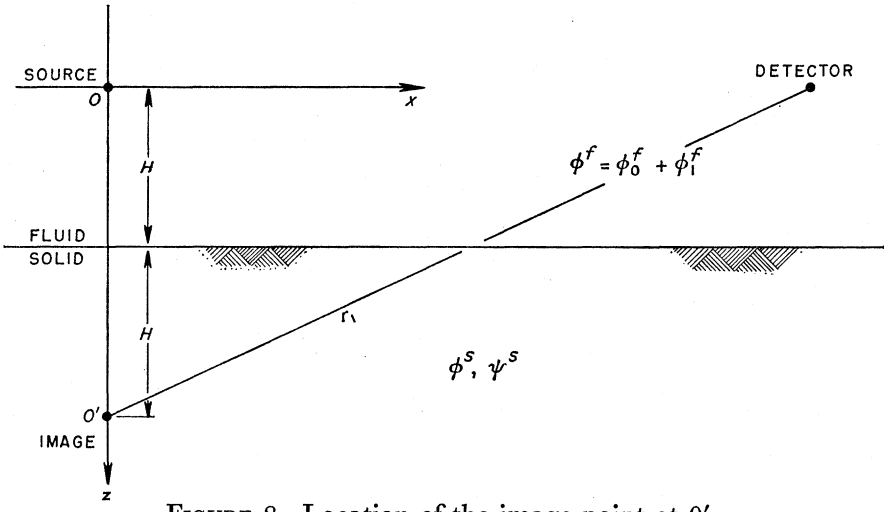


Figure 8. Location of the image point at 0′.

coefficient $A(q)$ into the integrand. For $\phi^s$ the term $\Gamma z$ in the exponent is replaced by $\sqrt{\{(1/a^2)-q^2\}}z$ and the transmission coefficient $B(q)$ incorporated into the integrand. Just as in (3·15$b$) we must have $$\mathscr{I}\sqrt{\{(1/a^2)-q^2\}} \lesseqgtr 0 \quad \text{for} \quad \omega \gtreqless 0. \tag{4·3$a$}$$

Similarly, $\psi^s$ is constructed by replacing $\Gamma z$ by $\sqrt{\{(1/b^2)-q^2\}}z$ with $C(q)$ as the undetermined coefficient. Also $$\mathscr{I}\sqrt{\{(1/b^2)-q^2\}} \lesseqgtr 0 \quad \text{for} \quad \omega \gtreqless 0. \tag{4·3$b$}$$

In this way we have constructed the set of potentials

$$\phi_1^f(x,z;\mathrm{e}^{\mathrm{i}\omega t}) = Q_0\int_{-\infty}^{+\infty}\frac{A(q)\exp\{-\mathrm{i}\omega[\Gamma(2H-z)+qx]\}}{\Gamma}\,\mathrm{d}q\,\mathrm{e}^{\mathrm{i}\omega t}, \tag{4·4$a$}$$

$$\phi^s(x,z;\mathrm{e}^{\mathrm{i}\omega t}) = Q_0\int_{-\infty}^{+\infty}\frac{B(q)\exp\left(-\mathrm{i}\omega[\sqrt{\{(1/a^2)-q^2\}}z+qx]\right)}{\Gamma}\,\mathrm{d}q\,\mathrm{e}^{\mathrm{i}\omega t}, \tag{4·4$b$}$$

$$\psi^s(x,z;\mathrm{e}^{\mathrm{i}\omega t}) = Q_0\int_{-\infty}^{+\infty}\frac{C(q)\exp\left(-\mathrm{i}\omega[\sqrt{\{(1/b^2)-q^2\}}z+qx]\right)}{\Gamma}\,\mathrm{d}q\,\mathrm{e}^{\mathrm{i}\omega t}, \tag{4·4$c$}$$

where the coefficients $A$, $B$ and $C$ are determined in the usual manner from the three conditions that the normal stress $\sigma_{zz}$ and normal displacement $w$ be continuous and the tangential stress $\sigma_{zz}$ vanish at the interface at $z = H$ for all $x$.

For our purposes, only the determination of the reflexion coefficient $A(q)$ is necessary, and since the algebraic manipulation is identical to that in the derivation of the well-known reflexion coefficient for plane waves impinging upon a fluid/solid interface, only the final result will be given, i.e.

$$A(q) = \Gamma g(q) - \frac{\rho^f}{\rho^s}\sqrt{\left(\frac{1}{a^2}-q^2\right)} \Big/ \Gamma g(q) + \frac{\rho^f}{\rho^s}\sqrt{\left(\frac{1}{a^2}-q^2\right)}, \tag{4·5}$$

where
$$g(q) = (1-2b^2q^2)^2 + 4b^4q^2\sqrt{\left\{\left(\frac{1}{a^2}-q^2\right)\left(\frac{1}{b^2}-q^2\right)\right\}}, \tag{4·6}$$

whose vanishing yields $q = 1/V_R$, i.e. the reciprocal of the Rayleigh wave velocity $V_R$ for a free boundary semi-infinite elastic solid.

Hence, at any point $(x, z)$ in the fluid the harmonic pressure response is given by

$$p^f = p_0^f + p_1^f, \tag{4·7}$$

with
$$p_1^f(x, z; e^{i\omega t}) = \frac{P_0}{2i}\int_{-\infty}^{+\infty}\frac{A(q)}{\Gamma}\exp\{-i\omega[\Gamma(2H-z)+qx]+i\omega t\}\,dq, \tag{4·8}$$

and $p_0^f$ is given by (3·14).

In order to obtain a non-dimensional form for further calculation let us introduce the new integration variable $u$ by

$$u = cq, \tag{4·9}$$

so that according to (3·13) the variable $u$ is simply the sine of the angle that the propagation vector of the elementary plane waves makes with the normal to the fluid/solid interface. Then $A(q)$ can be re-expressed as

$$A(u) = \frac{N(u)}{D(u)} = \frac{\gamma f(u) - (\rho^f/\rho^s)\,K_2^4\alpha}{\gamma f(u) + (\rho^f/\rho^s)\,K_2^4\alpha}, \tag{4·10}$$

where
$$f(u) = (K_2^2-2u^2)^2 + 4u^2\alpha\beta, \tag{4·11}$$

and we have introduced

$$K_1 = \frac{c}{a},\quad K_2 = \frac{c}{b},\quad \alpha = \sqrt{(K_1^2-u^2)},\quad \beta = \sqrt{(K_2^2-u^2)},\quad \chi = c\Gamma = \sqrt{(1-u^2)}. \tag{4·12}$$

The reflected part of $p_1^f$ of the pressure response becomes in the $u$ plane

$$p_1^f(x, z; e^{i\omega t}) = \frac{P_0}{2i}\int_{-\infty}^{+\infty}\frac{A(u)}{\gamma}\exp\{-i(\omega/c)\,(ux+\gamma z)\}\,du\,e^{i\omega t}. \tag{4·13}$$

At this point it is convenient to introduce the $s$-multiplied Laplace transform by considering the coefficient of $e^{i\omega t}$ in (4·13) with $s = i\omega$ to be the transform of the reflected part of the response to a step-function excitation of the source. At the same time it is convenient to rotate the path of integration to the imaginary axis as designated by $C$ in figure 9.

$$\bar{p}_1^f(x, z; \text{step}) = \frac{P_0}{2i}\int_{-\infty}^{+\infty}\frac{A(u)}{\gamma}e^{-s\tau}\,du, \tag{4·14}$$

with
$$\tau = u\frac{x}{c} + \gamma\frac{2H-z}{c}. \tag{4·15}$$

Another distortion of the contour of interest is that designated $C'$ which surrounds the cuts on the positive real $u$ axis.

In order to co-ordinate this theoretical development with the experimental discussion of part I, we shall carry along separate numerical investigations as in figure 9 for the pitch and plaster of paris solids. Theoretically, the division into cases 1 and 2 is made according to the possible existence of a critically refracted $S$ wave. Thus, case 2 is defined by the requirement that the critically refracted $S$ wave arrive before the reflected spherical wave-front, i.e. that $b > (r_1/x)\,c$. This condition is not exactly the same as the $b > c$ condition of part I, but for $x = 10\ (2H-z)$ as assumed in the experimental work it follows that $r_1/x = 1{\cdot}005$ and the difference between the two conditions is not important here.

Since we shall carry along exact theoretical curves for pitch and retarded plaster of paris, the necessary parameters† reproduced from part I are listed in table 3 ($x = 10\ (2H-z)$ in both cases).

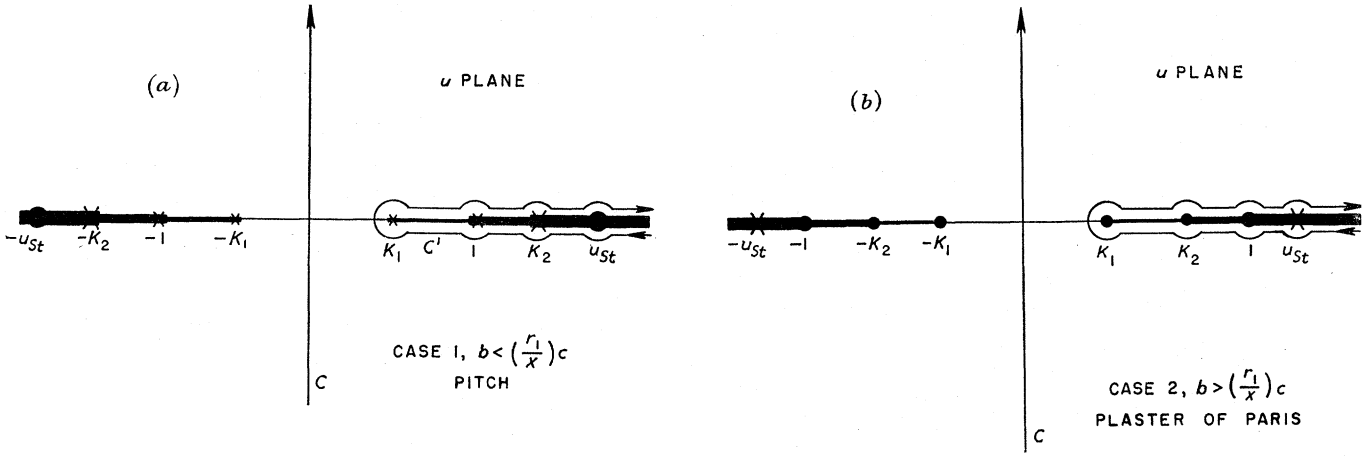


FIGURE 9. Contour for integral (4·14).

TABLE 3. VELOCITY AND SPECIFIC GRAVITY DATA FOR PITCH AND PLASTER OF PARIS

| case 1, pitch, | case 2, plaster of paris, |
|---|---|
| $\sigma = 0{\cdot}401$ | $\sigma = 0{\cdot}275$ |
| $K_1 = 0{\cdot}6144$ | $K_1 = 0{\cdot}4401$ |
| $K_2 = 1{\cdot}497$ | $K_2 = 0{\cdot}8052$ |
| $u_R = c/V_R = 1{\cdot}588$ | $u_R = c/V_R = 0{\cdot}8714$ |
| $\rho^f/\rho^s = 0{\cdot}787$ | $\rho^f/\rho^s = 0{\cdot}524$ |
| $c = 1501$ m/s | $c = 1484$ m/s |

The integrand of (4·14) contains branch points at $\pm K_1$, $\pm K_2$, and $\pm 1$, and simple poles $\pm u_{St}$ on the axis as determined by the vanishing of the denominator of the integrand. These latter poles give rise to Stoneley interface waves for the fluid/solid system.

Just as in the development of the source problems in § 3, figure 7, we here find it desirable to choose our branch cuts along the real $u$ axis from the branch points to infinity. The phases of the radicals $\alpha$ and $\beta$ are like $\gamma$ chosen to be zero in between the pairs of the respective

† The parameters of table 3 do not agree exactly with those of table 2 of part I, but except for the compressional velocity of plaster of paris they are in better than 1% agreement. The exception corresponds to profile rather than average data. Owing to various factors such as ageing of the solid material it was frequently necessary to modify the experimentally measured velocities and it was not convenient to modify so frequently the theoretical computations.

branch points at $\pm K_1$, $\pm K_2$ and $\pm 1$. This implies a phase $-$i above and $+$i below the respective cuts on the positive real $\tau$ axis. This range of phase will define the upper Riemann sheets for all radicals. In this convention the phase $-$i will be on the upper sheet.

The existence of a pole in $A(U)$ for the fluid/solid interface yielding a Stoneley-type interface wave has been known (Scholte 1948) for some time. Sato (1954) has discussed some of the harmonic properties of this interface wave, and extensive tabulated data have been prepared by Strick & Ginzbarg (1956). Referring to these latter tables we find that $u_{St} = c/V_{St} = 1{\cdot}830$ for pitch and $u_{St} = c/V_{St} = 1{\cdot}092$ for plaster of paris.

It is also important for our theoretical development to know that no other poles in $A(U)$ other than the above Stoneley pole and its negative exist on the top Riemann sheet as defined above. Cagniard (1939) has shown that only a single Stoneley pole and its negative exist for a solid/solid interface, and Spencer (1956) has carried out a similar analysis with similar results for our fluid/solid interface. However, these investigations were carried out under the assumption of the branch cuts directly joining the respective positive with negative branch points whereas our cuts proceed from the branch points to infinity. Consequently, our choice of the top Riemann sheet differs from that selected by Cagniard and Spencer, and as a result it is necessary to carry out an analogous proof for our investigation. This is shown in appendix 5 with numerical curves for pitch and plaster of paris. The generalization to an arbitrary solid follows just as in the afore-mentioned papers.

Following Cagniard we next consider (4·15) as a transformation of variable from the $u$ plane to the $\tau$ plane after which the positive real value of the complex variable $\tau$ can be interpreted as the time variable $t$.

The branch points at $K_1$ and $K_2$ go over by (4·15) directly into $t_P$ and $t_S$, respectively, where

$$t_P = K_1\frac{x}{c}+\frac{2H-z}{c}\sqrt{(1-K_1^2)}, \quad t_S = K_2\frac{x}{c}+\frac{2H-z}{c}\sqrt{(1-K_2^2)}. \tag{4·16a, b}$$

We can easily invert (4·15) to obtain $u$ as a function of $\tau$, i.e.

$$u = u(\tau) = \sin\theta = \frac{c\tau}{r_1}\frac{x}{r_1}-\frac{2H-z}{r_1}\delta, \tag{4·17}$$

where
$$\delta = \sqrt{\{1-(c\tau/r_1)^2\}}, \tag{4·18a}$$

and where
$$r_1 = \sqrt{\{x^2+(2H-z)^2\}} \tag{4·18b}$$

is the image-detector distance. Also

$$\alpha_\tau = \sqrt{(K_1^2-u^2)}\big|_{u=u(\tau)} \quad \text{and} \quad \beta_\tau = \sqrt{(K_2^2-u^2)}\big|_{u=u(\tau)}, \tag{4·18c, d}$$

where $u = u(\tau)$ is an abbreviation for (4·17).

The branch point at $u = 1$ associated with the radical $\gamma$ disappears in the transformation (4·15), being replaced by $\tau = r_1/c$ in the radical $\delta$. For $\gamma$ it follows that

$$\gamma = \sqrt{(1-u^2)} = \cos\theta = \frac{c\tau}{r_1}\frac{2H-z}{r_1}+\frac{x}{r_1}\delta, \tag{4·19}$$

and
$$\frac{\mathrm{d}u}{\gamma} = \frac{c}{r_1}\frac{\mathrm{d}\tau}{\delta}. \tag{4·20}$$

A sign ambiguity in $\delta$ appearing in equation (4·18$a$) due to the algebraic inversion of (4·15) has been resolved by the convergence requirements $\mathscr{R}\gamma \geqslant 0$ applied to (4·19). Thus, $\delta$ has phase zero for $\tau < r_1/c$.

Finally, in the $\tau$ plane the integral (4·14) takes on the form

$$p_1^f(x, z; \text{step}) = \frac{P_0 c}{2\mathrm{i} r_1} \int_{c_t} \frac{A(u)|_{u=u(\tau)}}{\delta} \mathrm{e}^{-s\tau}\, \mathrm{d}\tau, \tag{4·21}$$

where $u(\tau)$ is given by (4·17).

Numerical values of the branch points and poles as they appear in the right half of the $\tau$ plane are listed below in table 4 for cases 1 and 2.

TABLE 4. NUMERICAL VALUES OF BRANCH POINTS AND POLES IN THE $\tau$ PLANE IN MICROSECONDS

| | case 1, pitch | case 2, plaster of paris |
|---|---|---|
| $t_P$ | 44·64 | 35·71 |
| $t_S$ | 99·73 − i7·42 | 58·26 |
| $\tau_{1/c}$ | 66·96 | 67·72 |
| $\tau_{St}$ | 121·93 − i10·21 | 73·58 − i2·96 |

The contours $C$ and $C'$ obtained respectively from $C$ and $C'$ of figure 9 are shown in figure 10. Considering the transformation $C$ to $C_\tau$ first we note that $C_\tau$ is the same curve for both cases 1 and 2 if one assumes the same fluid velocity for both cases, since the transformation (4·15) is independent of the parameters of the solid. $C_\tau$ crosses the $t$ axis at $t = 3H - z/c$. The contour curves away from the imaginary axis for large $\tau$.

The transition from $C'$ to $C'_\tau$ is somewhat more complicated than that from $C$ to $C_\tau$. For $u < x/r_1$ the contour $C'$ which hugs the cuts in the $u$ plane transforms into a portion of $C'_\tau$ which similarly hugs the cuts in the $\tau$ plane up to $\tau = r_1/c$. Then, as $u$ proceeds in a semicircle about $u = x/r_1$ in a direction of increasing positive real $u$, the contours in the $\tau$ plane loop about branch point at $t = r_1/c$ crossing the cut for the radical $\delta$, thereby entering the lower sheet of this radical.† As $u$ proceeds further from $x/r_1$ to 1, the contour in the $\tau$ plane still hugging the cuts travels along the $t$ axis towards the origin from $t = r_1/c$ to $t = x/c$ still on the lower $\delta$ sheet. Then, as $u$ goes through a semicircle about $u = 1$, $\tau$ travels through an infinitesimal arc away from the real $t$ axis. Increasing $u$ above 1 takes $\tau$ farther away from the real $t$ axis on the bottom $\delta$ sheet in the manner of the dotted lines of figure 10.

A detail of contour $C'_\tau$ for plaster of paris of case 2 with a choice of $x = 2(2H - z)$ instead of $x = 10(2H - z)$ is shown in figure 11. The point $u = x/r_1$ now occurs at 0·895 instead of 0·995 and is now sufficiently removed from $u = 1$ to allow a corresponding separation of $r_1/c$ from $x/c$ in the $\tau$ plane. For $x$ equal to 10 cm we find, using data from table 3, that the path above the positive real axis in $(K_2, \infty)$ (shown in the upper part of figure 11) is mapped into the path shown in the bottom of figure 11. The corresponding part of the contour $C'$ in the $u$ plane that travels below the cuts transforms into the mirror image about the $t$ axis of that shown above for the above cut transformation. The locations of the points on the contours in the complex $\tau$ plane for $C'$ above the cut are complex conjugate to those below the cut.

† The complete specification of a Riemann sheet requires that we state the phase of all three radicals. However, in order to simplify notation here and elsewhere in this paper we shall adopt the understanding that unless there is a statement to the contrary, the phase of the unmentioned radicals will refer to their upper sheets.

Referring back to our discussion of the transformation of the unprimed contour $C$ to $C_\tau$ which showed a tendency to enclose the $t$ axis of the $\tau$ plane, we observe that the transformation of the primed contour $C'$ into the $\tau$ plane not only retains enclosure of the area on the top $\alpha$ and $\beta$ sheets exterior to the positive real $t$ axis, but also gathers in a portion of the

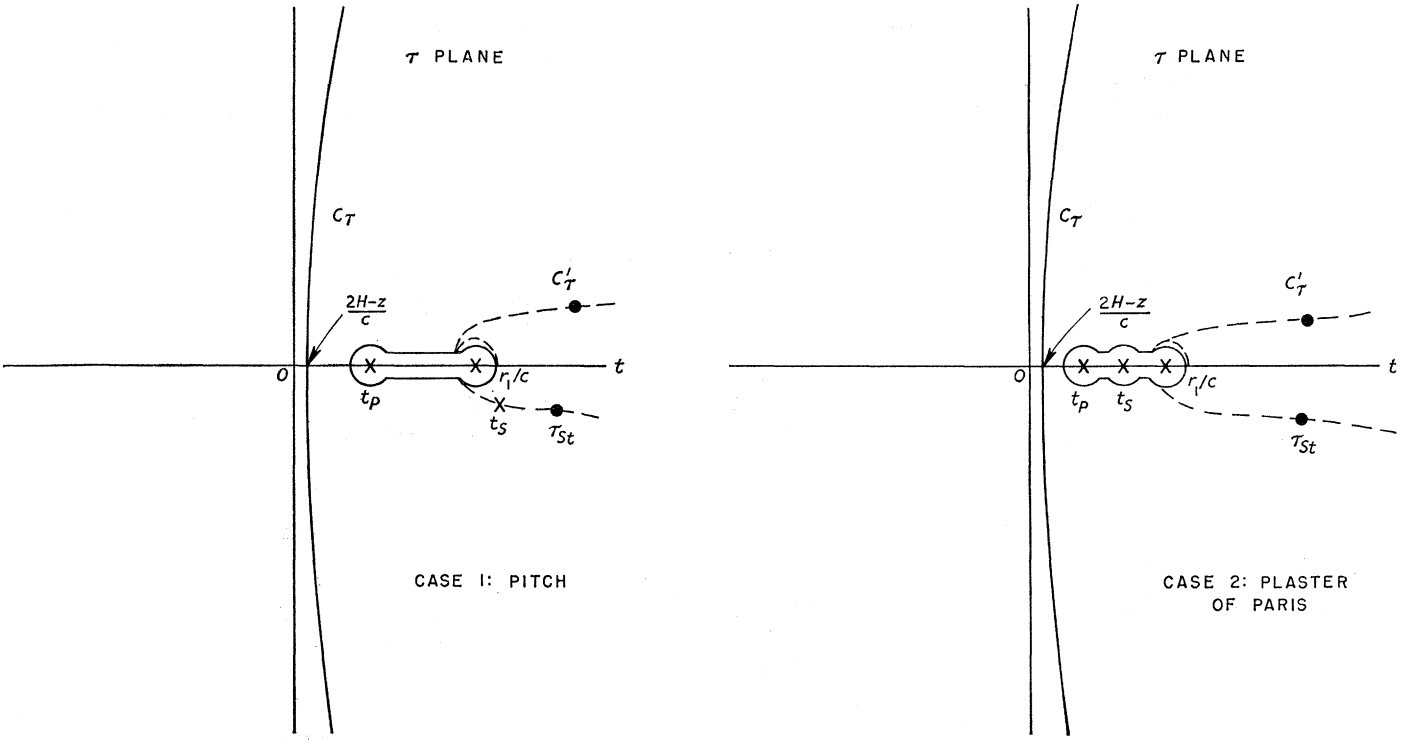


FIGURE 10. Contours and branch cuts in the $\tau$ plane (not to scale).

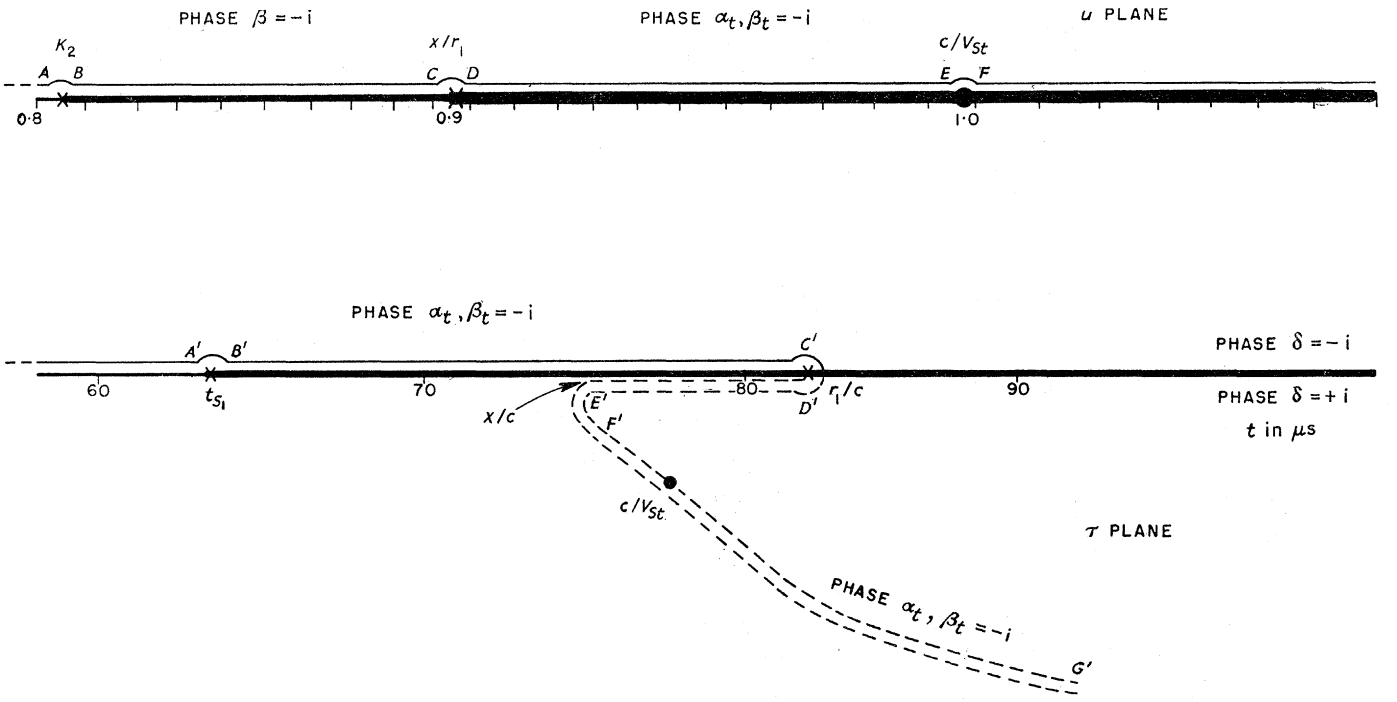


FIGURE 11. Detail of figure 10*b* with $x = 2(2H-z) = 10$ cm (not to scale).

area on the lower $\delta$ sheet on both sides of the axis. In order to see this double overlapping effect a little better, let us consider the phase behaviour of the radical $\alpha_\tau$ as we follow a complete circle of finite radius centred at $\tau = \tau_P$ on the top sheet defined by that radical having a phase in the range $-\mathrm{i}$ to $+\mathrm{i}$. Starting at the point in the $\tau$ plane designated $G'$, where the phase of $\alpha_\tau$ is $-\mathrm{i}$ and proceeding in a counterclockwise fashion to the right of the branch point of $\delta$ at $t = r_1/c$ we note that the area between the curve $D'E'F'G'$ and the cut for the radical $\delta$ is on the lower $\delta$ sheet. As our loop crosses the $\delta$ cut, where $\alpha_\tau$ has a phase in its fourth quadrant, it comes to the top $\delta$ sheet. We now follow a complete rotation of $2\pi$ about the $\alpha_\tau$ branch point in the $\tau$ plane during which, because of (4·15), the phase change of $\alpha_\tau$ is less than $\pi$. During this rotation the loop does not pass through the point $G'$ (which is on the lower $\gamma$ sheet) from which it started, but instead passes just above it on the top $\gamma$ sheet. In a similar vein it does not cross the cuts for $\alpha_\tau$ and $\beta_\tau$ since they are also here on the lower $\gamma$ sheet. Continuing on across the positive real $t$ axis the loop goes back down into the lower $\gamma$ sheet where the phase of $\alpha_\tau$ is now in its first quadrant. Finally, when the point in the $\tau$ plane which is complex conjugate to $G'$ is reached, the phase loop of $\alpha_\tau$ from $-\mathrm{i}$ to $+\mathrm{i}$ is completed.

In appendix 5 it is shown the existence of only one pair of poles, i.e. $\pm c/v_{St}$, on the top Riemann sheet of the $u$ plane, and since $\tau$ is a single-valued function of $u$ on these overlap regions on the lower sheet, there can be no other poles on these overlap regions other than the Stoneley pole. Therefore, the half of the $C'_\tau$ contour as illustrated in figure 11*b* can be distorted to follow just above the positive real $t$ axis now being wholly on the top $\alpha_\tau$, $\beta_\tau$ and $\delta$ sheets. Along this path to the right of $t = r_1/c$ the phases $\alpha_\tau$ and $\beta_\tau$ are in their fourth quadrants, whereas $\delta$ is of course always $-\mathrm{i}$. Similarly, the other half of the contour $C'_\tau$, which is complex conjugate to the half which we have just distorted, can also be distorted downward where it will come to the top sheets on the lower side of the $\delta$ cut on the $t$ axis. The phases of $\alpha_\tau$ and $\beta_\tau$ to the right of $r_1/c$ are in their first quadrants, and the phase of $\delta$ is always $+\mathrm{i}$. Note that in making such a distortion of the contour $C'_\tau$, the Stoneley pole has been left on the lower $\delta$ sheet of the $\tau$ plane. Also, in case 1 we see in figure 10*a* that the branch point $t_S$ as well as its cut falls completely on the lower $\delta$ sheet, and is consequently left behind when the contour is distorted to the real $t$ axis.

Along our new contour which hugs the positive real $t$ axis from $t_P$ to infinity in a clockwise direction the radicals below the axis are complex conjugate to those above the axis. It follows that $A(u)$ is similarly related about the positive real axis in the $\tau$ plane. We now find it advantageous to extend the contour from $t_P$ to the origin of the $\tau$ plane so as to hug completely the whole positive real $t$ axis. Now, making use of the fact that the integrand of (4·21) beneath the positive real $t$ axis is complex conjugate to that above, the integral (4·21) can be re-expressed in the form where the contour is above the $t$ axis:

$$\bar{p}_1^f(x, z; \text{step}) = \frac{P_0 c}{r_1} \mathscr{I} \int_0^\infty \frac{A(u)|_{u=u(\tau)}}{\delta} e^{-s\tau} \, \mathrm{d}\tau. \tag{4·22}$$

In this integral, since $\tau$ is always positive real, we may replace $\tau$ by the time $t$. Similarly, $t$ will be used in place of $\tau$ in all expressions to follow.

In order to get the integral into the form of an $s$-multiplied Laplace transform integral we multiply (4·22) through by the factor $s$. Since the elastic wave system is initially quiescent,

we can interpret $s\bar{p}_1^f(\text{step})$ as the transform $\bar{p}_1^f(\text{delta})$ of the response to a delta-function excitation of the source. Then, making use of Lerch's uniqueness theorem, we can write

$$p_1^f(x,z;\text{delta}) = \frac{P_0 c}{r_1}\mathscr{I}\left[\frac{A(u)|_{u=u(t)}}{\delta}\right]\mathbf{H}(t-t_P), \tag{4·23}$$

where use has been made of the fact that the bracketed term is real for $t \leqslant t_P$. On this positive real $t$ axis, the phases of the radicals $\alpha_t$, $\beta_t$ and $\delta$ where

$$\alpha_t = \sqrt{(K_1^2-u^2)}|_{u=u(t)}, \quad \beta_t = \sqrt{(K_2^2-u_2)}|_{u=u(t)},$$

and

$$\delta = \sqrt{\{1-(ct/r_1)^2\}},$$

are shown in figure 12.

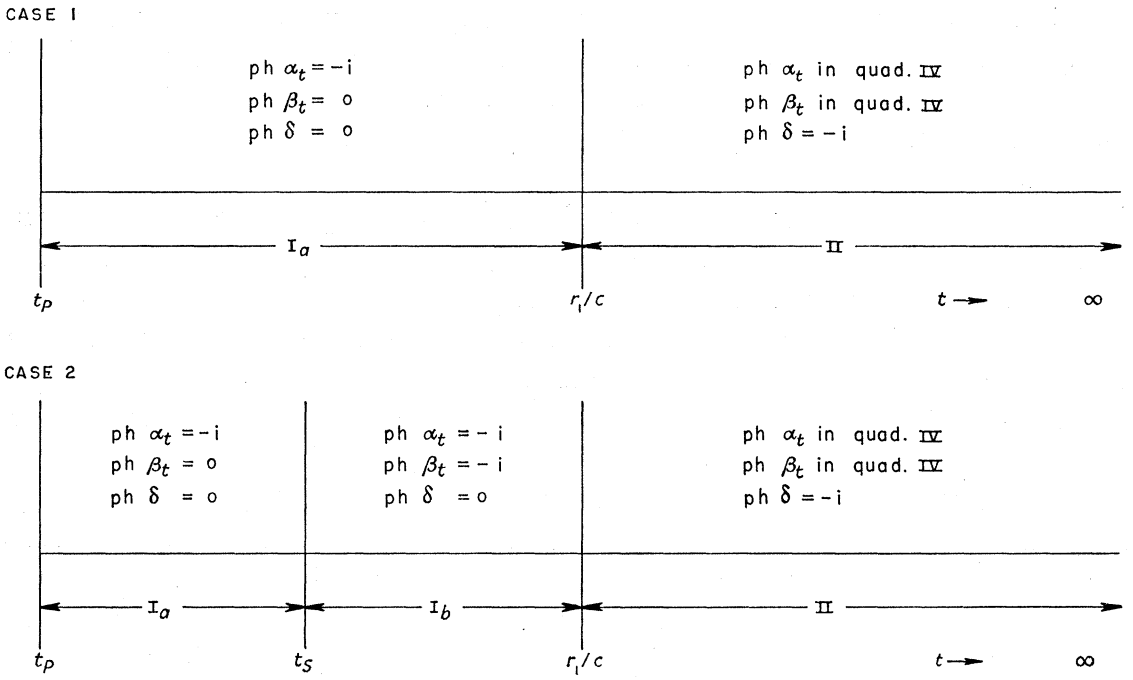


FIGURE 12. Phases of the radicals $\alpha_t$, $\beta_t$ and $\delta$ for ranges of the time $t$.

To response (4·23) we must according to (4·7) add the direct wave $p_0^f$ as given by (3·6) in order to obtain the total response $p^f$. In this way we find

$$p^f(x,z;\text{delta}) = \frac{P_0 c}{r}\frac{\mathbf{H}(t-r/c)}{\sqrt{\{(ct/r)^2-1\}}} + \frac{P_0 c}{r_1}\mathscr{I}\left[\frac{A(u)|_{u=u(t)}}{\delta}\right]\mathbf{H}(t-t_P), \tag{4·24}$$

where $r^2 = x^2+z^2$ and $r_1^2 = x^2+(2H-z)^2$. Also, $A(u)$ is defined by (4·10), $u(t)$ by (4·17) and $t_P$, $t_S$, by (4·16).

It is interesting to note that $A(u)$ has the algebraic form of the complex reflexion coefficient for reflexion from the fluid/solid interface if the intermediate variable $u$ is interpreted by (3·13) and (4·9) as the sine of the angle of incidence ($\theta$) between the direction of the propagation vector of the elementary plane waves and the normal to the interface.

In figure 12 there has been a decomposition of the response into regions I and II, depending upon whether or not the response time is less than or greater than $r_1/c$. The time $t_P$ as given by (4·16$a$) is, of course, the classic minimum time expression for the arrival of the

critically refracted $P$ wave as utilized in part I. Likewise, $t_S$ corresponds to the arrival time for a critically refracted $S$ wave. Finally, $r_1/c$ being the time for the arrival of a wave-front from the image point is the classic expression for the true reflexion arrival.

Thus, the response before the arrival of the direct and reflected wave-fronts is proportional to the imaginary part of the reflexion coefficient divided by a function which is related to the image source function. The angle of incidence $\theta$ is here positive real and a monotonically increasing function of the time $t$. Therefore, in this region, there exists a one-to-one correspondence between the angle of incidence $\theta$ and observed events on a wave-form.

After the time $t > r_1/c$ the response becomes proportional to the real part of the reflexion coefficient divided by the image source function. In this region where we expect to find a reflected cylindrical wave as well as the Stoneley interface wave we note that the angle of incidence becomes complex and is no longer easily interpretable.

Making use of the phase description in figure 12 we can further express the response $p_1^f$ in the following real form:

$$\textit{Region } I_a \begin{cases} \text{case 1:} & t_P \leqslant t \leqslant \dfrac{r_1}{c} \quad \text{or} \quad K_1 \leqslant u \leqslant \dfrac{x}{r_1}, \\ \text{case 2:} & t_P \leqslant t < t_S \quad \text{or} \quad K_1 \leqslant u \leqslant K_2, \end{cases}$$

so that

$$p_1^f(x,z;\text{ delta}) = \frac{2(\rho^f/\rho^s)\,K_2^4 P_0 c}{r_1 \delta}\left[\frac{\gamma(K_2^2-2u^2)^2\sqrt{(u^2-K_1^2)}}{\gamma^2(K_2^2-2u^2)^4-\alpha_t^2\{4u^2\beta_t\gamma+(\rho^f/\rho^s)\,K_2^4\}^2}\right]_{u=\frac{x}{r_1}\frac{ct}{r_1}-\frac{2H-z}{r_1}\delta} \tag{4·25}$$

$$\textit{Region } I_b \begin{cases} \text{case 1:} & p_1^f \equiv 0 \text{ in region } I_b, \\ \text{case 2:} & t_S < t < \dfrac{r_1}{c} \quad \text{or} \quad K_2 < u < \dfrac{x}{r_1}, \end{cases}$$

so that

$$p_1^f(x,z;\text{ delta}) = \frac{2P_0(\rho^f/\rho^s)\,K_2^4 c}{\delta r_1}\left[\frac{\gamma\sqrt{(u^2-K_1^2)}f(u)}{\gamma^2\{f(u)\}^2-\alpha_t^2(\rho^f/\rho^s)^2K_2^8}\right]_{u=\frac{x}{r_1}\frac{ct}{r_1}-\frac{2H-z}{r_1}\delta}, \tag{4·26}$$

where

$$f(u) = (K_2^2-2u^2)^2-4u^2\sqrt{(u^2-K_1^2)}\,\sqrt{(u^2-K_2^2)}. \tag{4·27}$$

*Region II*, both cases: $t \geqslant \dfrac{r_1}{c}$ or $u \geqslant \dfrac{x}{r_1}$,

$$p_1^f(x,z;\text{ delta}) = \frac{P_0 c}{r_1\delta}\left[\frac{|\gamma|^2|f(u)|^2-K_2^8(\rho^f/\rho^s)^2|\alpha|^2}{|D|^2}\right]_{u=\frac{x}{r_1}\frac{ct}{r_1}+i\frac{2H-z}{r_1}\sqrt{\left\{\left(\frac{ct}{r_1}\right)^2-1\right\}}}, \tag{4·28}$$

where $f(u)$ is defined by (4·11) and

$$D(u) = \gamma f(u)+(\rho^f/\rho^s)\,K_2^4\alpha, \tag{4·29}$$

so that

$$|D|^2 = DD^* = |\gamma|^2|f(u)|^2+K_2^8(\rho^f/\rho^s)^2|\alpha|^2+2K_2^4(\rho^f/\rho^s)\,\mathscr{R}\,[\gamma f(u)\,\alpha^*]. \tag{4·30}$$

By means of the parameters of table 3, the theoretical pressure response curves for pitch (case 1) and plaster of paris (case 2) have been calculated and are illustrated in figures 13 and 14, respectively. In each case the corresponding experimental curve from part I is reproduced for comparison. It should be noted here that what is actually shown is a comparison of the theoretical response from a delta-function excitation of a line source with that due experimentally to a 6 to 12 $\mu$s exponentially decaying excitation of a point source. However, the discussion of the point source representation in §3 (*a*) (ii) has led us to expect similar response wave-forms as is borne out by figures 13 and 14.

The computation time of a complete pressure response curve of the type shown in figures 13 and 14 is about 2 h for 100 time points using a medium speed computer (Elecom 120). It was originally intended to carry out a similar theoretical calculation using a point source. However, the numerical work would have been much greater, being roughly 100 h

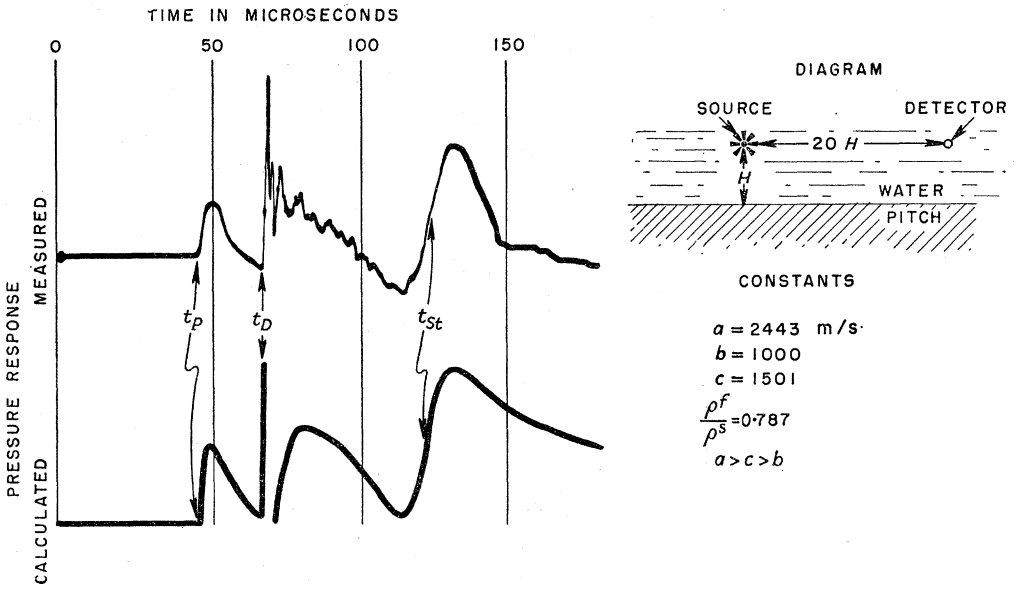


FIGURE 13. Pressure response at a water/pitch interface.

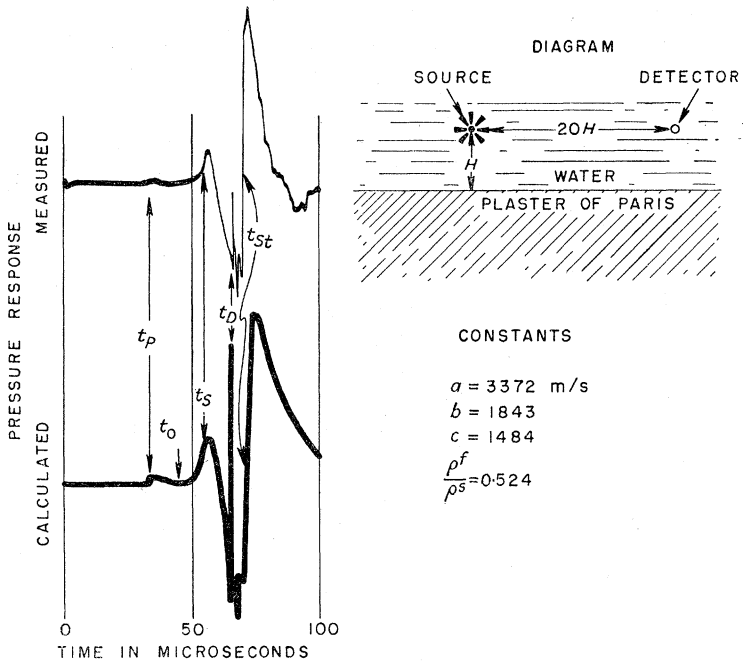


FIGURE 14. Pressure response at a water/plaster of paris interface.

for the same curve; and considering the close agreement obtained using our approximate viewpoint, it was decided not to make the more exacting point source calculations at this time.

One major disadvantage attendant with the use of the mathematically simple line source (3·6) is the inability, due to the singularity, of assigning an amplitude to the excitation. This

difficulty could have been avoided by the use of equation (A 4·10) in appendix 4. However, this requires an extra time integration which, although elementary, would not materially aid in the interpretation of the results of this paper. For our discussion we have found it sufficient to equate the theoretical and experimental amplitudes at an arbitrary point, which is usually the peak-to-peak amplitude of the Stoneley wave.

## 5. Discussion of results

Now let us analyze in detail the wave-forms of figures 13 and 14. The very first arrival at time $t_P$ is of course the critically refracted $P$ wave, being much more pronounced for pitch in figure 13 than for plaster of paris in figure 14. The amplitude variation of the critically refracted $P$ wave in figure 13 is described mathematically by (4·25). For $t \sim t_P$, the pressure builds up as $\sqrt{(u-K_1)}$ with $u(t)$ given by (4·17). The positive maximum can be obtained from the vanishing of the time derivative of (4·25), but such a lengthy expression is not very useful. The wave-form of this critically refracted $P$ wave with its single positive maximum is in good accord with other theoretical investigations beginning with Jeffreys's (1949) early work which first indicated its possible existence. The critically refracted $P$ wave is terminated at $t = t_D = r/c$ at 66·62 $\mu$s by the direct arrival with its positive singularity as given by (3·6). Very soon thereafter at $t = r_1/c = 66{\cdot}96$ $\mu$s region II starts with the simple reflexion of the spherical wave-front accompanied by a similar but negative singularity due to the vanishing of $\delta$. In order to simplify comparison with experiment, this portion of the wave-form containing the two singularities has been omitted. The curve starts again with the decay of the simple reflexion. It appears as though the whole of region II of the complete wave-form has been shifted upwards which we might expect from the tail effect of the two-dimensional delta-function-excited line source. Continuing on, we note that at $t = t_{St} = 122{\cdot}2$ $\mu$s corresponding to the arrival of the point of symmetry between the negative and positive extremums in the pressure response, occurs what we identify as the Stoneley arrival for the water/pitch interface. As mentioned in the discussion following table 3, the Stoneley equation for such an interface yields for a corresponding harmonic excitation the Stoneley velocity $V_{St} = c/1{\cdot}830$. Assuming in the usual fashion the instantaneous beginning of the generation of the interface wave at the epicentre, the arrival time $t_{St}$ is simply $x/V_{St}$ which yields 121·9 $\mu$s. This agreement, although close, is not exact. Referring to (4·28) we note that the vanishing of the numerator yields an equation which, although similar, is not the Stoneley equation for harmonic wave propagation, the latter being given by the vanishing of the denominator of (4·10). For our pulsed wave propagation the intermediate variable $u$ is in general a complex function of $x$, $2H-z$, $c$ and $t$ instead of being simply $c/V_{St}$, and one has to calculate $t_{St}$ for varying $x$ subject to the vanishing of the numerator in order to determine the incremental Stonely velocity. However, if we assume that $x \gg 2H-z$ so that we can neglect the imaginary part of $u(t)$, then $u = ct/x = c/(x/t)$ is real and we obtain the same relation as for harmonic excitation. It should be noted that the arrival time $t_{St}$ of the Stoneley wave for pulsed excitation is not the same as the absolute value nor the real part of the complex value of $\tau_{St}$ given in table 4. The latter is the location in the $\tau$ plane of the Stoneley pole in the $u$ plane as transformed according to (4·15). In our method of solving the problem, the solution in region II appears as a superposition of the reflected and interface waves, the

latter not appearing as an isolated pole contribution. The effect of the pole which is on the lower $\delta$ sheet in the complex $\tau$ plane is to distort the integrand of (4·22) into the wave-form of the interface wave. For $x \gg 2H-z$ this complex pole approaches the real $t$ axis.

The most apparent discrepancy between the theoretical and experimental wave-forms of figure 13 lies in the rapid oscillations that occur in the experimental wave-form between $t_D$ and $t_{St}$. These rapid oscillations do not appear in the theoretical calculations which were taken to an accuracy of seven significant figures and seem to lie in some experimental aspect as discussed in part I.

Replacing the pitch by plaster of paris whose shear wave velocity $b$ is greater than the water velocity $c$ results in (see figure 14) a diminishing of the amplitude of the critically refracted $P$ wave and an increase in the amplitude of the interface wave. Furthermore, there is a definite compression of the wave-form in time of both of these arrivals. The critically refracted $P$ wave for plaster of paris starts at 35·71 $\mu$s and lasts apparently until a zero in the response curve is reached at the point designated $t_0$ at 44·02 $\mu$s. The width of the critically refracted $P$ wave here is 8·31 $\mu$s as compared with 21·98 $\mu$s for pitch. If we define the width of the Stoneley interface wave as the time difference in the arrivals of the negative and positive peaks, then the width of the interface wave for plaster of paris in figure 14 is 6·23 $\mu$s as compared with 16·8 for pitch. Owing to a slightly different water velocity in table 3 the direct arrival is observed as in table 4 at 67·72 $\mu$s. The zero of the Stoneley interface wave is calculated to be at 73·75 $\mu$s. Just as in the case for pitch, use of the Stoneley wave charts (Strick & Ginzbarg 1956) gives $c/V_{St} = 1{\cdot}092$ for plaster of paris which yields an arrival time for harmonic wave propagation of 73·59, which is in rather good agreement. The reason for this close agreement here is that, as given in table 4, the Stoneley pole in the time plane has a rather small imaginary component.

The remaining feature of the pressure wave-form of figure 14 is the rather large amplitude variation between the critically refracted $P$ wave and the direct arrival. We noted earlier that for case 2 region I is divided into two parts with the separation time given by $t_S$ which is defined in (4·16$b$). This latter expression is, however, precisely that for a critically refracted $S$ wave which travels along the interface with the shear wave velocity $b$ of the plaster of paris, With the use of (4·16$b$), table 4 shows such an arrival should occur at 58·26 $\mu$s. However, such a value of $t_S$ occurs well up and near, but not on, the peak of the positive pressure swing in region $I_b$. It is difficult to see from this that a critically refracted $S$ head wave exists in this wave-form. The beginning of this large positive pressure build-up apparently occurs at the afore-mentioned time $t_0 = 44{\cdot}02$ $\mu$s, which is well within region $I_a$, which is much too early to explain by any minimum time path of the type associated with $t_S$.

Then there is the large negative (but finite) swing in the pressure response occurring after the positive peak is reached. Since this is not characteristic of the critically refracted $P$ wave, we might also not expect it to be characteristic of the critically refracted $S$ wave. Comparing the Stoneley wave of figure 14 with that of figure 13 suggests the possibility that this negative swing might be attributed to the very beginning of the Stoneley interface wave, which occurs before the direct arrival even though the arrival of the zero of the Stoneley wave occurs later.

Another complication in the interpretation occurs when we consider the behaviour of the point of zero amplitude on the wave-form which occurs between $t_S$ and $t_D$. Referring back to equation (4·26) we note that the only point of zero amplitude in region $I_b$ occurs when $f(u)$

vanishes. But the vanishing of $f(u)$ as defined by (4·27) is, except for the presence of $c$ instead of $b$ in the independent variable, precisely the known Rayleigh wave equation for surface waves travelling with a velocity $V_R$ along a semi-infinite elastic solid. If we let $u = c/V_R$ in (4·15) and take the time derivative holding $z$ = constant, then we find that

$$\partial x/\partial t = V_R, \tag{5·1}$$

i.e. this point of zero amplitude travels along the interface with exactly the true Rayleigh wave velocity of the solid as though the fluid were not present. Since one would certainly expect a true Rayleigh wave to exist if we were to go to the limit of vanishing fluid density, it is further suggestive that the build-up before the minimum time $t_S$ is related in some way to the Rayleigh wave. Since we have already shown in appendix 5 that only the pole associated with the Stoneley interface wave (and its negative) can exist on the top Riemann sheet, the pseudo-Rayleigh† pole must occur on a lower Riemann sheet of the $u$ plane.

Thus, we reach the rather attractive hypothesis that the large pressure variation in region $I_b$ is due to a linear superposition of pseudo-Rayleigh, Stoneley, and critically refracted shear waves. This hypothesis will be verified in part III of this paper.

Another point of interest is associated with the horizontal velocity of the zero amplitude point $t_0$ of region $I_a$ along the interface. Referring to equation (4·25) we note that the pressure vanishes for $u = K_2^2/\sqrt{2}$. Again applying the time derivative to (4·15) holding $z$ = constant we find that

$$\partial x/\partial t = \sqrt{2}\, b, \tag{5·2}$$

i.e. that the point of zero amplitude occurring at time

$$t_0 = \frac{x}{\sqrt{2}\, b} + \frac{2H-z}{c}\sqrt{\left(1-\frac{c^2}{2b^2}\right)}, \tag{5·3}$$

travels along the interface with a horizontal phase velocity equal to $\sqrt{2}$ times the shear wave velocity of the solid being independent not only of the existence of the fluid but also of the density and compressional velocity of the solid.

## 6. Conclusions

In figures 13 and 14 are given examples of the very close wave-form agreement between theory and experiment that can be obtained when a fluid/solid interface is excited by a transient point or line source located in the neighbourhood of the interface. For a delta-function excitation of a line source the complete pressure response solution is given in an exact closed form. It is also shown that for large distance as measured along the interface (i.e. $x \gg 2H-z$) the above exact solution for the line source can be reinterpreted as an approximate first-term asymptotic expansion for the pressure response due to the excitation of a point source that lies intermediate between that of a step and a delta function.

For a pitch/water interface (figure 13) there are four distinct arrivals: (1) critically refracted $P$ wave, (2) direct, (3) reflected, and (4) Stoneley interface waves. The critically

† Scholte (1949) has designated as a pseudo-Rayleigh wave the behaviour of the true Rayleigh wave when one takes into account the existence of the atmosphere over the semi-infinite solid. In order to avoid confusion we are extending his definition to that for a fluid/solid interface. Although we find this use of the adjective pseudo to be somewhat unsatisfactory (we prefer the adjective 'radiating'), we believe the whole nomenclature of interface waves to be in need of revision and are therefore not introducing new terminology at this time.

refracted $P$ wave and the Stoneley interface wave are both large in amplitude and extended in time, being the most significant events on the response curve. The direct and reflected arrivals seem to have a much higher frequency content.

For a plaster of paris/water interface there is a compression of the wave-form in time of the critically refracted $P$ wave and the Stoneley interface wave, but they are still major events on the response curve. Since the shear wave velocity of the plaster of paris is greater than the water velocity, we are led to expect a critically refracted $S$ wave to exist between the critically refracted $P$ wave and the direct arrival. However, the wave-form variation in this region does not show any indications of the existence of such a critically refracted $S$ wave. If it exists at all, it must be rather small. There is, however, a large pressure wave-form in this region which will be investigated in part III of this paper. For the present, we suggest that it is a combination of critically refracted $S$, pseudo-Rayleigh, and Stoneley interface waves.

It has been shown (Cagniard 1939) that when a step-excited point source is located in the vicinity of an interface between two media, there will be a logarithmic singularity in the response curve just before the arrival of the reflexion. In our exact solution for the response due to a delta-function excitation of a line source the only singularity that we observe that occurs before the reflexion is of the same nature as that of the source itself; furthermore, if we apply a time integration to our solution in order to recover the response to a step-function excitation, we do not find singularities of any kind except at $t =$ infinity.

## III. THE PSEUDO-RAYLEIGH WAVE

By E. STRICK

### 7. Introduction

The basic idea behind the possible existence of a pseudo-Rayleigh wave for propagation along a fluid/solid interface lies in the known behaviour of the response when the fluid is taken to be a low-density atmosphere. For then the elastic wave system is very close to that for the propagation of a true Rayleigh wave along the free boundary of a semi-infinite elastic solid, which has been studied in detail by many writers. Cagniard (1939, chap. XIV) has shown that the presence of the atmosphere perturbs the propagation of the Rayleigh wave to a negligible extent when the source is placed near the boundary. However, this method of solution which neglects higher powers of the density ratio $\rho^f/\rho^s$ is unsuitable for use in our study of the propagation along a water/solid interface.

Scholte (1949) in written communication with Cagniard reaches the conclusion that a pseudo-Rayleigh wave should not be observable if the density of the fluid approaches that of water. On the other hand, in our discussion of equation (4·26) in the preceding part it was conjectured that the presence of a pseudo-Rayleigh wave might account for much of the variation of the pressure response observed between the times $t_0$ and $t_D$ in figure 14 for the excitation of a water/plaster of paris interface.

Osborne & Hart (1945) essentially repeat Cagniard's perturbation calculation in that they neglect instead higher powers of the deviation of the horizontal phase velocity from that

of the true Rayleigh wave velocity, and arrive at an expression almost identical to Cagniard's for the complex propagation velocity of the pseudo-Rayleigh wave. Although they assume that the water correction term to the original velocity equation is small, nevertheless, they do apply the derived expression to a water/steel interface and reach the conclusion that for this system a pseudo-Rayleigh wave can exist.

If we are to prove that the above-mentioned wave-form variation in figure 14 is primarily due to the existence of a pseudo-Rayleigh wave, then we must also be able to explain why such an arrival does not appear in the wave-form for a water/pitch interface as shown in figure 13 of part II. From the parameters of pitch given in table 3 of part II we can determine from the well-known Rayleigh equation that $b/V_R = 0{\cdot}948$. Thus, $u_R = c/V_R = 1{\cdot}583$. However, in the neighbourhood of the time $t = x/V_R = 106{\cdot}7\ \mu$s of figure 13 there is no visible indication of such a pseudo-Rayleigh wave.

In this paper we shall first discuss some properties of the pseudo-Rayleigh wave that are similar to those of a true Rayleigh wave. Then we shall discuss other properties of the pseudo-Rayleigh wave that are reminiscent of a critically refracted arrival. From this investigation we shall find that the pseudo-Rayleigh wave has the dual set of properties such that measurement on the solid would lead us to think of the arrival as a modified Rayleigh wave, whereas measurement in the fluid would lead us to think of it as a critically refracted wave.

Since the true Rayleigh wave properties of the pseudo-Rayleigh wave will be discussed first, it is necessary that we state clearly just what these properties are. First of all, the true Rayleigh wave travels along the boundary with a horizontal phase velocity determined by the well-known Rayleigh cubic equation. We have already seen in §5 of part II, that the pressure zero of the pseudo-Rayleigh wave also travels with this true Rayleigh wave velocity. The particle displacement of the true Rayleigh wave as was initially determined by Lamb (1904) has been referred to by many investigators, as has the 'ellipsoid' of retrograde particle motion. In §9 we shall find that after some modification these properties are carried over into the pseudo-Rayleigh wave. There are, in addition, other properties connected with attenuation with distance both parallel to and normal to the boundary that are usually associated with the true Rayleigh wave. For harmonic excitation these amplitude-distance relations are simple and well understood, but for transient excitation one obtains rather complicated dependences which depend upon the actual excitation utilized. For this reason, attenuation-distance comparisons will not be made.

In addition to the above comparison of physical wave-forms it is of interest to investigate a very important mathematical feature that distinguishes boundary waves from all other arrivals. A true Rayleigh wave and the Stoneley wave of figures 13 and 14 are both mathematically obtainable as the contribution from a pole singularity on the upper Riemann sheet of the integrand, whereas the other arrivals are all associated with branch point contributions. This aspect of the problem is investigated in §10 and it leads to some insight into the apparent non-existence of the pseudo-Rayleigh wave at a water/pitch interface. In the course of the investigation of the pole contribution where we are led into a discussion of the migration of the Rayleigh pole on to lower Riemann sheets of the complex $u$ plane, other poles located on lower Riemann sheets of our integrand are investigated. Although these latter poles do not contribute to an observable arrival as does the pseudo-Rayleigh pole, in §11 we shall see that the location of one or more of them is, in some as yet unexplained




PHILOSOPHICAL TRANSACTIONS OF THE ROYAL SOCIETY A MATHEMATICAL, PHYSICAL & ENGINEERING SCIENCES

fashion, associated with an algebraic condition that apparently maximizes the total pressure response curve.

In § 11 we shall return to an analysis of the response within the fluid where we shall discuss some of the properties such as an apparent minimum time path and velocity normal to the interface that would lead us to think of the pseudo-Rayleigh wave as a modified critically refracted wave. Finally, in this same section we shall discuss a practical method for utilizing the pseudo-Rayleigh and Stoneley interface arrivals to measure *in situ* the rigidity of bottom sediments in water-covered areas.

However, before attempting to study in detail the pseudo-Rayleigh arrival that we found in the water/plaster of paris interface in figure 14, we shall first show that it is easily possible to find media which will yield response curves where the pseudo-Rayleigh wave is clearly isolated from all of the other arrivals. This will now be accomplished in § 8.

## 8. Isolation of the pseudo-Rayleigh wave

Some experimental evidence of the existence of this pseudo-Rayleigh wave has been found by several investigators. Osborne & Hart (1945) suggest among several possibilities that such an arrival may be the cause of a 'precursor' which is an oscillation that they observe to precede the explosion wave as it travels along a steel plate in water. McMillen (1946) in an experimental approach utilizing spark shadowgrams showed the existence of such a pseudo-Rayleigh wave when a brass cylinder in water was excited on a lateral side. However, when he extended his experiment to that of a steel block in water, the identification of the pseudo-Rayleigh wave required a rather unsatisfactory extrapolation from the brass cylinder experiment. In this section we shall clearly isolate the pseudo-Rayleigh arrival both experimentally and theoretically so that it can be studied in great detail.

In order to isolate the pseudo-Rayleigh wave from the critically refracted wave it is apparent from travel-time considerations that we must have $V_R \ll b$. On the other hand, in order to isolate it from the direct arrival we should require that $V_R \gg c$. Both of these conditions can best be satisfied if we require that $K_2 = c/b \ll 1$ and $a/b \gg 1$.

In figure 15 we show the pressure response obtained by further increasing the velocity contrasts from that of water/plaster of paris of figure 14 to that of water/iron. The theoretical pressure response calculated according to equations (4·25) through (4·28) of part II is shown at the left of figure 15. The corresponding experimentally measured response curve as obtained by Roever & Vining using the experimental procedure of part I and an iron block of 99·9 % pure Swedish iron is shown at the right of figure 15. Since it was not feasible to core the iron block, they were limited to velocity data obtained by taking seismic profiles over the block and studying refracted arrivals through a corner of the block. Their results are included below in table 5 and were used in the calculations of the theoretical curve of figure 15.

Referring to figure 15, notice once again the very close wave-form agreement that we have obtained between theory and experiment. Just as we had anticipated, the amplitude of the critically refracted $P$ wave arriving at $t_P$ is very small. The critically refracted $S$ wave should come in at the time designated $t_S$ which is well before the positive peak of region $I_b$, but is not evident. The point of zero-pressure amplitude in region $I_b$ is designated $t_{pR}$ and is now quite isolated. The wave-form antisymmetric about this time $t_{pR}$ is now attributed to the pseudo-

Rayleigh wave. Much later in time just before the direct arrival at $t_P$ we observe a large negative pressure variation. This we attribute to the beginning of the Stoneley wave. The solution of the Stoneley wave equation for the parameters of table 5 is $u_{St} = c/V_{St} = 1{\cdot}0004$. For $x = 10$ cm this corresponds to an arrival time from the epicentre for harmonic waves of $66{\cdot}69\ \mu$s, which is earlier than the calculated simple reflexion at $t_{\text{refl.}} = r_1/c = 67{\cdot}00\ \mu$s. This is, of course, impossible and only reflects what is quite apparent from equation (4·28)

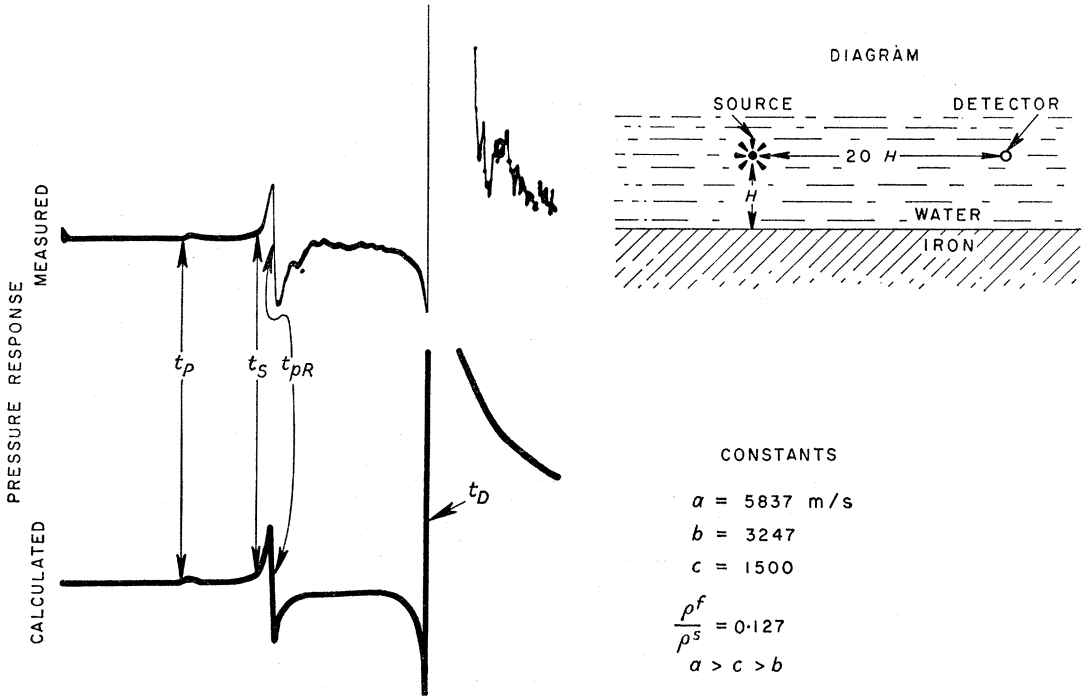


FIGURE 15. Case 2, $a > b > c$.

TABLE 5. VELOCITY AND SPECIFIC GRAVITY DATA FOR IRON

case 2, iron/water interface,
$\sigma = 0{\cdot}272$
$K_1 = 0{\cdot}2570$
$K_2 = 0{\cdot}4620$
$c = 1500$ m/s
$u_R = c/V_R = 0{\cdot}5003$
$\rho^f/\rho^s = 0{\cdot}127$ (*Handbook Chem. Phys.*)

of part II, i.e. that our naïve assumption of $t_{St} = x/V_{St}$ is an approximation with increasing accuracy for large horizontal distances. The vanishing of the numerator of (4·28) yields an intermediate variable $u$ which is complex and which is associated with a real $t$. For $x$ sufficiently large that we can neglect the imaginary part of $u$ we obtain the Stoneley wave equation. Since the Stoneley interface wave is non-dispersive, we can expect a similar result when an accurate harmonic analysis is carried out.

Even though the arrival time for the Stoneley wave is apparently inaccurate when calculated in the above manner, it is certainly true that the time of the Stoneley arrival is indeed very close to the arrival of the simple reflexion. Also, if we extrapolate from figures 13 and 14 to figure 15, we should expect the Stoneley wave to be extremely compressed in time. On the other hand, increasing the contrast makes the reflexion look more like

that from a rigid boundary so that the reflected wave has the same sign and differs only slightly in wave-form from the direct arrival. The result is that the body of the Stoneley arrival is over-shadowed by the reflected wave, and that the only visible portion of the Stoneley wave is that which comes in before the direct arrival at $t_D$. The apparent high frequency appearing on the experimental pressure response is the same as that occurring in figures 13 and 14 after the reflexion has arrived, but is of rather large amplitude here.

Making use of the transformation (4·15) of part II we list in table 6 for iron the numerical values of the branch points and poles in the $\tau$ plane in microseconds just as we did in table 4 of part II for pitch and plaster of paris.

TABLE 6. NUMERICAL VALUES OF BRANCH POINTS AND POLES IN THE $\tau$ PLANE IN MICROSECONDS

case 2, iron/water interface

| | |
|---|---|
| $t_P = 23{\cdot}57$ | $t_D = 66{\cdot}67$ |
| $t_0 = 28{\cdot}08$ | $r_1/c = 67{\cdot}00$ |
| $t_S = 36{\cdot}71$ | $t_{St} \cong 66{\cdot}69$ |
| $t_{pR} = 39{\cdot}16$ (from $u_R = c/V_R = 0{\cdot}5002$) | $\tau_{St} = 66{\cdot}69 - \mathrm{i}0{\cdot}19$ |

## 9. DISPLACEMENT RESPONSE DETERMINATION

In §4 of part II we determined the reflexion coefficient $A(q)$ as given by (4·5) from the requirement that the potentials of $\phi_1^f$, $\phi^s$ and $\psi^s$ represented in (4·4) satisfy the boundary conditions on the continuity of the normal stress and normal displacement and the vanishing of the tangential stress. In so doing we obtained three simultaneous equations in the coefficients $A(q)$, $B(q)$ and $C(q)$ contained in (4·4). At that time we did not find it necessary to solve for the coefficients $B(q)$ and $C(q)$. Since we now desire to determine the two components of displacement of the solid at the interface, we need these latter coefficients which are easily shown to be

$$B(u) = \frac{\gamma(K_2^2 - 2u^2)}{\alpha K_2^2}[1 - A(u)] \exp\{-\mathrm{i}\omega H/c(\gamma - \alpha)\}, \tag{9·1a}$$

$$C(u) = \frac{-2u\gamma}{K_2^2}[1 - A(u)] \exp\{+\mathrm{i}\omega H/c(\beta - \gamma)\}, \tag{9·1b}$$

where we have already made the transformation into the $u$ plane by (4·9). $A(u)$ is the reflexion coefficient in the $u$ plane defined by (4·10). $H$ is as before the distance of the source from the interface.

The solid displacement potentials $\phi^s$ and $\psi^s$ (4·4$b$, $c$) are thus uniquely represented in the $u$ plane and by (3·36) we find for the solid displacements $U^s$ and $W^s$

$$U^s(x, z; \mathrm{e}^{\mathrm{i}\omega t}) = \frac{-P_0}{2\rho^f \omega c}\int_{-\infty}^{+\infty}\left[\frac{u}{\gamma}B(u) \exp\{-\mathrm{i}\omega/c(\alpha z + ux)\} + \frac{B}{\gamma}C(u) \exp\{-\mathrm{i}\omega/c(\beta z + ux)\}\right] \mathrm{d}u\, \mathrm{e}^{\mathrm{i}\omega t}, \tag{9·2a}$$

$$W^s(x, z; \mathrm{e}^{\mathrm{i}\omega t}) = \frac{-P_0}{2\rho^f \omega c}\int_{-\infty}^{+\infty}\left[\frac{\alpha}{\gamma}B(u) \exp\{-\mathrm{i}\omega/c(\alpha z + ux)\} - \frac{u}{\gamma}C(u) \exp\{-\mathrm{i}\omega/c(\beta z + ux)\}\right] \mathrm{d}u\, \mathrm{e}^{\mathrm{i}\omega t}. \tag{9·2b}$$

Inserting (9·1) into (9·2) we find integrals analogous to (4·13). At the same time, we can introduce the $s$-multiplied Laplace transform variable $s = \mathrm{i}\omega$, rotate the contour to the

imaginary axis and consider the transform of the displacement response to a step-function excitation of the line source to be

$$\bar{U}^s(x,z;\text{step}) = \frac{P_0 \mathrm{i}}{K_2^2 \rho^f c s} \int_{-\mathrm{i}\infty}^{+\mathrm{i}\infty} u[1-A(u)] \Big[ -\frac{(K_2^2-2u^2)}{2\alpha} \exp\left[-(s/c)\{(z-H)\alpha+\gamma H\}\right] + \beta \exp\left[-(s/c)\{(z-H)\beta+\gamma H\}\right] \Big] \mathrm{e}^{-sux}\,\mathrm{d}u, \quad (9{\cdot}3a)$$

$$\bar{W}^s(x,z;\text{step}) = \frac{-P_0 \mathrm{i}}{K_2^2 \rho^f c s} \int_{-\mathrm{i}\infty}^{+\mathrm{i}\infty} [1-A(u)] \Big[ \frac{(K_2^2-2u^2)}{2} \exp\left[(s/c)\{(z-H)\alpha+\gamma H\}\right] + u^2 \exp\left[-(s/c)\{(z-H)\beta+\gamma H\}\right] \Big] \mathrm{e}^{-sux}\,\mathrm{d}u. \quad (9{\cdot}3b)$$

These integrals are of the form of (4·14). The exponents, however, are slightly more complicated than $-s\tau$ where $\tau$ was defined by (4·15) in that they involve two radicals. Cagniard (1939) has discussed this transformation in chapter V of his book. We are at present only interested in the displacements on the interface where $z = H$. Our integrals may then be condensed into

$$\bar{U}^s(x,H;\text{step}) = \frac{+P_0 \mathrm{i}}{2K_2^2 \rho^f c s} \int_{-\mathrm{i}\infty}^{+\mathrm{i}\infty} \frac{u}{\alpha} [2\alpha\beta - (K_2^2-2u^2)]\,[1-A(u)]\,\mathrm{e}^{-s\tau}\,\mathrm{d}u, \quad (9{\cdot}4a)$$

$$\bar{W}^s(x,H;\text{step}) = \frac{-P_0 \mathrm{i}}{2\rho^f c s} \int_{-\mathrm{i}\infty}^{+\mathrm{i}\infty} [1-A(u)]\,\mathrm{e}^{-s\tau}\,\mathrm{d}u, \quad (9{\cdot}4b)$$

where on the interface

$$\tau = \frac{\gamma H}{c} + \frac{ux}{c}. \quad (9{\cdot}5)$$

Just as in §4, we may now distort the contour to surround the cuts on the real $u$ axis and then make the transformation to the $\tau$ plane using (9·5). Equations of the types (4·17) through (4·20) are still valid here with $z = H$, and we obtain:

$$\bar{U}^s(x,H;\text{step}) = \frac{-P_0 \mathbf{H}(t-t_P)}{K_2^2 \rho^f s r_1} \mathscr{I} \int_0^{\infty} \frac{\gamma}{\delta} \frac{u}{\alpha} [2\alpha\beta - (K_2^2-2u^2)]\,[1-A(u)]\,\mathrm{e}^{-s\tau}\,\mathrm{d}\tau, \quad (9{\cdot}6a)$$

$$\bar{W}^s(x,H;\text{step}) = \frac{P_0 \mathbf{H}(t-t_P)}{\rho^f s r_1} \mathscr{I} \int_0^{\infty} \frac{\gamma}{\delta} [1-A(u)]\,\mathrm{e}^{-s\tau}\,\mathrm{d}\tau, \quad (9{\cdot}6b)$$

where we have made use of the fact that the integrand below the cut is the complex conjugate of that above the cut.

In order to identify integrals (9·6) with the definition of the $s$-multiplied Laplace transform we need a power of $s$ on the right side of (9·6) that is 2 degrees higher than exists there. Since our system is initially quiescent, we have three choices of interpretation. We can write down directly the particle acceleration response to a step-function excitation of the line source, the particle velocity response to a delta-function excitation of the line source, or the particle displacement response to a derivative of the delta-function excitation of the source. These representations are, of course, equivalent, but in order to facilitate comparison with the developments of parts I and II we shall make use of the second interpretation. We then have as in part II

$$\dot{U}^s(x,H;\text{delta}) = \frac{P_0 \mathbf{H}(t-t_P)}{K_2^2 \rho^f r_1} \mathscr{I} \Big[ \frac{\gamma}{\delta} \frac{u}{\alpha} \{-2\alpha\beta + (K_2^2-2u^2)\}\{1-A(u)\} \Big]_{u=u(t)}, \quad (9{\cdot}7a)$$

$$\dot{W}^s(x,H;\text{delta}) = \frac{P_0 \mathbf{H}(t-t_P)}{\rho^f r_1} \Big[ \frac{\gamma}{\delta} \{1-A(u)\} \Big]_{u=u(t)}, \quad (9{\cdot}7b)$$

where $u(t)$ is by (4·17) at $z = H$ $\quad u = u(t) = \dfrac{ct}{r_1}\dfrac{x}{r_1} - \dfrac{H}{r_1}\delta.$ (9·8)

We can compare (9·7) with the total pressure response (4·24) at the interface. For $z = H$ it follows that $r = r_1 = (x^2+H^2)^{\frac{1}{2}}$ and $p^f$ reduces to

$$p^f(x, H;\ \text{delta}) = \frac{P_0 c\mathbf{H}(t-t_P)}{r_1}\mathscr{I}\left[\frac{1+A(u)}{\delta}\right]_{u=u(t)}. \tag{9·9}$$

Just as the pressure response $p_1^f$ (delta) given by (4·23) was decomposed into three separate regions as given by (4·25), (4·26) and (4·28) we can similarly subdivide our particle velocity response (9·7). In regions $I_a$ and $I_b$ we shall find it convenient to express $\dot{U}^s$ and $\dot{W}^s$ in terms of $p^f$ as given by (4·25) and (4·26) at $z = H$.

$$\textit{Region } I_a \begin{cases} \text{case 1:} & t_P \leqslant t \leqslant r_1/c \quad \text{or} \quad K_1 \leqslant u \leqslant x/r_1, \\ \text{case 2:} & t_P \leqslant t \leqslant t_S \quad \text{or} \quad K_1 \leqslant u \leqslant K_2. \end{cases}$$

$$U^s(x, H;\text{delta}) = \frac{u(z\beta\gamma+(\rho^f/\rho^s)\,K_2^2)}{K_2^2-2u^2}\bigg|_{u=u(t)} \cdot \frac{p^f(\text{delta})}{\rho^f c}, \tag{9·10a}$$

$$\dot{W}^s(x, H;\ \text{delta}) = -\gamma\Big|_{u=u(t)} \cdot \frac{p^f(\text{delta})}{\rho^f c}. \tag{9·10b}$$

$$\textit{Region } I_b \begin{cases} \text{case 1:} & \dot{U}^s \text{ and } \dot{W}^s \text{ are} \equiv 0 \text{ in region } I_b, \\ \text{case 2:} & t_S \leqslant t \leqslant r_1/c \quad \text{or} \quad K_2 \leqslant u \leqslant x/r_1, \end{cases}$$

$$\dot{U}^s(x, H;\ \text{delta}) = \frac{-(\rho^f/\rho^s)\,K_2^2 u}{r_1}\,\frac{(2u^2-K_2^2-2\sqrt{(u^2-K_1^2)}\,\sqrt{(u^2-K_2^2)})}{f(u)}\bigg|_{u=u(t)} \cdot \frac{p^f(\text{delta})}{\rho^f c}, \tag{9·11a}$$

$$\dot{W}^s(x, H;\ \text{delta}) = -\gamma\Big|_{u=u(t)} \cdot \frac{p^f(\text{delta})}{\rho^f c}. \tag{9·11b}$$

*Region* II, both cases: $t > r_1/c \quad$ or $\quad u > x/r_1$,

$$\dot{U}^s(x, H;\ \text{delta}) = \frac{2P_0 K_2^2[\gamma^* u^*(K_2^2-2u^2-2\alpha\beta)^* D(u)]}{r_1\rho^s\sqrt{\{(ct/r_1)^2-1\}}\,|D|^2}\bigg|_{u=u(t)}, \tag{9·12a}$$

$$W^s(x, H;\ \text{delta}) = \frac{2P_0 K_2^4\{|\gamma|^2\mathscr{R}[\alpha^* g(u)]+(\rho^f/\rho^s)\,K_2^4|\alpha|^2\mathscr{R}\gamma\}}{r_1\rho^s\sqrt{\{(ct/r_1)^2-1\}}\,|D|^2}\bigg|_{u=u(t)}, \tag{9·12b}$$

where $D$ and $|D|^2$ are defined by (4·29) and (4·30).

The vertical velocity response $\dot{W}^s$ is in regions $I_a$ and $I_b$ very much like that of the pressure response in these regions, after due regard is taken for the sign inversion. The factor $\gamma$ is always positive and is a slowly varying function of $t$ except in the neighbourhood of $r_1/c$. The relationship of the horizontal velocity response $U^s$ to the pressure response $p^f$ is a little more involved. In region $I_a$ the factor $u[2\alpha\beta+(\rho^f/\rho^s)\,K_2^2]$ is always positive. The denominator term $K_2^2-2u^2$, however, goes through a sign change at $u = K_2/\sqrt{2}$. This corresponds to precisely that time $t = t_0$ at which the pressure response was shown in §5 to reach a zero value. Although it appears from (9·10$a$) that $\dot{U}^s$ becomes infinite at $u = K_2/\sqrt{2}$, the singularity is cancelled out by a squared term appearing in $p^f$ in (4·25). Thus, the horizontal velocity response crosses the time axis at $t = t_0$, whereas the pressure and vertical velocity responses only touch the axis at this time.

This horizontal velocity $\dot{U}^s$ given by (9·11 $a$) differs sufficiently from $p^f$ to make a comparison somewhat difficult. The quantity $u$ and the bracketed term to the right of it in (9·11 $a$) are both always positive real in region $I_b$. In the denominator we have $f(u)$ which was defined by (4·27) and whose vanishing yields the Rayleigh wave equation. In § 5 we made use of the existence of this term in the numerator of (4·26) to prove (5·1), i.e. that the points of zero amplitude in region $I_b$ travel along the interface with the true Rayleigh wave velocity. Inserting (4·26) into (9·11 $a$) we see that $f(u)$ cancels out. Thus, $\dot{U}^s$ does not have a zero amplitude at $t = t_{pR}$ as do $p^f$ and $\dot{W}^s$. Calculation also shows that it has neither a maximum nor minimum at this time. In fact, there does not appear to be any feature of the response in region $I_b$ that travels along the interface with the Rayleigh wave velocity.

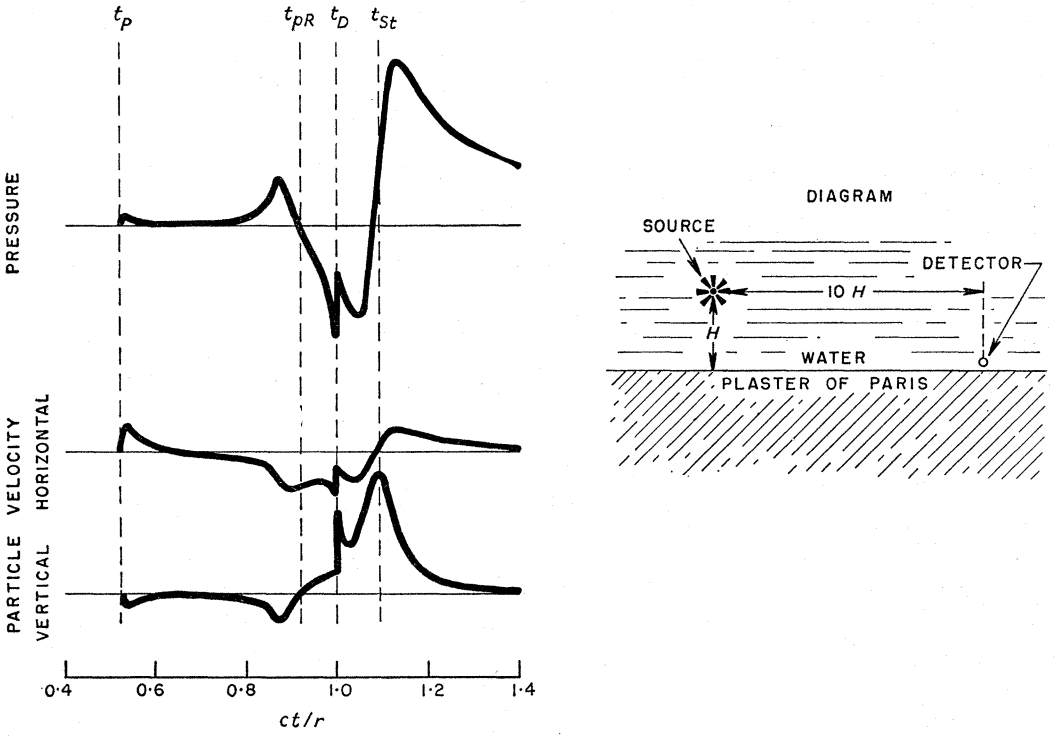


FIGURE 16. Comparison of particle velocity with pressure response at a water/plaster of paris interface.

The tail of the direct arrival raises the response in region II, so that we should pick the point of antisymmetry in the wave-form rather than the point of zero amplitude as the arrival time of the Stoneley wave. Since we are here concerned primarily with the existence of the pseudo-Rayleigh wave, we shall not discuss the Stoneley arrival in further detail.

In figure 16 are plotted the pressure (4·24); horizontal particle velocity $\dot{U}^s$ (9·10 $a$), (9·11 $a$), (9·12 $a$); and the vertical particle velocity $\dot{W}^s$ (9·10 $b$), (9·11 $b$), (9·12 $b$) when the detector is placed on the water/plaster of paris interface. Simultaneous with relocating the detector to the interface we have shortened the horizontal distance by a factor two. In this way we have kept the ratio $x/(2H-z)$ fixed so that $u$ and therefore $p_1^f$ is invariant. Therefore, the pressure curve in figure 16 is identical to the theoretical curve in figure 14 except for a rather minor difference which occurs when the direct arrivals which have travelled slightly

different distances are added in. However, in regions $I_a$ and $I_b$ which include the pseudo-Rayleigh wave under discussion the two curves are identical.

Upon comparing the vertical velocity response $\dot{W}^s$ with the pressure response in figure 16 we note that before the direct arrival at $t_D$ the two curves are just as we discussed earlier, very much alike apart from the negative sign. After the direct arrival, however, it appears that the vertical particle velocity has a positive peak instead of a point of antisymmetry to correspond to the arrival time of the Stoneley wave. The horizontal particle velocity response $\dot{U}^s$ yields a critically refracted $P$ wave which looks very much like the critically refracted $P$ wave of the pressure response. At $t = t_0$ it crosses the time axis, whereas the pressure only touched the axis and remained positive. At $t = t_{pR}$ it is very close, but not exactly, at a negative peak.

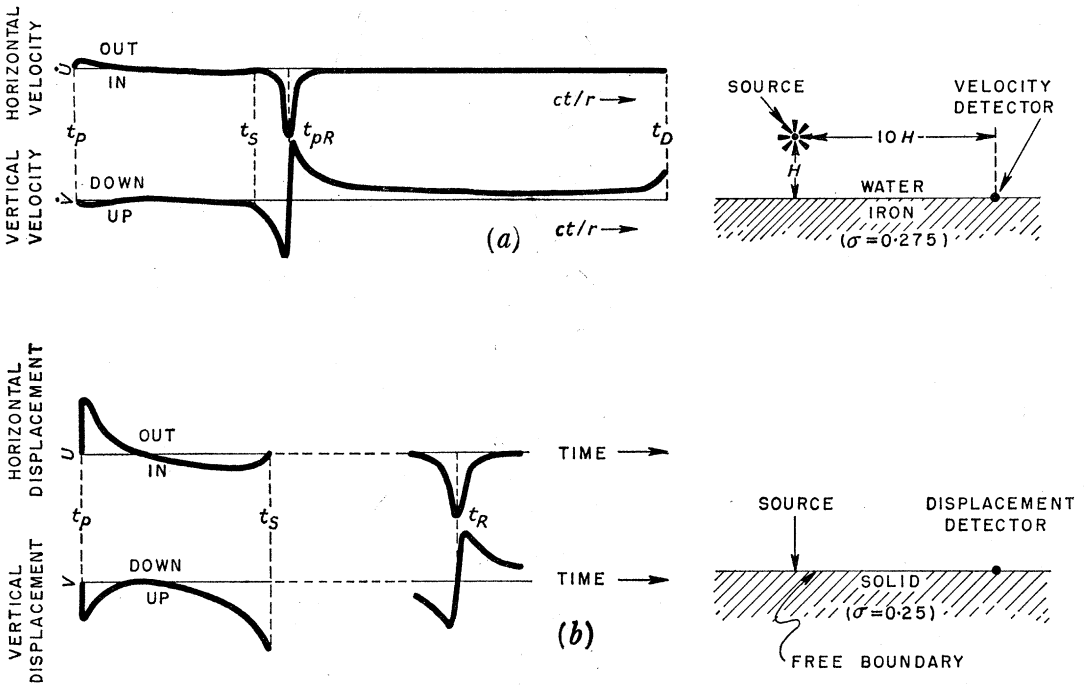


FIGURE 17. Particle velocity response curves: (*a*) For a water/iron interface, (*b*) for the Lamb problem (free boundary semi-infinite solid).

This is in line with our previous discussion that there is apparently not any point on the wave-form of $\dot{U}^s$ that travels with the velocity of the true Rayleigh wave. In the Stoneley wave region we observe that the horizontal velocity response is very much like the pressure response, except that the arrival time of the Stoneley wave again does not correspond exactly to the arrival of the point of antisymmetry on the wave-form.

Next we take advantage of our ability to isolate the pseudo-Rayleigh arrival by considering the propagation along a water/iron interface. In figure 17*a* are shown the horizontal and vertical components of particle velocity for times before the direct arrival. Since the ratio $(2H-z)/x$ has been unchanged, these curves are directly comparable with the pressure curve of figure 15. The critically refracted $P$ wave is very much like that for the water/plaster of paris interface in figure 16. Its amplitude is actually somewhat smaller, but its scale has been altered so as to allow a better comparison with figure 17*b*. The behaviour in the neighbourhood of $t = t_0$ is also very much the same in figures 16 and 17*a*. At $t = t_S$, the

arrival time for a possible critically refracted $S$ wave, we observe that there is a distinct change in the slope of the horizontal velocity curve which takes place at a point of zero amplitude. It appears that there is actually a critically refracted $S$ wave arriving at this time and that its amplitude is of the order of magnitude of that of the critically refracted $P$ wave, the latter being roughly one-fiftieth of that of the pseudo-Rayleigh wave amplitude. The critically refracted $S$ wave is not so discernible in the vertical velocity response curve. On the other hand, the beginning of the Stoneley wave which occurs just before the direct arrival is quite evident in the vertical velocity and non-evident in the horizontal velocity curve.

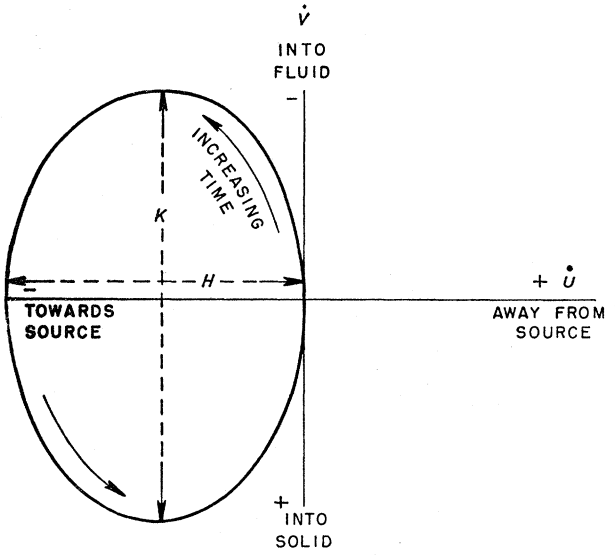


FIGURE 18. Orbit of retrograde motion of the pseudo-Rayleigh wave at a water-iron interface.

It is the region about the arrival time of the pseudo-Rayleigh wave that is of primary interest. Just as in figure 15, the pseudo-Rayleigh wave is well isolated, except for a possible overlapping with the critically refracted $S$ wave. However, the overlapping occurs at a time much earlier than $t_{pR}$ and therefore does not have an appreciable effect on the pseudo-Rayleigh wave. The vertical velocity response $\dot{W}^s$ about $t = t_{pR}$ is essentially the negative of the pressure response of figure 15, as we are led to expect from our earlier discussion. At $t = t_{pR}$ the amplitude is zero and this zero travels along the interface with the true Rayleigh wave velocity of the solid. The horizontal velocity response, on the other hand, has a negative minimum at a time very close to $t_{pR}$. From our discussion of the corresponding response in figure 16 we see that this minimum does not occur at exactly $t_{pR}$. However, from our calculations of figure 17$a$ we can ascertain that the negative peak occurs within 0·03 microsecond of the value of $t_{pR} = 39{\cdot}16\ \mu$s given in table 6. Thus, the better the isolation of the pseudo-Rayleigh wave, the closer the time of the negative peak of $\dot{U}^s$ is to the zero of $\dot{W}^s$.

In figure 17$b$ we show a reproduction of response curves taken from the classic paper by Lamb (1904) on the propagation of elastic waves along the free surface of a semi-infinite elastic solid. If we disregard for a moment the discrepancy in our ordinates, which is discussed in appendix 6, i.e. Lamb has calculated displacements rather than velocities, then we observe a very close wave-form correlation between the two sets of response curves. The behaviour between the times $t_P$ and $t_S$ is almost identical. A similar statement can be made

for the behaviour about the times $t_{pR}$ for the pseudo-Rayleigh wave and the time $t_R$ for the true Rayleigh wave. Lamb carried out separate calculations for the two regions of the response curves, and they are plotted to different scales. If we are to compare our response curves in figure 17 with Lamb's, then we should join Lamb's curves together in such a manner that the negative swing on the vertical displacement just before $t = t_S$ is part of the negative swing on the true Rayleigh wave. If we continue to ignore the discrepancy in the ordinate variables in figure 17, then we can plot the 'so-called' ellipsoid of retrograde motion for the two problems. This has been done in figure 18 for the water/iron interface. Not only is the motion retrograde, but the ratio of axis is 1·47 which compares very favourably with the value of 1·49 that we would find for a true Rayleigh wave propagation over a free boundary semi-infinite elastic solid of $\sigma = 0{\cdot}275$. Lamb's calculations were made for a solid of $\sigma = 0{\cdot}25$. His ellipsoid of motion is shown in his figure 7 and is very much like ours. He finds (on page 19 of his paper) a ratio $K'/H' = 1{\cdot}468$. We find $K/H \approx 1{\cdot}49$ for our iron/water interface.

## 10. Mathematical relation to the true rayleigh wave

In § 5 it was mentioned that the pole associated with the pseudo-Rayleigh wave cannot, because of the development in appendix 5, exist on the top Riemann sheet and we must therefore look for it on a lower Riemann sheet. But if such a pole lies on a lower Riemann sheet, then we should be extremely careful in assigning any attenuation property to the imaginary part of the complex phase velocity derived from such a pole location.

In §§ 8 and 9 we isolated the pseudo-Rayleigh wave and determined some of its properties. Although we have seen that these properties are almost identical with many of those of the true Rayleigh wave, we have not yet studied an actual limiting transition to the true Rayleigh wave. We have also yet to see why there is apparently no visible evidence of the existence of a pseudo-Rayleigh wave in figure 13 where we considered the propagation of elastic waves along a pitch/water interface; for, after all, a true Rayleigh wave can certainly propagate along the free surface of a semi-infinite medium of pitch. We should also like to be able to account for the existence of the pseudo-Rayleigh wave if we were to attempt a solution to the problem using an asymptotic method such as the saddle-point method of van der Waerden (1950). In this latter method the contour is distorted to surround all branch points and poles in quadrant IV of the top Riemann sheet of the $u$ plane; since the pseudo-Rayleigh wave does not directly arise from a pole or branch point contribution on the top Riemann sheet, it will have to be accounted for by its relation to the true Rayleigh pole.

The answer to all these questions is tied up with the migration of the true Rayleigh pole into a lower Riemann sheet when the free boundary of the semi-infinite solid is continuously transformed, by adding a fluid of increasing density, to the fluid/solid interface that we have studied. In line with our previous contention, the branch cuts are taken along the real $u$ axis from the branch points to infinity as in figure 9. The phase range of the radicals is again $-\mathrm{i}$ to $+\mathrm{i}$ with $-\mathrm{i}$ just above the cut on the top sheet. The locations of the true Rayleigh poles and the branch points in the $u$ plane are given in Tables 3 and 5.

In figures 19 *a* and *b* are illustrated the migration of the Rayleigh pole into the complex plane for iron/water and plaster of paris/water, respectively. Both poles starting as the true Rayleigh poles on the real $u$ axis migrate into quadrant IV of the $u$ plane. In doing so, they

pass on to the lower Riemann sheets of both of the radicals $\alpha$ and $\beta$. However, the poles remain on the top $\gamma$ sheet so that the convergence of integrals such as (4·13) is maintained. The migration of the poles is such that the real part of $u_R$ is continuously decreasing as the density ratio is continuously increasing. Thus, one cannot identify the $\mathscr{R}(u)$ with the ratio

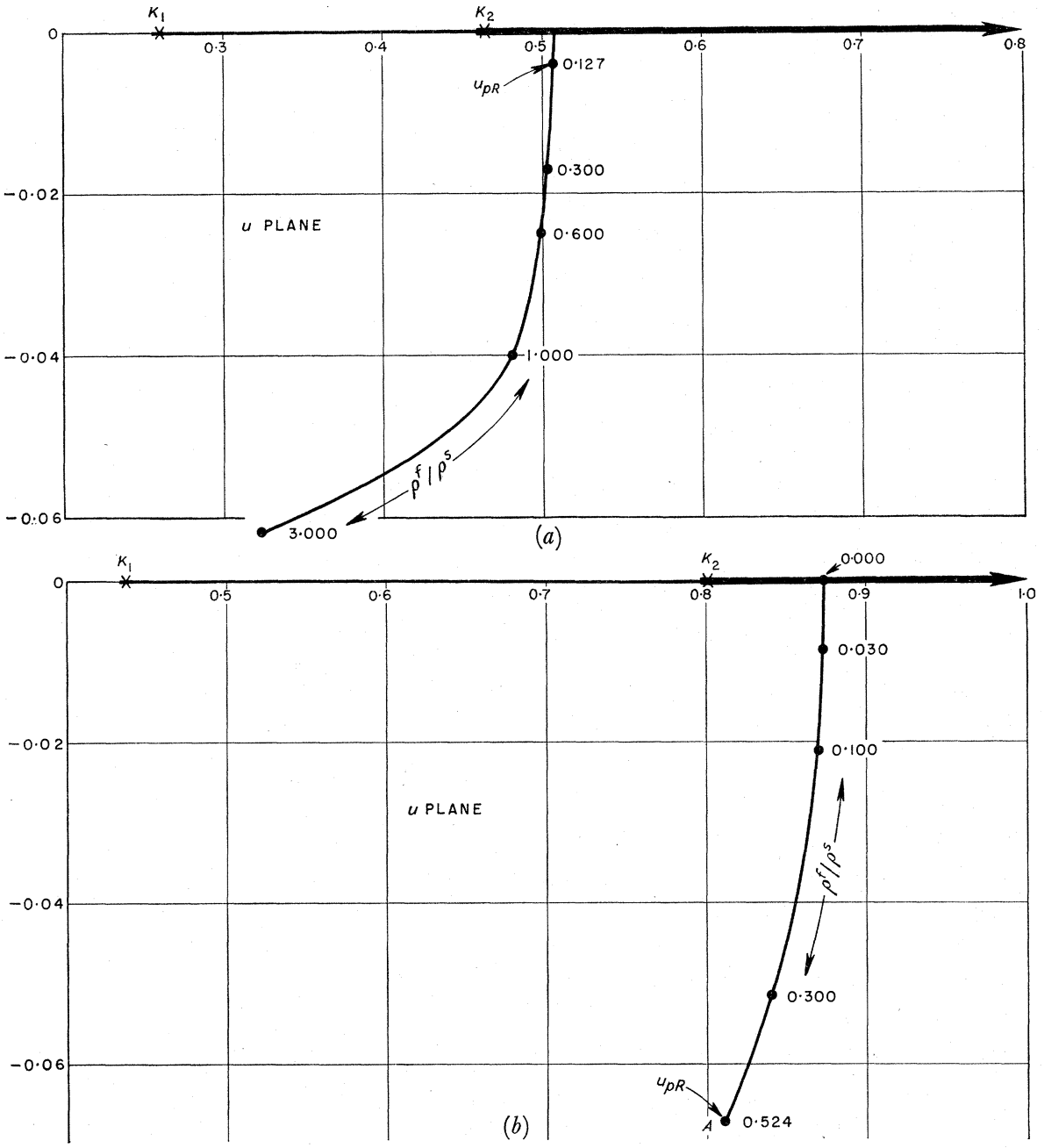


FIGURE 19. Migration of the Rayleigh pole into the complex plane: (*a*) For a water/iron interface, (*b*) for a water/plaster of paris interface.

$c/V_{pR}$. This is especially true in view of the fact pointed out in equation (5·1), that the point of zero amplitude on the pressure response curve associated with the pseudo-Rayleigh wave travels with exactly the true Rayleigh wave velocity of the solid and is independent of the existence of the fluid.

Although it is not rigorously valid to do so, it is tempting to follow other investigators such as Osborne & Hart (1945) and insert the value of $u_{pR}$ for the pseudo-Rayleigh poles into the exponent of the integrand of (4·13) in order to obtain some measure of the attenuation of harmonic pseudo-Rayleigh waves with distance. Our computations yield the results shown in table 7.

TABLE 7. LOCATION OF RAYLEIGH AND PSEUDO-RAYLEIGH POLES IN THE $u$ AND $\tau$ PLANES

| | iron/water | plaster of paris/water |
|---|---|---|
| $u_R = c/V_R$ | 0·500208 | 0·8714 |
| $u_{pR}$ | 0·499941 − i0·005456 | 0·812343 − i0·073604 |
| $\alpha$ | −0·006360 − i0·428834 | −0·0875176 − i0·684394 |
| $\beta$ | −0·014243 − i0·191494 | −0·238605 − i0·251028 |
| $\gamma$ | 0·866082 + i0·003149 | 0·596298 + i0·100271 |
| $\tau_{pR}$ | (39·1035 − i0·34274) $\mu$s | (58·7583 − i5·6355) $\mu$s |

From these values we obtain attenuation distances $x_d$ (in metres) along the interface of

$$\left.\begin{aligned} x_d = c/\omega\,|\mathscr{I}u| &= 43{,}716/f \text{ for iron/water,} \\ x_d = c/\omega\,|\mathscr{I}u| &= 3208/f \text{ for plaster of paris/water,} \end{aligned}\right\} \tag{10·1}$$

where $f$ is the frequency in cycles/second. Owing to the fact that the imaginary part of $\gamma$ is positive, the amplitude increases as we proceed into the liquid normally away from the interface. This increase is related to the radiation into the fluid by the harmonic pseudo-Rayleigh wave as it propagated along the interface. For pulsed excitation our calculations also show an increase as we proceed away from the interface, but the increase is terminated as soon as the condition $t_S < r_1/c$ of region $I_b$ is violated. This increase has been found to be in good agreement with a corresponding experimental measurement by Roever & Vining using the technique of part I. If we further make use of (4·15) to calculate $\partial z/\partial t$ for constant $x$, we find using pulsed excitation

$$\frac{\partial z}{\partial t} = -\frac{c}{\sqrt{\{1-(c/V_R)^2\}}}, \tag{10·2}$$

for the zero point at $u = u_R$. Using the data from table 7 we find values of 1732 and 3025 m/s for water/iron and water/plaster of paris, respectively. These velocities are again in good agreement with experimentally measured velocities by Roever & Vining.

We shall next attempt to carry out the same pole migration for a water/pitch interface as we did in figure 19 for iron and plaster of paris. Referring to table 3, we find that the true Rayleigh wave root for pitch is $u_R = c/V_R = 1{\cdot}588$ and $K_2 = 1{\cdot}497$. However, in gradually introducing a fluid of increasing density ratio $\rho^f/\rho^s$ the pole at $u_R = 1{\cdot}588$ rapidly migrates far into the complex plane so that it could not conceivably be associated with the origin of the pseudo-Rayleigh wave at the pitch/water interface. Therefore, a different approach will be tried. Since we know the location of the pseudo-Rayleigh pole for a water/plaster of paris interface ($u_{pR}$ in table 7), and since the essential difference here in these two solid media lies in their values of $K_2$, it is suggestive that we search for the $u_{pR}$ for a fluid/solid interface which has the values of $K_1$ and $\rho^f/\rho^s$ which are the same as water/plaster of paris and a value of $K_2$ which is equal to that for the water/pitch interface. This pole is easy to find and occurs at the point designated $B$ in figure 20 rather close to $u_{pR}$ for water/plaster of paris which is located at $A$. In order to arrive at the pseudo-Rayleigh pole for the water/pitch interface we

now need only to increase the value of $K_2$ from 0·8052 to 1·497. In doing so, the pole so to speak 'takes off' and migrates rapidly upward in the $u$ plane. At $C$ at about $K_2 = 1{\cdot}10$ the migration crosses the branch cut at about $u = 0{\cdot}805$. Note that as we increase $K_2$, the branch point for $K_2$ moves continuously to the right. Therefore, we are crossing the branch cut line to the left of the branch point at $u = K_2$; i.e. we are crossing only the branch cut associated with the branch point at $u = K_1$. Since we were initially on the lower $\alpha$, lower $\beta$, top $\gamma$ sheet, we must now be on the top $\alpha$, lower $\beta$, top $\gamma$ sheet. If we now increase $K_2$ from 1·10 to 1·497, then we arrive at the pseudo-Rayleigh pole for the water/pitch interface indicated $D$ in figure 20. The value of $u_{pR}$ at $D$ is

$$u_{pR} = 0{\cdot}8595 + i0{\cdot}2117. \tag{10·3}$$

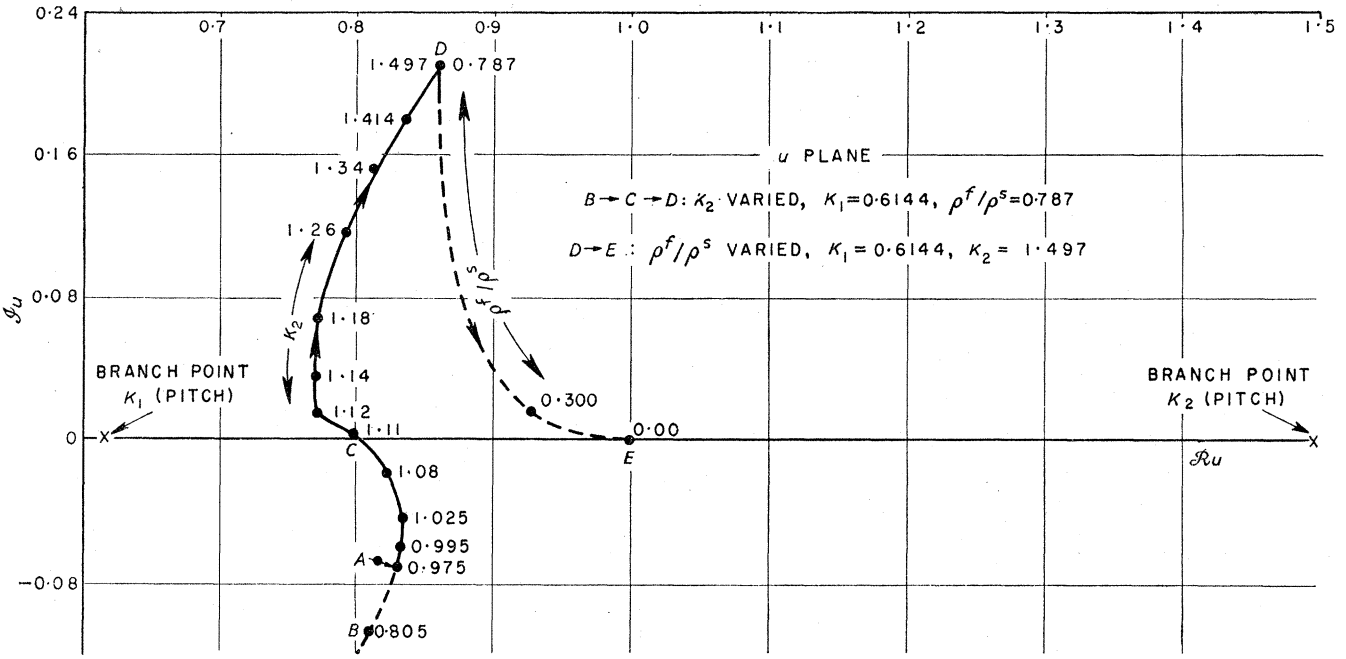


FIGURE 20. Further migration of the pseudo-Rayleigh pole in the complex $u$ plane.

If we attempt to establish an attenuation distance for water/pitch just as we did for the other interfaces in (10·1), then, owing to the fact that the imaginary part of $u_{pR}$ is positive, the amplitude of the wave associated with such a pole increases as the wave moves along the interface. This physically disagreeable result points out clearly the mistake that we can make in attributing a physical significance to a complex pole when it falls on a lower Riemann sheet. The imaginary part of $\gamma_{pR}$ is now negative yielding an exponential decay as we proceed normally away from the interface. Although this would describe the behaviour of the pseudo-Rayleigh wave for a water/pitch interface, as we stated earlier, the pressure response curve of figure 13 gives little indication of its existence. This may be due to the fact that the branch point at $K_2 = 1{\cdot}497$ is now sufficiently far removed from the $u_{pR}$ of (10·3) that according to the method of the saddle point (van der Waerden 1950), the effect of the pole on the function at the branch point is negligible.

Starting with the pole for the pitch/water interface at $D$, we can successively decrease the density ratio $\rho^f/\rho^s$ from 0·787 to the vanishing point. The pole then migrates along the path of figure 20 to $E$, terminating at the branch point for the reflected arrival at $u = 1$. We now

see that the pole at $D$ was no longer a pseudo-Rayleigh pole since it was closer to the branch point at $u = 1$ than to the branch point at $u = K_2$. This change in character of the pole as it migrated across the real $u$ axis at $C$ was unexpected, and is in keeping with the conclusion that wave propagation along a simple fluid/solid interface is not nearly as simple as it was generally thought to be.

Since we have now lost the pseudo-Rayleigh pole as far as it may be used to account for the existence of the true Rayleigh wave on a pitch boundary, the conclusion is inescapable that it is the Stoneley wave that becomes the true Rayleigh wave when the density ratio $\rho^f/\rho^s$ for case 1 $[b < (r_1/x)\, c]$ is made to vanish. This result is consistent with the limiting velocity behaviour of the Stoneley wave velocity for vanishing $\rho^f/\rho^s$ as can be seen from figure 8 *a* and *b* of the Stoneley wave charts of Strick & Ginzbarg (1956).

## 11. Discussion of results

We have seen that the pseudo-Rayleigh wave has the wave-form and retrograde motion of the true Rayleigh wave. Its zero also travels along the interface with exactly the true Rayleigh wave velocity of the solid as though the fluid were not present. In addition, in those liquid-solid systems where it is observable, it goes over into a true Rayleigh wave if the fluid density is made to vanish.

On the other hand, we have seen that certain properties consistent with radiation into the fluid are evident. The amplitude increases as we proceed normally away from the interface in much the same way as does the critically refracted $P$ wave. There exists a velocity of propagation normal to the interface which is also in agreement with experiment. Another interesting radiation property of the pseudo-Rayleigh wave follows from its arrival time formula. Since the arrival time $t_{pR}$ is defined by the vanishing of the pressure amplitude in region $I_b$ which in turn occurs when $u = u_R = c/V_R$, we can obtain $t_{pR}$ by direct substitution into (4·15):

$$t_{pR} = \frac{x}{V_R} + \frac{2H - z}{c} \sqrt{\left\{1 - \left(\frac{c}{V_R}\right)^2\right\}}. \tag{11·1}$$

But (11·1) has the form of the minimum-time formula (4·16) for the critically refracted $P$ and $S$ waves. Thus, if we consider the path of figure 21 which is incident upon the solid at an angle $\theta_0 = \sin^{-1}(c/V_R)$ and travels along the interface with the true Rayleigh wave velocity of the solid, then we have tagged a point on the wave-form that as far as measurement in the fluid is concerned has one of the essential properties of a critically refracted wave. Of course, the true Rayleigh wave velocity is not a body velocity, but if one were for some reason not to know the body velocities, then, owing to the constancy of $V_R$ along the interface, he could easily come to the conclusion that he was observing the arrival of a critically refracted wave. We can make a similar statement about the point $t_0$ which arrives, according to equation (5·3), after travelling along the interface with a velocity of $\sqrt{2}$ times the shear wave velocity $b$.

In summarizing, we find that from measurement made on the solid one would be led to think of the pseudo-Rayleigh arrival as a modified true Rayleigh wave. On the other hand, measurement in the fluid would yield properties of critically refracted wave propagation. For this reason, it would perhaps be more proper to call the arrival a radiating Rayleigh wave rather than a pseudo-Rayleigh wave.

In the experimental investigation in part I, Roever & Vining had only a pressure detector suitable for use in recording the response curves. They were therefore able to make measurements only in the fluid and initially came to the tentative conclusion that what we have called a pseudo-Rayleigh arrival was actually a critically refracted $S$ wave. This, of course, led to a difficulty in picking the arrival time of the critically refracted $S$ wave since the parameters of (4·16$b$) were accurately known.

We have discussed in great detail the existence of the pseudo-Rayleigh wave, but up to now we have carefully avoided any reference to the actual existence of a critically refracted $S$ wave. There is no prominent feature in figures 14, 15, 16, that we can readily identify with such a critically refracted wave. However, in figure 17$a$ we do observe in the horizontal velocity response an abrupt change in the slope of the response about $t = t_S$. From an accurate detailed expansion calculation of the response about $t = t_S$ on this curve it has been concluded that a critically refracted $S$ wave of the order of magnitude of the critically refracted $P$ wave appears to exist, but for our distance ratio $(2H-z)/x$ it cannot be isolated from the pseudo-Rayleigh wave. For a radially symmetric line source it is an unimportant contribution.

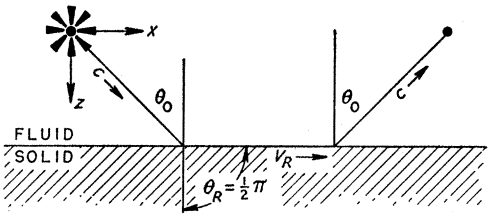


FIGURE 21. The apparent minimum time path of the pseudo-Rayleigh arrival.

Mathematically speaking, the essential difference between a pseudo-Rayleigh wave and a true Rayleigh wave is that the former arises from a pole in the complex $u$ plane, whereas the latter arises from a pole on the real axis of that plane. An interesting situation exists when we consider the parameters associated with the location of the pseudo-Rayleigh pole on the real $u$ axis at $C$ in figure 20. We have $K_1 = 0{\cdot}6144$, $K_2 \approx 1{\cdot}10$, $\rho^f/\rho^s = 0{\cdot}787$ with the pole at $u_{pR} \approx 0{\cdot}805$. Unlike that of the true Rayleigh wave, our pole lies between $K_1$ and $K_2$ rather than to the right of both of the branch points. Also, it lies on the top $\alpha$, lower $\beta$, top $\gamma$ sheets, i.e. on the lower $\beta$ rather than the upper $\beta$ sheet. Therefore, we cannot expect to find a true Rayleigh wave with these parameters. The most striking feature we have observed on the pressure response curve arising from this region of the $u$ axis between $K_1$ and $K_2$ was the zero point $t_0$ on the response curve which came from $u = K_2/\sqrt{2}$. Notice how closely the above parameters for the point $C$ fit this condition. It is suggestive that we assume this condition to hold at the point $C$ and find out if the Stoneley wave equation yields a root on the real $u$ axis of the top $\alpha$, lower $\beta$, top $\gamma$ Riemann sheet. In appendix 7 we see that such will be the case if the further condition

$$u = \frac{K_2}{\sqrt{2}} = \frac{1}{\sqrt{\{1+(\rho^f/\rho^s)^2\}}}, \tag{11·2}$$

is satisfied. For $K_2$ to be less than unity this condition requires that $\rho^f/\rho^s$ be greater than unity. Such a requirement is not met for most fluid/solid media. As we shall see in a moment, this does, however, lead to an interesting limiting condition. Referring again to appendix 7 we

see that there are three other pairs of roots of the Stoneley wave equation all at the point described by equation (11·2), but on different Riemann sheets. Because of the highly singular nature of the region about $u = K_2/\sqrt{2}$ it was decided to study, for example, the pressure wave-form as the density ratio is increased from a small value through a value consistent with (11·2). Use of the same velocity parameters as for the water/iron interface of table 5 and increasing the density ratio $\rho^f/\rho^s$ in ratio steps of 2·185 from 0·127 to 6·3206 gives the set of pressure wave-forms shown in figure 22. It is quite evident that the pressure

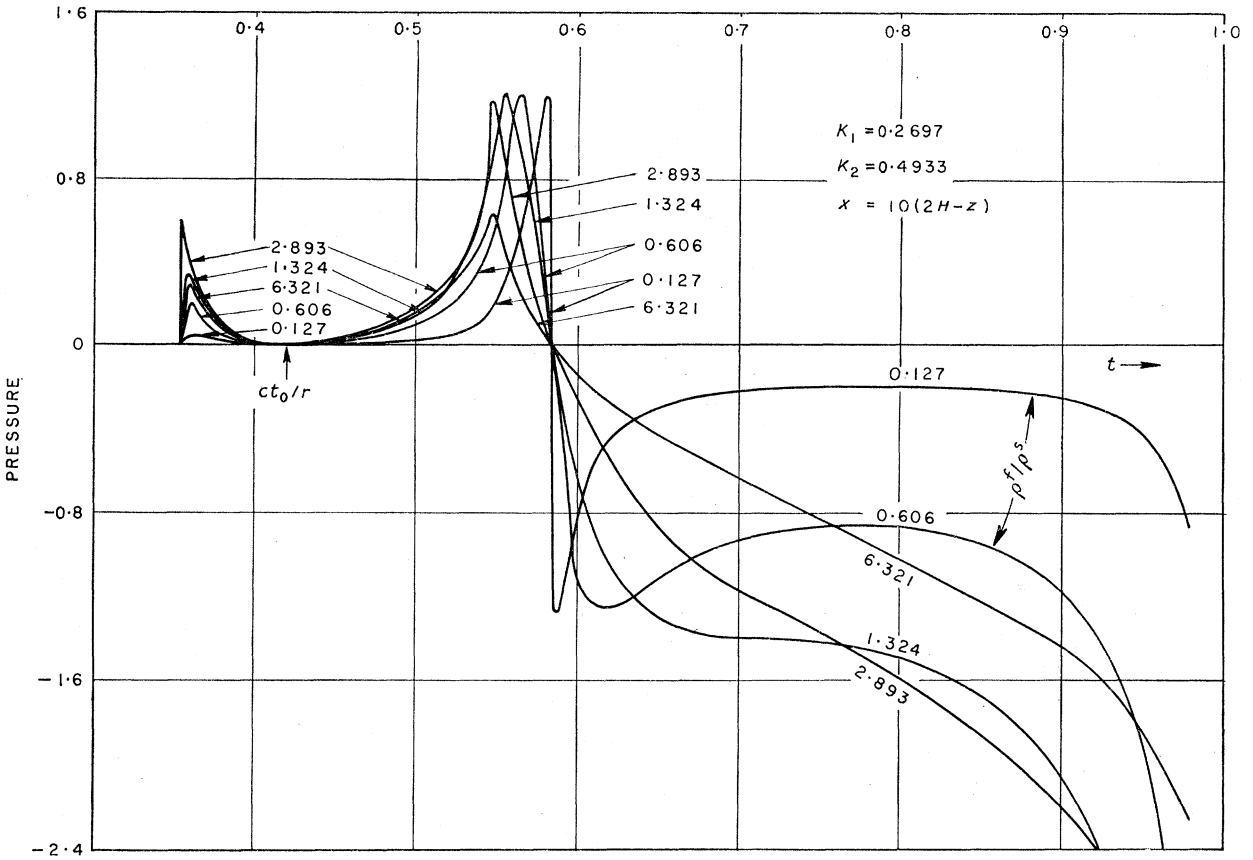


FIGURE 22. Pressure wave-forms showing the apparent maximizing property of equation (11·2) for $\rho^f/\rho^s = 2{\cdot}893$.

wave-form (for $\rho^f/\rho^s = 2{\cdot}185$) that is consistent with (11·2) covers for the most part a larger area for all time up to the direct arrival than the neighbouring curves. Although we have not studied the corresponding behaviour of the wave-form in region II which comes after the reflexion, there is an indication from the large negative swing of the beginning of the Stoneley wave just before the direct arrival that region II also goes through some similar kind of maximizing behaviour.

We have shown that the contribution of the pseudo-Rayleigh wave to the total response arises from a pole which lies on a lower Riemann sheet. When this pole is near the real axis of the $u$ plane, the integrand of integrals such as (4·13) is sufficiently affected to cause the resulting pseudo-Rayleigh wave-form when a solution is obtained using the technique of Cagniard. Since this pole is not on a top Riemann sheet, the question naturally arises how could we obtain its contribution if we were to use an asymptotic method of solution. There

are many formulations of the asymptotic method; we shall use that form developed by van der Waerden (1950). For example, reintroduce $\omega = -is$ and the harmonic factor $e^{i\omega t}$ into (4·21). In order to avoid confusion let the integration variable be designated $\xi$. Then orient the co-ordinate system to agree with van der Waerden's by introducing the change of variable to the $\xi$ plane by $\xi = i\tau$. In the $\xi$ plane the branch cuts and Stoneley pole are now on the positive imaginary axis. Following van der Waerden we move the cuts so that they proceed from the respective branch points along a path parallel to the positive real $\xi$ axis to infinity. The contour is then distorted to surround the branch cuts and Stoneley pole in the manner shown in figure 23.

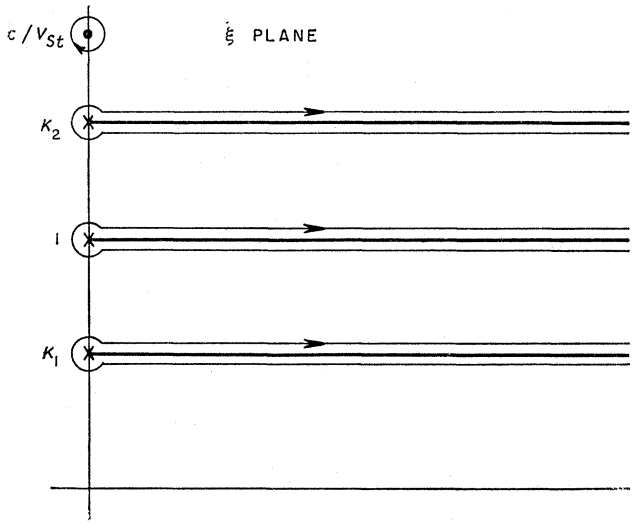


FIGURE 23. Choice of branch cuts and distortion of contour suitable for asymptotic solution.

Now in this distortion of the branch cuts the range of phase of the radicals defining the top sheets of $\alpha_t$, $\beta_t$ and $\delta$ is a variable quantity, being $-135$ to $+45°$ in the vicinity of the branch points and continuously changing to the range $-180$ to $0°$ as we move out to infinity along the cut. After the branch cuts have been moved, the result of appendix 5 that only the Stoneley poles appear on the top Riemann sheet is not necessarily valid. It is entirely possible that the pseudo-Rayleigh poles now can appear on the top sheet. Referring to table 7 we find from the complex values of $\alpha_t$ and $\beta_t$ at the pseudo-Rayleigh pole that the phase of $\alpha_t$ is $-90·9°$ and $\beta_t$ is $-94·25°$ for an iron/water interface and that the phase of $\alpha_t$ is $97·3°$ and $\beta_t$ is $-133·5°$ for a plaster of paris/water interface. Therefore the pseudo-Rayleigh pole for these two interfaces lies on the top Riemann sheet and must be accounted for in an asymptotic solution in exactly the same manner as the Stoneley pole. The contribution will appear with an exponential factor

$$\exp\{i\omega(t-t'_{pS})\}, \tag{11·3}$$

where $t'_{pS}$ is listed in table 7. Since we saw in figure 19 and table 7 the real part of $u_{pR}$ is not equal to $c/V_R$, the harmonically excited pseudo-Rayleigh wave does not travel along the interface with exactly the true Rayleigh wave velocity of the free boundary semi-infinite solid. On the other hand, we saw in §4, equation (4·29), that for a delta-function excitation the pseudo-Rayleigh wave does indeed travel with a velocity $V_R$.

Although the phases of the radicals $\alpha_t$ and $\beta_t$ put the location of the pseudo-Rayleigh pole on the top Riemann sheet for both iron and plaster of paris, the phase of $\beta_t$ for the plaster of paris/water interface puts it rather close to the new branch cut for $\beta_t$. Referring to figure 19*b* we see that the real part of the pseudo-Rayleigh pole is only slightly greater than $K_2$ when $\rho^f/\rho^s = 0{\cdot}524$ and that it would require only a slight increase in $\rho^f/\rho^s$ to make the real part of $u_{pS}$ less than $K_2$. Distorting the branch cut $\beta$ to an asymptotic form as before would now leave the pseudo-Rayleigh pole on the lower Riemann sheet for $\beta$. Under this condition the contribution of the pseudo-Rayleigh pole to the total response would appear in a different way. Although we have discussed this point in the original $u$ plane, the same argument should hold if we were to apply it in the $\xi$ plane.

In order to see how the location of the pseudo-Rayleigh pole on the lower $\beta_t$ sheet would affect the response, let us consider just the contribution from that part of the contour which surrounds the branch cut for $\beta_t$. The branch point is at $\xi = it_S$ where $t_S$ is given by (4·16*b*). In order to obtain the contribution from that part of the contour about the branch cut, van der Waerden expands the integrand into an equivalent Laurent series about the branch point at $\xi_S = \mathrm{i}t_S$. Thus, if our integral is of the form

$$I = \int_{C_s} P(\xi)\, \mathrm{e}^{-\omega\xi}\, \mathrm{d}\xi \quad (\omega > 0), \tag{11·4}$$

where the contour $C_S$ refers to the contour about the branch cut, then the expansion

$$P(\xi) = \sum_{n=-1,\,0} b_n (\xi - \mathrm{i}t_S)^{\frac{1}{2}n} \tag{11·5}$$

leads to the asymptotic solution

$$I = 2\, \mathrm{e}^{\mathrm{i}\omega(t-t_S)} \sum_{n=0,\,1,\,2}^{\infty} b_{2n-1} \frac{\Gamma(n+\frac{1}{2})}{\omega^{n+\frac{1}{2}}} + K, \tag{11·6}$$

where

$$b_{2n-1} = \frac{1}{4\pi\mathrm{i}} \int_{\mathrm{d.c.}} \frac{P(\xi)\, \mathrm{d}\xi}{(\xi - \mathrm{i}t_S)^{n+\frac{1}{2}}}, \tag{11·7}$$

and $K$ is given by van der Waerden. In the integral (11·7) the contour d.c. refers to a double circle about the branch point at $\xi = \mathrm{i}t_S$, i.e. over both Riemann sheets associated with the branch point. The radius of the d.c. is that of the largest circle about $\xi = \mathrm{i}t_S$ which does not touch the nearest other singular point on the top Riemann sheet of the $\xi$ plane. The contour d.c. can, however, include singularities on the lower $\beta_t$ sheet. Our pseudo-Rayleigh pole is just such a singularity. But according to (11·6) the propagation will appear in the form

$$\exp\{\mathrm{i}\omega(t - t_S)\}, \tag{11·8}$$

as compared with (11·3). Thus, the pseudo-Rayleigh arrival now appears as a distortion of the $S$-head wave at $t_S$ rather than as an independent arrival at $t = \mathscr{R}(t'_{pR})$.

We now also see why the pseudo-Rayleigh wave is not observed for a pitch/water interface, for then the pseudo-Rayleigh pole always remains on the lower Riemann sheet after the branch cut is moved. Referring to figure 10*a* under the ninety-degree rotation, introduced by the variable $\xi = \mathrm{i}t$, we see that $\mathrm{i}t_S$ is itself not on the imaginary axis so that $t_S$ in the exponent of (11·6) is complex. Thus, the $S$-head wave as distorted by the pseudo-Rayleigh pole is rapidly damped out.

In the course of preparing this paper and the Stoneley wave charts (Strick & Ginzbarg 1956), it became apparent that one might be able to utilize the arrival times of the pseudo-Rayleigh and Stoneley waves to determine *in situ* the shear modulus $\mu = \rho^s b^2$ of the solid medium as a function of other known parameters of the system.

In all response curves the compressional body velocity, $a$, would be determined from $t_P$ by means of formula (4·16$a$). $\rho^f/\rho^s$ would be an intelligent guess. One might be able to make use of a strong dependence of the period of the pseudo-Rayleigh wave on $\rho^f/\rho^s$ in order to make this guess.

By means of 'series $b$' of the Stoneley wave charts we can readily determine $b/c$ as a function of $\sigma$, $\rho^f/\rho^s$ and $V_{St}/b$. Again, for fixed $x$ and $2H-z$ we can use (11·1) to obtain $V_R$ as

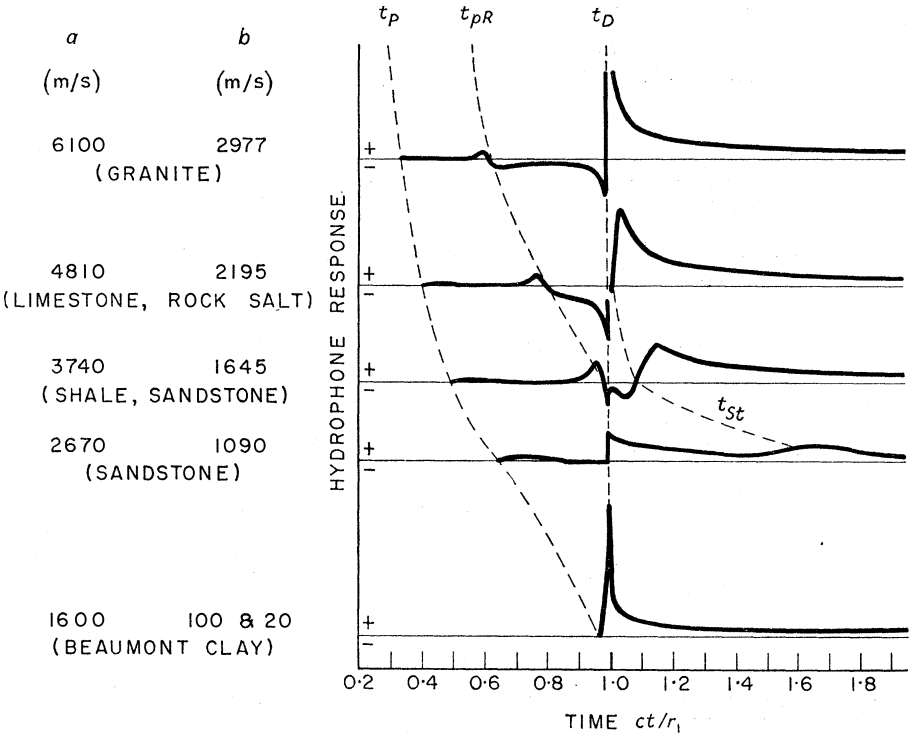


FIGURE 24. Pressure response curve for idealized rock media.

a function of $\sigma$, $\rho^f/\rho^s$ and $t_{pR}$ so that the shear wave velocity $b$ can be uniquely determined from $V_R$ by the Rayleigh cubic equation. In order to clarify this procedure we have prepared figures 24 and 25 which illustrate the complete wave-forms in both pressure and vertical particle velocity that one can observe over a wide range of idealized rock media.

Although in principle one could use either detector for such a determination of the rigidity, the vertical velocity detector located on the interface seems to give rise to Stoneley waves whose amplitude is almost independent of the body velocities of the solid and for this reason seems to be the preferable of the two to use. Therefore, we shall restrict our discussion to the vertical particle velocity response of figure 25. Therein the period of the Stoneley wave seems to be almost inversely proportional to the shear wave velocity $b$. It is evident from these curves that for case 2 media where the pseudo-Rayleigh wave does not exist we can use the arrival time of the peak of the Stoneley waves from which we can calculate $b$ and therefore $\mu$. On the other hand, for case 1 media the Stoneley wave is coming in almost on

top of the direct and reflected waves and cannot be used. The zero of the pseudo-Rayleigh wave is always easy to locate and it can be used to determine $b$ and $\mu$. There is an overlap region where $b \approx (r_1/x)\, c$ where both interface waves appear and either may be so utilized.

In the above discussion, as elsewhere in this report, we have made the assumption that $V_{St} = x/t_{St}$. This is not strictly true. For example, the motion of the point determined by the vanishing of the numerator of (4·28), which is not equivalent to the Stoneley wave equation for a fluid/solid interface, is a rather involved expression since the intermediate variable $u$ is complex. However, for $x \gg 2H - z$ the variable $u$ approaches real values and the assumption above is a good approximation.

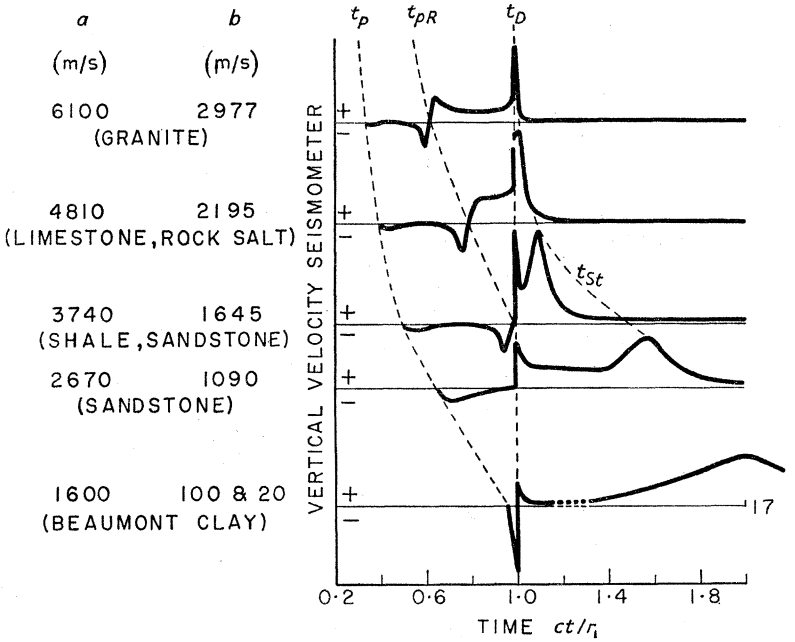


FIGURE 25. Vertical particle velocity response curves for idealized rock media.

## 12. CONCLUSIONS

The wave-form variation in region $I_b$ of figure 14 of part II which was therein hypothesized to be a superposition of pseudo-Rayleigh, Stoneley, and critically refracted $S$ waves has been investigated and the hypothesis verified. The existence of the pseudo-Rayleigh wave at a water/solid interface as exemplified by figure 17 $a$ is in direct contradiction to a statement of Cagniard (1939) at the beginning of chapter XIV of his book. Although Cagniard calls both pseudo-Rayleigh and Stoneley waves by the single designation of Rayleigh waves, he is therein referring to our pseudo-Rayleigh wave. Scholte (1949) in agreeing with Cagniard points out that only the Stoneley wave will exist for fluid density greater than that of air. Our conclusion, as we have found in figure 16, is that both types of Rayleigh waves can be important at a fluid/solid interface.

The origin of the pseudo-Rayleigh wave from a pole off the axis on a lower Riemann sheet points out the importance of the contribution of complex poles on lower Riemann sheets, that are so often ignored by investigators, to the complete solution of a wave propagation problem. In accord with this conclusion, it is also shown that the location of other poles on lower Riemann sheets is possibly associated with a maximization of the amplitude of the total response.

The evaluation of the phase velocities of the pseudo-Rayleigh and Stoneley waves from their arrival times, and the respective relations of these velocities to the rigidity of the solid medium and other parameters of the elastic system, imply that it might be possible to make use of such a scheme to determine the rigidity *in situ* of the bottom sediments in water-covered areas.

The present experimental and theoretical study of the existence of the pseudo-Rayleigh wave as illustrated by figure 15 should aid in clarifying the work of many experimenters. For example, Weinstein (1952) in an experimental study of the reflexion of a narrow ultrasonic beam from a water/aluminum interface finds a strong disagreement with plane wave theory for angles of incidence of about 30°. From our investigation we should expect such a narrow beam to excite a pseudo-Rayleigh wave which according to our figure 21 should occur at just about 30°. In another experiment O'Brien (1955) in observing the wave-form for a water/concrete interface interprets as a critically refracted $S$ wave an arrival that we are inclined to reinterpret as a pseudo-Rayleigh wave.

The authors of Part I would like to extend their appreciation to C. van der Poel of the Laboratory N.V. De Bataafsche Petroleum Maatschappij. Amsterdam who first suggested to us the possibility of utilizing pitch as a medium for studying elastic wave propagation at high frequencies.

The authors would like to express their deepest appreciation to Dr A. S. Ginzbarg for the many illuminating discussions which contributed to the conclusions reached in this paper. They would also like to express their thanks to Mr A. E. Perry for his instrumentation work in part I and to Miss E. E. Allen for machine programming and computational work for parts II and III.

## Appendix 1. The delta-function-excited line source

The simple boundary-value problem for a cylindrical source of radius $r_0$ is given by the wave equation or its transform

$$\left(\nabla^2-\frac{1}{c^2}\frac{\partial^2}{\partial t^2}\right)p_0^f(r,t)=0,\quad \left(\nabla^2-\frac{s^2}{c^2}\right)\bar{p}_0^f(r,s)=0, \tag{A 1·1}$$

subject to the boundary conditions

$$p_0^f(r_0,t)=\mathbf{H}(t-0)=\begin{cases}0 & \text{for}\quad t<0,\\ 1 & \text{for}\quad t>0,\end{cases} \tag{A 1·2$a$}$$

$$p_0^f(\infty,t)=0. \tag{A 1·2$b$}$$

The Laplace transform of (A 1·1) because of (A 1·2$b$) has the convergent solution

$$\bar{p}_0^f(r,s)=A(s)\,K_0(rs/c)\quad (r\geqslant r_0), \tag{A 1·3}$$

where $A(s)$ is determined by (A 1·1). Since the $s$-multiplied transform of $\mathbf{H}(t-0)$ is 1, we have

$$A(s)=\frac{1}{K_0(r_0s/c)}. \tag{A 1·4}$$

Inverting $\bar{p}_0^f(r,s)$ by means of the Mellin inversion theorem we obtain

$$p_0^f(r;\text{step})=\frac{1}{2\pi i}\int_{-i\infty}^{+i\infty}\frac{ds}{s}\frac{K_0(sr/c)}{K_0(sr_0/c)}\,e^{st}. \tag{A 1·5}$$

In particular, for $s = \mathrm{i}\omega$ we have the harmonic form

$$p_0^f(r; \mathrm{e}^{\mathrm{i}\omega t}) = \frac{1}{2\pi\mathrm{i}} \int_{-\infty}^{+\infty} \frac{\mathrm{d}\omega}{\omega} \frac{H_0^{(2)}(\omega r/c)}{H_0^{(2)}(\omega r_0/c)} \mathrm{e}^{\mathrm{i}\omega t}. \tag{A 1·6}$$

If

$$\frac{1}{2\pi\mathrm{i}} \int_{-\infty}^{+\infty} \frac{\mathrm{d}\omega}{\omega}$$

is to be considered as the step operator, then the harmonic response to a line source must be given by

$$p_0^f(r; \text{step}) = \frac{1}{2\pi\mathrm{i}} \int_{-\infty}^{+\infty} \frac{\mathrm{d}\omega}{\omega} \frac{H_0^{(2)}(\omega r/c)}{H_0^{(2)}(\omega r_0/c)} \mathrm{e}^{\mathrm{i}\omega t}. \tag{A 1·7}$$

This form is, however, much too complicated to use as a source function because of the presence of the Hankel function in the denominator. It is customary to make the assumption that $r_0$ is sufficiently small that

$$\omega \ll \lim_{r_0 \to 0} \left(\frac{c}{r_0}\right), \tag{A 1·8}$$

for all $\omega$. We then obtain the form (3·3)

$$p_0^f(r; \mathrm{e}^{\mathrm{i}\omega t}) = -\tfrac{1}{2}\pi\mathrm{i} P_0 H_0^{(2)}(\omega r/c)\, \mathrm{e}^{\mathrm{i}\omega t}. \tag{3·3}$$

Application of the step-and delta-function operators lead to (3·5) and (3·6), respectively

$$p_0^f(r; \text{step}) = P_0 \cosh^{-1}(ct/r)\, \mathbf{H}(t - r/c), \tag{3·5}$$

$$p_0^f(r; \text{delta}) = P_0 \frac{c}{r} \frac{\mathbf{H}(t - r/c)}{\sqrt{\{(ct/r)^2 - 1\}}}. \tag{3·6}$$

Lord Rayleigh (1888) derived the harmonic form (3·3) by considering the line source to be a superposition of harmonic point sources of the form

$$P_0 \frac{\exp\{-\mathrm{i}(\omega/c)\sqrt{(r^2+y^2)} + \mathrm{i}\omega t\}}{\sqrt{(r^2+y^2)}}, \tag{A 1·9}$$

distributed along the $y$ axis normal to the plane of figure 6; i.e.

$$p_0^f(r; \mathrm{e}^{\mathrm{i}\omega t}) = P_0 \int_{-\infty}^{+\infty} \mathrm{d}y \frac{\exp\{-\mathrm{i}(\omega/c)\sqrt{(r^2+y^2)} + \mathrm{i}\omega t\}}{\sqrt{(r^2+y^2)}}. \tag{A 1·10}$$

We can modify this derivation by considering the coefficient of $\mathrm{e}^{\mathrm{i}\omega t}$ in (A 1·9) with $s = \mathrm{i}\omega$ to be the transform of the response to a step-function-excited line source:

$$p_0^f(r; \text{step}) = 2P_0 \mathscr{R} \int_0^{\infty} \mathrm{d}y \frac{\exp\{-(s/c)\sqrt{(r^2+y^2)}\}}{\sqrt{(r^2+y^2)}}. \tag{A 1·11}$$

Let

$$c^2\tau^2 = r^2 + y^2, \tag{A 1·12}$$

so that in the $\tau$ plane

$$\bar{p}_0^f(r; \text{step}) = 2\frac{P_0 c}{r} \mathscr{R} \int_0^{\infty} \mathrm{d}\tau \frac{\mathrm{e}^{-s\tau} \mathbf{H}(\tau - r/c)}{\sqrt{\{(c\tau/r)^2 - 1\}}}. \tag{A 1·13}$$

Because we are using the $s$-multiplied Laplace transform, we need to have a factor $s$ multiplying the integral (A 1·13) if we are to compare that integral with the definition of the transform. Therefore, on multiplying through by $s$ we have

$$s\bar{p}_0^f(r; \text{step}) = 2P_0 \frac{sc}{r} \int_0^{\infty} \mathrm{d}\tau \frac{\mathrm{e}^{-s\tau} \mathbf{H}(\tau - r/c)}{\sqrt{\{(c\tau/r)^2 - 1\}}}. \tag{A 1·14}$$

The left-hand side of (A1·14) is simply the transform to the response to a delta-function excitation. We can now invert the transform and on applying the uniqueness theorem to identify $\tau$ with the time $t$ we arrive at equation (3·6).

## Appendix 2. Application of the method of Cagniard to the line-source integral

The transform $\bar{p}_0^f$ of the response to a step-function excitation of the line source is given by (3·16)

$$\bar{p}_0^f(x,z;\text{step}) = \frac{P_0}{2\mathrm{i}}\int_{-\mathrm{i}\infty}^{+\mathrm{i}\infty}\frac{\exp\{-s(qx+\Gamma z)\}}{\Gamma}\,\mathrm{d}q, \tag{3·16}$$

where $\Gamma$ was defined in (3·15$a$). Introducing as in (4·9) the variable $u$ by $u = cq$ we find (this step is not necessary here but is included so as to make formal comparison with the development in §4 easier):

$$\bar{p}_0^f(x,z;\text{step}) = \frac{P_0}{2\mathrm{i}}\int_{-\mathrm{i}\infty}^{+\mathrm{i}\infty}\frac{\exp\{-(s/c)\,(ux+\gamma z)\}}{\gamma}\,\mathrm{d}u. \tag{A2·1}$$

Now let
$$\tau = \frac{ux}{c}+\frac{\gamma z}{c}, \tag{A2·2}$$

from which
$$u = u(\tau) = \frac{c\tau}{r}\frac{x}{r}-\frac{z}{r}\delta_0, \tag{A2·3}$$

$$\gamma = \frac{c\tau}{r}\frac{z}{r}+\frac{x}{r}\delta_0, \tag{A2·4}$$

and
$$\frac{\mathrm{d}u}{\gamma} = \frac{c\,\mathrm{d}\tau}{r\delta_0}, \tag{A2·5}$$

where
$$\delta_0 = \sqrt{\{1-(c\tau/r)^2\}}, \tag{A2·6}$$

and
$$r = \sqrt{(x^2+z^2)}. \tag{A2·7}$$

In the $\tau$ plane the integral (A2·1) becomes

$$\bar{p}_0^f(r;\text{step}) = \frac{P_0 c}{2\mathrm{i}r}\int_C \frac{\mathrm{e}^{-s\tau}}{\delta_0}\,\mathrm{d}\tau, \tag{A2·8}$$

where the branch point at $u = 1$ has been replaced by one at $\tau = r/c$. The cut in the $\tau$ plane for $\delta_0$ is taken to be $(r/c,\infty)$ and just as in §4 the contour $C$ can be distorted to hug both sides of this cut. Since $\delta_0$ below the cut is complex conjugate to that above the cut, we can write

$$\bar{p}_0^f(r;\text{step}) = \frac{P_0 c}{r}\int_{r/c}^{\infty}\mathscr{I}\left(\frac{\mathrm{e}^{-s\tau}}{\delta_0}\right)\mathrm{d}\tau. \tag{A2·9}$$

The variable $\tau$ is now positive real and may therefore be replaced by the time variable $t$. Also, since $\delta_0$ has an imaginary part only for $t > r/c$, we can extend the lower limit to zero by inserting the factor $\mathbf{H}(t-r/c)$ and obtain

$$\bar{p}_0^f(r;\text{step}) = \frac{P_0 c}{r}\int_0^{\infty}\frac{\mathbf{H}(t-r/c)\,\mathrm{e}^{-st}}{\delta_0}\,\mathrm{d}t. \tag{A2·10}$$

In order to make a comparison with the definition of the $s$-multiplied Laplace transform we need to multiply through by $s$ so that

$$s\bar{p}_0^f(r;\,\text{step}) = s\frac{P_0 c}{r}\int_0^\infty \frac{\mathbf{H}(t-r/c)\,\mathrm{e}^{-st}}{\delta_0}\,\mathrm{d}t, \tag{A2·11}$$

from which since the elastic system is initially quiescent it follows that

$$p_0^f(r;\,\text{delta}) = \frac{P_0 c}{r}\frac{\mathbf{H}(t-r/c)}{\sqrt{\{1-(ct/r)^2\}}}, \tag{A2·12}$$

which is identical with (3·6).

## Appendix 3. Reduction of the $K_0$ form of the Sommerfeld integral for the point source to its radially symmetric solution

Consider the integral (3·27)

$$\bar{p}_0^f(\text{step}) = \pm\mathrm{i}\frac{P_0 s}{\pi}\int_{-\mathrm{i}\infty}^{+\mathrm{i}\infty} K_0(sq\rho)\exp\left(-s\Gamma|z|\right)\frac{q}{\Gamma}\mathrm{d}q, \tag{3·27}$$

where $\Gamma$ was defined after (3·21). $K_0(sq\rho)$ has the well-known integral representation

$$K_0(sq\rho) = \int_0^\infty \exp\left(-sq\rho\cosh\eta\right)\mathrm{d}\eta. \tag{A3·1}$$

Introduce just as in appendix 2 the variable $u$ by $u = cq$, $\gamma = c\Gamma$, and also designate

$$X = \rho\cosh\eta, \tag{A3·2}$$

so that the transformation

$$\tau = \frac{uX}{c} + \frac{\gamma|z|}{c}, \tag{A3·3}$$

is analogous to (A2·2). Then, just as in appendix 2

$$u = \frac{c\tau}{R_1}\frac{X}{R_1} - \frac{|z|}{R_1}\delta_1, \tag{A3·4}$$

$$\gamma = \frac{c\tau}{R_1}\frac{|z|}{R_1} + \frac{X}{R_1}\delta_1, \tag{A3·5}$$

and

$$\frac{\mathrm{d}u}{\gamma} = \frac{c}{R_1}\frac{\mathrm{d}\tau}{\delta_1}, \tag{A3·6}$$

where

$$\delta_1 = \sqrt{\{1-(c\tau/R_1)^2\}}, \tag{A3·7}$$

and

$$R_1 = \sqrt{(z^2+X^2)}. \tag{A3·8}$$

In the $\tau$ plane the integral (3·27) becomes

$$\bar{p}_0^f(R;\,\text{step}) = \pm\frac{\mathrm{i}sP_0}{\pi R_1}\int_C \mathrm{d}\tau\int_0^\infty \mathrm{d}\eta\,\frac{u\mathrm{e}^{-s\tau}}{\delta_1}. \tag{A3·9}$$

We continue to follow the development in appendix 2 in distorting the contour around the cut and refer the integrand to the upper side of the cut where $\delta_1$ is negative imaginary.

$\tau$ is now positive real and may be identified with the time $t$, and the integration over $t$ identified with the definition of the $s$-multiplied Laplace transform

$$p_0^f(R;\text{step}) = \mp\frac{2P_0}{\pi R_1}\int_0^\infty \mathrm{d}\eta\, \mathscr{I}\left(\frac{u}{\delta_1}\right)\mathbf{H}(t-R_1/c), \tag{A 3·10}$$

or

$$p_0^f(R;\text{step}) = \mp\frac{2P_0}{\pi}\int_0^\infty \frac{\mathrm{d}\eta}{R_1}\mathscr{R}\frac{u}{\sqrt{\{(ct/R_1)^2-1\}}}\mathbf{H}(t-R_1/c). \tag{A 3·11}$$

Now,

$$\mathscr{R}(u) = \frac{ct}{R_1}\frac{\rho}{R_1}\cosh\eta. \tag{A 3·12}$$

Also, since the integrand is zero for $t < R_1/c$, we find from (A 3·2) and (A 3·4) that

$$\cosh\eta < \sqrt{\{(ct/\rho)^2-(z/\rho)^2\}}, \tag{A 3·13}$$

so that

$$p_0^f(R;\text{step}) = \mp\frac{2P_0}{\pi}\int_0^{\cosh^{-1}\sqrt{\{(ct/\rho)^2-(z/\rho)^2\}}}\mathrm{d}\eta\,\frac{ct}{R_1^2}\frac{\rho}{R_1^2}\frac{1}{\sqrt{\{(ct/R_1)^2-1\}}}. \tag{A 3·14}$$

$R_1$ depends on $\eta$ through (A 3·2) and (A 3·8). Introduce the physically significant radial co-ordinate variable $R$ by

$$R = \sqrt{(z^2+\rho^2)}. \tag{A 3·15}$$

and the new variable of integration $Y$ by

$$Y = \rho\sinh\eta = \sqrt{(R_1^2-R^2)}. \tag{A 3·16}$$

Then

$$p_0^f(R;\text{step}) = \mp\frac{2P_0 ct}{\pi}\int_0^{\sqrt{(c^2t^2-R^2)}}\frac{\mathrm{d}Y}{(Y^2+R^2)\sqrt{(c^2t^2-R^2-Y^2)}}. \tag{A 3·17}$$

Next we introduce the variable of integration $w$ by

$$Y = \sqrt{(c^2t^2-R^2)}\sin w, \tag{A 3·18}$$

which gives

$$p_0^f(R;\text{step}) = \mp\frac{2P_0}{\pi R}\frac{ct}{R}\int_0^{\frac{1}{2}\pi}\frac{\mathrm{d}w}{(ct/R)^2\sin^2 w+\cos^2 w}. \tag{A 3·19}$$

Finally, if we let

$$v = (ct/R)\tan w, \tag{A 3·20}$$

it follows that

$$p_0^f(R;\text{step}) = \mp\frac{2P_0}{\pi R}\int_0^\infty\frac{\mathrm{d}v}{1+v^2}\mathbf{H}(t-R/c). \tag{A 3·21}$$

The integral in (A 3·21) is well known to be $\frac{1}{2}\pi$ so that (A 3·21) reduces to the desired result:

$$p_0^f(R;\text{step}) = \mp\frac{P_0\mathbf{H}(t-R/c)}{R}. \tag{A 3·22}$$

Comparison with (3·18) requires that we choose the lower sign in (3·24) and in the integrals that follow.

## Appendix 4. Evaluation of the first-order response by use of the product theorem

The 'imaginary part of' operator, $\mathscr{I}$, can be inserted in place of the factor i of the integrals in (3·26) and (3·27), because the $s$-multiplied transform of (3·18) is positive real, being simply

$$P_0\,\mathrm{e}^{-sR/c}/R.$$

In order to evaluate integrals of the type (3·30) without discarding the factor $s^{\frac{1}{2}}$ let us first follow the procedure of appendixes 2 and 3 and introduce the variable of integration $u$ by $u = cq$. Then (3·30) takes the form

$$\bar{p}_0^f(\rho, z; \text{step}) = P_0\sqrt{\left(\frac{s}{2\pi\rho c}\right)}\,\mathscr{I}\int_{-i\infty}^{+i\infty}\frac{\sqrt{u}}{\gamma}\exp\{-(s/c)\,(u\rho+\gamma\,|z|)\}\,\mathrm{d}u. \tag{A 4·1}$$

If we now let

$$\tau = \frac{u\rho}{c}+\frac{\gamma|z|}{c}, \tag{A 4·2}$$

in analogy with (A 2·2) and (A 3·3), and continuing as before we have

$$u = u(\tau) = \frac{c\tau}{R}\frac{\rho}{R}-\frac{|z|}{R}\sqrt{\left\{1-\left(\frac{c\tau}{R}\right)^2\right\}}, \tag{A 4·3}$$

$$\frac{\mathrm{d}u}{\gamma} = \frac{c}{R}\frac{\mathrm{d}\tau}{\sqrt{\{1-(c\tau/R)^2\}}}, \tag{A 4·4}$$

and $R$ is defined by (3·19). In the $\tau$ plane the integral (A 4·1) then becomes

$$\bar{p}_0^f(\rho, z; \text{step}) = \frac{P_0}{R}\sqrt{\left(\frac{sc}{2\pi\rho}\right)}\,\mathscr{I}\int_{C_\tau}\frac{\sqrt{u}\,\mathrm{e}^{-s\tau}}{\sqrt{\{1-(c\tau/R)^2\}}}\,\mathrm{d}\tau. \tag{A 4·5}$$

It is important to realize here that the validity of the asymptotic expansion (3·28) for the phase range of the argument of $K_0$ from $-\pi$ to $+\pi$ requires that the cut for the radical $u^{\frac{1}{2}}$ be taken from the origin of co-ordinates to infinity along the negative real $u$ axis. Therefore, the contour of (A 4·1) from $-i\infty$ to $+i\infty$ has to proceed to the right of the origin of the $u$ plane. It can therefore be distorted to surround only the cut from $u = 1$ to $u = \infty$ along the positive real $u$ axis. The transformation (A 4·2) takes the origin of the $u$ plane into the point $z/c$ in the $\tau$ plane. The branch point at $u = 1$ disappears, being replaced by one at $t = R/c$. The contour $C_\tau$ can now be taken to surround the cut from $t = R/c$ to $t = +\infty$.

The assumption (3·29) requires that $q$, $u$, and therefore $\tau$ be large. In extending the contour to enclose the whole positive real $t$ axis we shall therefore ignore the extension of the cut for $u^{\frac{1}{2}}$ which goes up to $t = z/c$ in the $\tau$ plane. We then find

$$\bar{p}_0^f(\rho, z; \text{step}) = \frac{P_0}{R}\sqrt{\left(\frac{2sc}{\pi\rho}\right)}\,\mathscr{I}\left[\mathrm{i}\,\mathscr{I}\int_0^\infty\frac{\sqrt{u}\,\mathrm{e}^{-st}\mathbf{H}(t-z/c)}{\sqrt{\{1-(ct/R)^2\}}}\,\mathrm{d}t\right]+\ldots. \tag{A 4·6}$$

Integral (A 4·6) is of the form

$$\bar{p}(\text{step}) = s^{\frac{1}{2}}\int_0^\infty G(t)\,\mathrm{e}^{-st}\,\mathrm{d}t, \tag{A 4·7}$$

which becomes an $s$-multiplied Laplace integral on multiplication by $s^{\frac{1}{2}}$:

$$s^{\frac{1}{2}}\bar{p}(\text{step}) = s\int_0^\infty G(t)\,\mathrm{e}^{-st}\,\mathrm{d}t. \tag{A 4·8}$$

It is also well known from transform theory that

$$s^{\frac{1}{2}} = s\int_0^\infty\frac{\mathrm{e}^{-st}}{\sqrt{(\pi t)}}\,\mathrm{d}t, \tag{A 4·9}$$

so that the interpretation (McLachlan 1953) of the product of these transforms divided by $s$ is given simply by

$$p\,(\text{step}) = -\frac{1}{\sqrt{\pi}}\int_0^t \frac{G(t')}{\sqrt{(t-t')}}\,\mathrm{d}t', \tag{A 4·10}$$

which for our source problem becomes

$$p_0^f(R;\text{step}) = \begin{cases} 0 & \text{for} \quad (t < R/c), \quad \text{(A 4·11 } a\text{)} \\ \dfrac{P_0}{\pi R}\sqrt{\left(\dfrac{2c}{\rho}\right)}\,\mathscr{R}\displaystyle\int_0^t \frac{\sqrt{u}\,\mathrm{d}t'}{\sqrt{\{(ct'/R)^2-1\}}\sqrt{(t-t')}} & \text{for} \quad (t > R/c). \quad \text{(A 4·11 } b\text{)} \end{cases}$$

For $t > R/c$ (A 4·3) yields

$$\mathscr{R}\sqrt{u} = \frac{1}{\sqrt{2}}\sqrt{\left[\frac{ct'}{R}\frac{\rho}{R}+\sqrt{\left\{\left(\frac{ct'}{R}\right)^2-\left(\frac{z}{R}\right)^2\right\}}\right]}, \tag{A 4·12}$$

so that the integral becomes

$$p_0^f(R;\text{step}) = \frac{P_0}{\pi R}\frac{c}{\sqrt{(\rho R)}}\int_{R/c}^t \sqrt{\left[\frac{\dfrac{ct'}{R}\dfrac{\rho}{R}+\sqrt{\left\{\left(\dfrac{ct'}{R}\right)^2-\left(\dfrac{z}{R}\right)^2\right\}}}{\left[\left(\dfrac{ct'}{R}\right)^2-1\right]\left(\dfrac{ct}{R}-\dfrac{ct'}{R}\right)}\right]}\mathrm{d}t'+\ldots. \tag{A 4·13}$$

Next, introduce the transformation from the variable $t'$ to the variable by $\xi$

$$\frac{ct'}{R} = \frac{1}{2}\left(\frac{ct}{R}+1\right)+\frac{1}{2}\left(\frac{ct}{R}-1\right)\sin\frac{\pi}{2}\xi, \tag{A 4·14}$$

which yields

$$p_0^f(R;\text{step}) = \frac{P_0}{2R}\int_{-1}^{+1}\mathrm{d}\xi\sqrt{\left[\frac{\dfrac{ct'}{R}+\dfrac{R}{\rho}\sqrt{\left\{\left(\dfrac{ct'}{R}\right)^2-\left(\dfrac{z}{R}\right)^2\right\}}}{\dfrac{ct'}{R}+1}\right]}. \tag{A 4·15}$$

The integrand of (A 4·15) is a slowly varying positive real function of $\xi$ and is bounded between 1 and $\sqrt{(1+R/\rho)}$. An exact numerical evaluation of (A 4·15) is shown in figure 26 for values of $z/\rho = 0{\cdot}0, 0{\cdot}1$ and $0{\cdot}2$. The curves are indistinguishable from each other to three

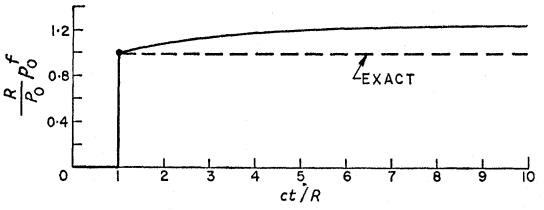


FIGURE 26. Comparison of the first-term approximation with the exact response to the step-function excitation of a point source in an infinite fluid.

significant figures. Upon comparing them with the exact step-function response which they are approximating it becomes apparent that by retaining the Cagniard formalism while making an asymptotic expansion of only part of the integrand, we obtain an exceedingly close approximation to the step-function excitation. This approximation is much closer to the actual response than we would obtain by applying the step-function operator to the first term of the saddle-point method such as that developed by van der Waerden (1950) and discussed in §11.

The upper limit of the response (A 4·15) occurs for $ct/R = \infty$ and is equal to

$$(P_0/R)\sqrt{\{1+(R/\rho)\}}.$$

This gives the maximum deviation from the exact step-function response which is less than 50 % for the three curves of figure 26. At $ct/R = \infty$ where the three curves differ the most we find a relative deviation of less than 0·6 % from $\sqrt{2}$. For a value of $z/\rho$ as high as 0·5 the upper limit becomes only 1·455. When a practical excitation such as an exponential decay is convoluted with the response of figure 26, we can expect a rather good amplitude agreement with the exact response. Therefore, in a boundary value problem such as that of the fluid/solid interface, the approximate integral (3·30) will greatly simplify the labour involved in evaluating the response for a point source and this large radial distance approximation should enable the evaluation of solution of the Cagniard problem for a point source which up to now has been limited to points on the $z$ axis where the Bessel function in (3·17) becomes unity.

## Appendix 5. Singularities of the function $A(u)$ on the upper Riemann sheet

The procedure, making use of 'the principle of the argument' (Copson 1944) to determine the zeros of the vanishing of the denominator of $A(u)$, is well established, and we shall therefore find it necessary to present only the briefest summary.

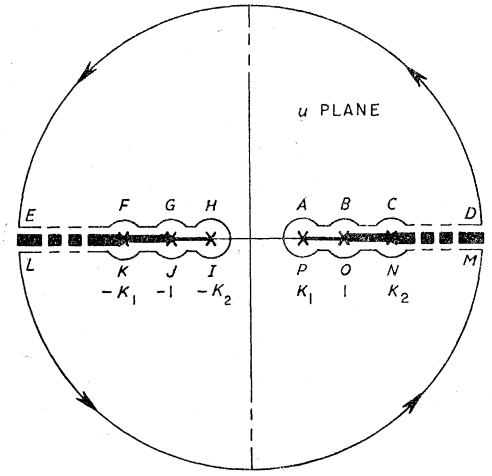


Figure 27*a*. Contour for determining the singularities of $A(u)$ on the top Riemann sheet. Case 1, pitch (figure 27*b*, for plaster of paris is identical except that branch points have been interchanged as mentioned in text).

Consider the behaviour of the contour of figure 27 in the $u$ plane as it appears in the $D$ plane where $D(u)$ is defined by (4·10) to be

$$D(u) = \gamma f(u) + (\rho^f/\rho^s)\, K_2^4 \alpha, \tag{A 5·1}$$

where

$$f(u) = (K_2^2 - 2u^2)^2 + 4u^2\alpha\beta, \tag{4·11}$$

and

$$\left.\begin{aligned} &\alpha = \sqrt{(K_1^2-u^2)} \text{ has phase 0 for } u < K_1 \text{ and phase } -\mathrm{i} \text{ for } u > K_1, \\ &\beta = \sqrt{(K_2^2-u^2)} \text{ has phase 0 for } u < K_2 \text{ and phase } -\mathrm{i} \text{ for } u > K_2, \\ &\gamma = \sqrt{(1-u^2)} \text{ has phase 0 for } u < 1 \text{ and phase } -\mathrm{i} \text{ for } u > 1. \end{aligned}\right\} \tag{A 5·2}$$

The circular path of the contour of figure 27*a* is taken at $|u| = \infty$. Figure 27*b* for case 2, plaster of paris, is of course identical to figure 27*a* except for an interchange of the order of positioning of the branch points 1 and $K_2$ as listed in table 3. The contour taken in the direction $A$ through $P$ appears as the contour designated $A'$ through $P'$ in the $D$ plane.

The transformation of the path $E$ through $H$, i.e. $E'$ through $H'$, is the image of $A'$ through $D'$ about the real $D$ axis. Furthermore, the path $I'$ through $L'$ is identical to $A'$ through $D'$ and the path $M'$ through $P'$ is identical to $E'$ through $H'$. The net result is that the complete contour $A'$ through $P'$ does not enclose the origin of the $D$ plane. A similar result is also found for case 2, plaster of paris, whose behaviour is described by the corresponding path $A'$ through $D'$ as is shown in figure 28*b*.

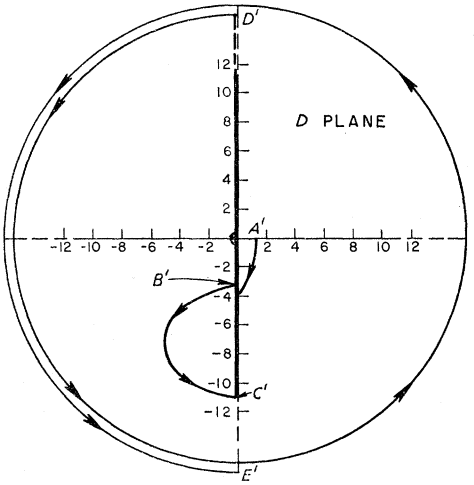


FIGURE 28*a*. The path $A'$ through $E'$ in the $D$ plane for case 1, pitch.

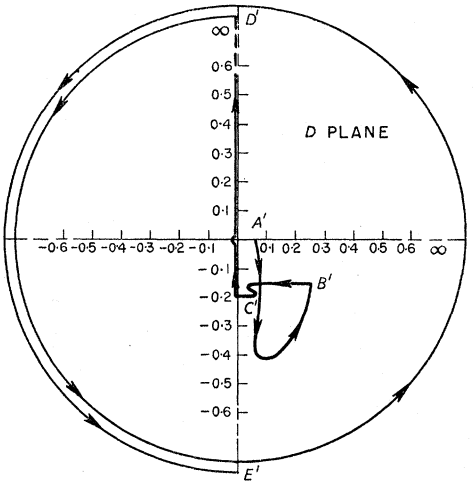


FIGURE 28*b*. The path $A'$ through $E'$ in the $D$ plane for case 2, plaster of paris.

Although we have shown that the origin of the $D$ plane is not enclosed for pitch and plaster of paris, this conclusion can easily be generalized to any physically interesting solids of cases 1 or 2 because the points designated $B'$ and $V'$, respectively, in figures 28*a* and *b* will always lie on the negative imaginary axis as can be seen from the fact that for $u = 1$

$$D(1) = -\mathrm{i}(\rho^f/\rho^s)\, K_2^4 \sqrt{(1-K_1^2)}.$$

Therefore, zeros of $D(u)$ or poles of $A(u)$ can occur on the top Riemann sheet as defined by (A 5·2) only on the cut along the real axis of figure 27. The single change of sign of $f(u)$ of (4·11) on this axis can be used to argue that only one pair of zeros can exist there. These zeros are just the Stoneley pair discussed by Spencer (1956) and numerically tabulated by Strick & Ginzbarg (1956).

## APPENDIX 6. FURTHER DISCUSSION OF THE LAMB PROBLEM

We shall account for the discrepancy in ordinate variables, which is apparent in the comparison of figure 17*a* with *b* in § 9. We saw in § 3 that the application of the unit function operator

$$\frac{1}{2\pi \mathrm{i}} \int_{\Omega} \frac{\mathrm{d}\omega}{\omega}$$

upon the harmonic response leads to the response to a step-function excitation given by (3·3). Likewise, the delta-function operator

$$\frac{1}{2\pi}\int_{\Omega} \mathrm{d}\omega$$

applied to (3·3) will yield the response (3·6) which we have designated as a delta-function source. The harmonic response (3·3) was then transformed into the form (3·14)

$$P_0(x, z; \mathrm{e}^{\mathrm{i}\omega t}) = \frac{P_0}{2\mathrm{i}}\int_{-\infty}^{+\infty} \frac{1}{\sqrt{\{(1/c^2)-q^2\}}} \exp\left(-\mathrm{i}\omega[\gamma\sqrt{\{(1/c^2)-q^2\}}\, z + qx]\right) \mathrm{d}q\, \mathrm{e}^{\mathrm{i}\omega t}, \quad (3\cdot14)$$

where the integration variable was related to the angle of incidence by

$$q = \frac{1}{c}\sin\theta, \quad (3\cdot13)$$

and

$$\sqrt{\left(\frac{1}{c^2}-q^2\right)} = \frac{1}{c}\cos\theta \quad \mathscr{I}\sqrt{\left(\frac{1}{c^2}-q^2\right)} \leqslant 0 \quad \text{for} \quad \omega \geqslant 0. \quad (3\cdot15)$$

At $z = 0$ our harmonic source becomes

$$p_0^f(x, 0; \mathrm{e}^{\mathrm{i}\omega t}) = \frac{P_0}{2\mathrm{i}}\int_{-\infty}^{+\infty} \mathrm{d}q \exp\left(-\mathrm{i}\omega q x + \mathrm{i}\omega t\right) \Big/ \sqrt{\left(\frac{1}{c^2}-q^2\right)}. \quad (\mathrm{A}\,6\cdot1)$$

Now let us consider Lamb's source which was defined by (an equation number with an L refers to such an equation in Lamb's paper; the notation, however, has been transcribed so as to correspond to our notation)

$$\sigma_{xz}^s|_{z=0} = 0, \quad \sigma_{zz}^s|_{z=0} = Y \exp\left(\mathrm{i}\xi x + \mathrm{i}\omega t\right). \quad (\mathrm{L}\,46)$$

Lamb constructs $\phi$ his source function by letting $Y = -P_0\,\mathrm{d}\xi/2\pi$ and integrating from $-\infty$ to $+\infty$.

$$\sigma_{zz}^s|_{z=0} = -\frac{P_0}{2\pi}\int_{-\infty}^{+\infty} \mathrm{d}\xi \exp\left(\mathrm{i}\xi x + \mathrm{i}\omega t\right). \quad (\mathrm{A}\,6\cdot2)$$

If we further apply the delta-function time operator

$$\frac{1}{2\pi}\int_{-\infty}^{+\infty} \mathrm{d}\omega,$$

then use the interpretations

$$\delta(x) = \frac{1}{2\pi}\int_{-\infty}^{+\infty} \mathrm{d}\xi\, \mathrm{e}^{\mathrm{i}\xi x}, \quad \delta(t) = \frac{1}{2\pi}\int_{-\infty}^{+\infty} \mathrm{d}\omega\, \mathrm{e}^{\mathrm{i}\omega t},$$

we quickly find that $\sigma_{zz}$ has the form $-P_0\delta(x)\,\delta(t)$; or since the pressure is negative to the stress, we see that the Lamb source has a positive delta function concentration in both $x$ and $t$.

If we now introduce the change of variable from $q$ to $\xi$ by

$$\xi = -\omega q, \quad (\mathrm{A}\,6\cdot3)$$

into our source integral (A 6·1), then we obtain

$$p_0^f(x, 0; \mathrm{e}^{\mathrm{i}\omega t}) = \frac{+P_0}{2\mathrm{i}}\int_{-\infty}^{+\infty} \mathrm{d}\xi \frac{\exp\left(\mathrm{i}\xi x + \mathrm{i}\omega t\right)}{\sqrt{\{(\omega/c)^2-\xi^2\}}}, \quad (\mathrm{A}\,6\cdot4)$$

which has exactly the same form as Lamb's source integral (A 6·2) except for the existence of the radical $\sqrt{\{(\omega/c)^2-\xi^2\}}$ in the denominator of (A 6·4). In §3 we based our development of

the source integral (3·14) on a summation of plane waves over angles of incidence $\theta$. The integration variable $\xi$ is related to $\theta$ according to (3·13) and (A 6·3) by

$$\xi = (\omega/c)\sin\theta. \tag{A 6·5}$$

From (4·17) we can easily ascertain that $\theta$ is a monotonically increasing function of $t$ for $t \leqslant r_1/c$ and complex for $t > r_1/c$. Thus, as is well known for the Rayleigh wave, the Stoneley interface wave is also excited by elementary plane waves incident at a complex angle, i.e. to a damped plane wave. Also, from a plane wave viewpoint, the reflexion coefficient is complex of magnitude unity in region $I_b$ (where $t_S \leqslant t \leqslant r_1/c$ or $c/b < \sin\theta < x/r_1$) and therefore corresponds to totally reflected waves. In region $I_a (t_P \leqslant t \leqslant t_S$ or $c/a \leqslant \sin\theta \leqslant c/b)$ the reflexion coefficient is complex of magnitude less than unity corresponding to partial reflexion and for $0 \leqslant t \leqslant t_P$ or $0 \leqslant \sin\theta \leqslant c/a$ it is real again of magnitude less than unity. Therefore, as far as transmission into the solid is concerned, we need consider only those values of $\theta$ which lie between 0 and $\sin^{-1} c/b$. In our interface problem where the source is a distance $H$ above the interface we would now like to picture the solid as initially being excited by a bundle of plane waves whose normals lie within the wedge formed by the angles $0 \leqslant \sin\theta \leqslant c/b$. That is, we would like to think of an equivalent source on the solid which is not quite as concentrated in space and time as is Lamb's delta-function source.

In terms of $\theta$ our bundle of plane waves is restricted to $0 \leqslant \sin\theta \leqslant \omega/b$ so that if $c \ll b$, we can approximate the radical in the denominator of (A 6·4) by $\omega/c$. This approximate form of (A 6·4) is then identical in form to Lamb's integral (A 6·2) aside from a coefficient $1/\mathrm{i}\omega$; i.e.

$$p_0^f(\mathrm{e}^{\mathrm{i}\omega t}) \approx -(1/\mathrm{i}\omega)\,\sigma_{zz}|_{z=0}^{\text{Lamb}}. \tag{A 6·6}$$

This coefficient $(1/\mathrm{i}\omega)$ will be carried along when the harmonic displacement response in both boundary value problems is determined. For example, the relation between the horizontal displacement responses can be expressed as

$$(\mathrm{i}\omega)\,U^s(\mathrm{e}^{\mathrm{i}\omega t}) \approx U(\mathrm{e}^{\mathrm{i}\omega t})|_{z=0}^{\text{Lamb}}. \tag{A 6·7}$$

Operationally, $\mathrm{i}\omega$ corresponds to a time differentiation so that the left side can be written as simply the horizontal velocity response $\dot{U}^s(\mathrm{e}^{\mathrm{i}\omega t})$. Therefore, we come to the conclusion that we should expect approximately the same response when we calculate velocities in our problem that Lamb obtains when he calculates displacements in his problem. This is precisely what we observe when we compare displacement responses in figures 17*a* and *b*.

Another way to relate our source to Lamb's source is as follows. Let us return to (3·14) and differentiate with respect to $z$. Then, upon introducing the transformation (A 6·3) we obtain at $z = 0$

$$\frac{\partial p_0^f}{\partial |z|} = +\frac{P_0}{2}\int_{-\infty}^{+\infty} \mathrm{d}\xi \exp(+\mathrm{i}\xi x + \mathrm{i}\omega t). \tag{A 6·8}$$

The integral in (A 6·8) is the same as that in (A 6·2) for Lamb's source so that we find

$$\frac{\partial p_0^f}{\partial |z|} = \frac{-1}{\pi}\sigma_{zz}|_{z=0}^{\text{Lamb}}. \tag{A 6·9}$$

Therefore, our source has a sort of dipole behaviour along the $z$ axis when compared with Lamb's monopole behaviour.

## Appendix 7. Singularities of the function $A(u)$ on the lower Riemann sheets

Here we consider only those poles of $A(u)$ which lie on the real axis on lower Riemann sheets. Therefore, we again consider the zeros of $D(u)$ defined by (A 5·1), but this time subject to a violation of the top sheet conditions (A 5·2). Furthermore, we restrict ourselves to searching for zeros of $D(u)$ on the real $u$ axis for which $u = u_0$ is less than $K_1$ and greater than both 1 and $K_2$; then

$$\begin{aligned} \alpha \text{ is pure imaginary} &= (\pm)\,\mathrm{i}\sqrt{(u_0^2 - K_1^2)}, \\ \beta \text{ is real} &= (\pm)\sqrt{(K_2^2 - u_0^2)}, \\ \gamma \text{ is real} &= (\pm)\sqrt{(1 - u_0^2)}, \text{ all radicals now being positive real.} \end{aligned}$$

Vanishing of the real and imaginary parts of $D(u_0)$ yields the equations

$$0 = \mathscr{R}\, D(u_0) = \gamma(K_2^2 - 2u_0^2)^2, \tag{A 7·1 a}$$

$$0 = \mathscr{I}\, D(u_0) = \alpha(4u_0^2\beta\gamma + (\rho^f/\rho^s)\, K_2^4). \tag{A 7·1 b}$$

The only solution that is compatible with both of these equations is found by inserting $u_0 = K_2/\sqrt{2}$ obtained from (A 7·1 $a$) into (A 7·1 $b$). We then find

$$K_2^2 = \frac{2}{1 + (\rho^f/\rho^s)^2}, \tag{A 7·2}$$

or

$$u_0 = \pm\frac{1}{\sqrt{1 + (\rho^f/\rho^s)^2}}, \tag{A 7·3}$$

the latter relations showing that one can always find such a real root merely by varying the density ratio $\rho^f/\rho^s$.

The solutions (A 7·2), (A 7·3) were obtained from the equation

$$4u_0^2\beta\gamma + (\rho^f/\rho^s)\, K_2^4 = 0, \tag{A 7·4}$$

which required only that either $\beta$ or $\gamma$ be negative real. Therefore we have the roots (A 6·3) existing at $u_0$ on the real axis on four different Riemann sheets:

$$\left.\begin{array}{llll} 1. & \text{upper } \alpha, & \text{lower } \beta, & \text{upper } \gamma, \\ 2. & \text{upper } \alpha, & \text{upper } \beta, & \text{lower } \gamma, \\ 3. & \text{lower } \alpha, & \text{lower } \beta, & \text{upper } \gamma, \\ 4. & \text{lower } \alpha, & \text{upper } \beta, & \text{lower } \gamma. \end{array}\right\} \tag{A 7·5}$$

These are the phase requirements on $\alpha$, $\beta$ and $\gamma$ just above the cut on the real $u$ axis and they account for four of the eight pairs of roots of the rationalized polynomial associated with the Stoneley wave equation for a fluid/solid interface (together with the true Stoneley pair and its images on the lowest Riemann sheet obtained by reversing the signs of all three radicals, $\alpha$, $\beta$ and $\gamma$, we are left with only two pairs of roots unaccounted for).

In § 10 we varied the value of $K_2$ and followed the root $u_0$ in the complex plane of figure 20 as it passed through the real point $u_0 = K_2/\sqrt{2}$. Although there are many transitions of the cut that could lead through the point $u_0$ on any of the four sheets listed in (A 7·4), the $u_0$ of interest here is associated with the crossing from lower $\alpha$, lower $\beta$, upper $\gamma$ to upper $\alpha$, lower $\beta$, upper $\gamma$; i.e. to the sheet first listed in (A 7·5).

## Notation

All equation numbers refer to parts II and III

*Interpretation and equation where first introduced*

| | |
|---|---|
| $a, b, \sigma, \rho^s, \lambda^s, \mu^s$ | Compressional and shear (rotational) velocities, Poisson's ratio, density, and Lamé constants of the solid. |
| $c, \rho^f, \lambda^f$ | Compressional velocity, density, and Lamé constant of the fluid. |
| $\omega$; $t$ | Angular frequency of harmonic excitation, time. |
| $P_{cr}, S_{ct}$ | Critically refracted longitudinal and transverse waves—used only in part I. |
| $w$ | Integration variable (3·4); $w = \frac{1}{2}\pi - (\theta + \chi)$. |
| $r$; $r_0$ | Radial response co-ordinate and radius of cylindrical source in cylindrical co-ordinates. The azimuthal and axial co-ordinates are not specified since, owing to azimuthal symmetry, all line-source problems can be reduced to a treatment in polar co-ordinates. |
| $r, \chi$; $x, z$ | Polar and rectangular co-ordinates in two-dimensional line-source problems. $x = r\cos\chi$, $z = \sin\chi$, figure 6. |
| $p_0$, $P_0$ | Pressure response and its amplitude from a source in an infinite medium (3·1). |
| $\theta$ | Angle of incidence with respect to normal to fluid/solid interface (3·8). |
| $\mathbf{k}$ | Propagation vector for plane waves in an infinite fluid $= \omega/c\, e^{i\theta}$, figure 6. |
| $q$ | Variable of integration $= (1/c)\sin\theta$ (3·13). |
| $\Gamma$ | $(1/c)\cos\theta = \sqrt{\{(1/c^2) - q^2\}}$. |
| $\lambda$ | Integration variable (3·17). |
| $s = i\omega$ | Positive real $s$-multiplied Laplace transform variable. |
| $U^f, W^f, \phi^f$ | Horizontal and vertical particle displacements and displacement potentials in fluid (3·32). |
| $U^s, W^s, \phi^s, \psi^s$ | Horizontal and vertical particle displacements and displacement potentials in solid (3·36). |
| $Q_0$ | (4·2). |
| $H$ | Distance of source from interface. |
| $u = cq$ | Variable of integration (4·9). |
| $V_R$ | Rayleigh wave velocity of solid medium. |
| $V_{St}$ | Stoneley wave velocity for fluid/solid media. |
| $u_R = c/V_R$ | Non-dimensional Rayleigh wave velocity parameter, table 3. |
| $u_{St} = c/V_{St}$ | Non-dimensional Stoneley wave velocity parameter, following table 3. |
| $A(q)$, $A(u)$ | Complex reflexion coefficient (4·5), (4·10). |
| $f(q), f(u)$ | (4·6), (4·11). |
| $K_1 = c/a$ | Non-dimensional velocity parameter (4·12). |
| $K_2 = c/b$ | Non-dimensional velocity parameter (4·12). |
| $\alpha, \beta, \gamma$ | Square root radicals (4·12). |
| $\tau$ | Variable of integration (4·15), (9·5), (A2·2), (A3·3) and (A4·2). |
| $t$ | The real axis of the complex variable $\tau$ and the time variable; it is not in general equal to the real part of $\tau$. |
| $t_P, t_S$ | Arrival times for critically refracted $P$ and $S$ waves (4·16). |




PHILOSOPHICAL TRANSACTIONS OF THE ROYAL SOCIETY A MATHEMATICAL, PHYSICAL & ENGINEERING SCIENCES

| | |
|---|---|
| $\delta$ | Square-root radical (4·18*a*). |
| $r_1$ | Image detector distance (4·18*b*). |
| $\alpha_\tau, \beta_\tau$ | $\alpha, \beta$ defined by (4·12) expressed in the variable $\tau$. |
| $\tau_{St}$ | The transformation by (4·15) or (9·5) of the Stoneley pole at $u_{St}$ to the $\tau$ plane. |
| $t_{St}$ | The arrival time of the Stoneley wave and $t_{St} \approx x/V_{St}$. It is not in general equal to the real part of $\tau_{St}$. |
| $u_{pR}$ | Location of the pseudo-Rayleigh pole in the complex $u$ plane. |
| $t_{pR}$ | The arrival time of the pseudo-Rayleigh wave; it is in general not equal to the real part of $\tau_{pR}$. |
| $\tau_{pR}$ | The transformation of $u_{pR}$ by (4·15) or (9·5) to the $\tau$ plane. |
| $D(u)$ | Denominator of complex reflexion coefficient for $u > x/r_1$ (4·29). |
| $t_0$ | Arrival time of zero-pressure amplitude in region $I_a$ (5·3). |
| $x_d$ | Attenuation distance (10·1). |
| $\xi$ | Variable of integration $= i\tau$ (11·4). |

## References


Arons, A. B. & Yennie, D. R. 1950 Phase distortion of acoustic pulses obliquely reflected from a medium of higher sound velocity. *J. Acoust. Soc. Amer.* **22**, 231–237.

Cagniard, L. 1939 *Réflexion et Réfraction des ondes Séismiques Progressives*. Paris: Gauthier-Villars.

Copson, E. T. 1944 *Theory of functions of a complex variable*, p. 118. Oxford University Press.

Dix, C. H. 1954 The method of Cagniard in seismic pulse problems. *Geophysics*, **19**, 722–738.

Dix, C. H. 1955 The mechanism of generation of long waves from explosives. *Geophysics*, **20**, 87–103.

Fay, R. D. 1954 Notes on the transmission of sound through plates. *J. Acoust. Soc. Amer.* **234** A, 528–541.

Garvin, W. W. 1956 Exact transient solution of the buried line source problem. *Proc. Roy. Soc.* A, **234**, 528–541.

Gilbert, F. 1956 Seismic wave propagation in a two-layer half-space. Unpublished Ph.D. thesis, Massachusetts Inst. Tech.

Heuter, T. F. & Bolt, H. 1955 *Sonics*, p. 151, figure 4.36. New York: Wiley.

Hughes, D. S., Pondrom, W. L. & Mims, R. L. 1949 Propagation of elastic pulses in metal rods. *Phys. Rev.* **75**, 1552–1556.

Jeffreys, H. 1949 On compressional waves in two superposed layers. *Proc. Camb. Phil. Soc.* **23**, 652–653.

Kaufman, S. & Roever, W. L. 1951 Laboratory studies of transient elastic waves. *Proc. Third World Petroleum Cong.* The Hague, Sect. 1.

Kennel, J. M. 1955 Dispersion of wave velocities in elastic solids. Thesis: University of Texas.

Knopoff, L. 1952 On Rayleigh wave velocities. *Bull. Seismol. Soc. Amer.* **42**, 307.

Knott, C. G. 1899 Reflection and refraction of elastic waves with seismological applications. *Phil. Mag.* **48**, 64–97.

Lamb, H. 1904 On the propagation of tremors over the surface of an elastic solid. *Phil. Trans.* A, **203**, 1–42.

Lapwood, E. R. 1949 The disturbance due to a line source in a semi-infinite elastic medium. *Phil. Trans.* A, **242**, 63–100.

McLachlan, N. W. 1953 *Complex variable theory and transform calculus*. Cambridge University Press.

McMillen, J. H. 1946 The velocity of dilatation and Rayleigh waves in metal bars. *J. Acoust. Soc. Amer.* **18**, 190–199.

Muskat, M. 1933 Theory of refraction shooting. *Physics*, **4**, 14–28.

Nakano, H. 1925 On Rayleigh waves. *Japanese J. Astr. Geophys.* **2**, 233–326.

Northwood, T. D. & Anderson, D. V. 1953 Model seismology. *Bull. Seismol. Soc. Amer.* **43**, 239–245.

O'Brien, P. N. S. 1955 Model seismology—the critical refraction of elastic waves. *Geophysics*, **20**, 227–243.

Osborne, M. F. M. & Hart, S. O. 1945 Transmission, reflection and guiding of an exponential pulse by a steel plate in water. I. Theory. *J. Acoust. Soc. Amer.* **17**, 1–18.

Pekeris, C. L. 1955*a* The seismic surface pulse. *Proc. Nat. Acad. Sci., Wash.*, **41**, 469–480.

Pekeris, C. L. 1955*b* The seismic buried pulse. *Proc. Nat. Acad. Sci., Wash.*, **41**, 629–639.

Pinney, E. 1954 Surface motion due to a point source in a semi-infinite elastic medium. *Bull. Seismol. Soc. Amer.* **44**, 571–590.

Rayleigh, Lord 1888 On point-, line-, and plane-sources of sound. *Proc. Lond. Math. Soc.* **19**, 504–507.

Roever, W. L. & Vining, T. F. 1956 Propagation of an impulse along a fluid-solid interface. Part I. Experimental (Abstract). *Bull. Amer. Phys. Soc.* **1**, no. 2, 98.

Sato, Y. 1954 Study on surface waves. XII. Non-dispersive surface waves. *Bull. Earthqu. Res. Inst. Tokyo*, **32**, 349.

Scholte, J. G. 1948 On the large displacements commonly regarded as caused by Love's waves and similar dispersive waves IV. *Proc. Kon. Ned. Akad. Wetensch. Amst.* **51**, p. 976.

Scholte, J. G. 1949 On true and pseudo Rayleigh waves. *Proc. Kon. Ned. Akad. Wetensch. Amst.* **52**, 652–653.

Sommerfeld, A. 1949 *Partial differential equations*, chap. VI. New York: Academic Press.

Spencer, T. W. 1956 Studies in acoustic pulse propagation. Ph.D. thesis, California Inst. Tech. Also *Geophysics*, **21**, 71–87 (1956).

Stoneley, R. 1924 Elastic waves at the surface of separation of two solids. *Proc. Roy. Soc.* A, **106**, 416–428.

Strick, E. 1956 Propagation of an impulse along a fluid-solid interface. Part II. Theoretical (abstract). *Bull. Amer. Phys. Soc.* **1**, no. 2, 98.

Strick, E. & Ginzbarg, A. S. 1956 Stoneley wave velocities for a fluid-solid interface. *Bull. Seismol. Soc. Amer.* **46**, 281–292.

Strick, E., Roever, W. L. & Vining, T. F. 1956 Theoretical and experimental investigation of a pseudo-Rayleigh wave (abstract). *J. Acoust. Soc. Amer.* **28**, 794.

Takeuchi, H. & Kobayashi, N. 1955 Wave generations from line sources within the ground. *J. Phys. Earth*, **3**, 7–15.

Tatel, H. E. 1954 On the nature of a seismogram II. *J. Geophys. Res.* **59**, 289–294.

Tsuboi, C. 1927 *Proc. Phys. Math. Soc. Tokyo*, (3), **9**, 93–97.

van der Waerden, B. L. 1950 On the method of saddle points. *Appl. Sci. Res.* B, **2**, 33–45.

Von Schmidt, O. 1938 Über Knallwellenausbreitung in Flussigkeiten und festen Korpen. *Z. tech. Phys.* **19**, 554–560.

Watson, G. N. 1952 *Theory of Bessel functions*, 2nd ed., p. 80, formula 18. Cambridge University Press.

Weinstein, M. S. 1952 On the failure of plane wave theory to predict the reflection of a narrow ultrasonic beam. *J. Acoust. Soc. Amer.* **24**, 284–287.

Yamaguichi, R. & Sato, Y. 1956 Stoneley wave—its velocity, orbit and the distribution of amplitude. *Bull. Earthqu. Res. Inst.* **33**, 549–559.



PHILOSOPHICAL TRANSACTIONS OF THE ROYAL SOCIETY A MATHEMATICAL, PHYSICAL & ENGINEERING SCIENCES